

**The spiral-pole antenna: An electrically small, resonant hybrid dipole with structural
modification for inherent reactance cancellation**

by

Ishrak Khair

A Thesis

Submitted to the Faculty

of the

WORCESTER POLYTECHNIC INSTITUTE

in partial fulfillment of the requirements for the

Degree of Master of Science

in

Electrical and Computer Engineering

by

August 2011

APPROVED:

Dr. Reinhold Ludwig, Committee Member (WPI)

Dr. Sabah Sabah, Committee Member (Vectron Intl.)

Dr. Sergey N. Makarov, Thesis Advisor (WPI)

Abstract

A small “spiralpole” antenna – the hybrid structure where one dipole wing is kept, but another wing is replaced by a coaxial single-arm spiral, is studied both theoretically and experimentally. Such a structure implies the implementation of an impedance-matching network (an inductor in series with a small dipole) directly as a part of the antenna body. The antenna impedance behavior thus resembles the impedance behavior of a small dipole in series with an extra inductance, which is that of the spiral. However, there are two improvements compared to the case when an equivalent small dipole is matched with an extra lumped inductor. First, the spiralpole antenna has a significantly larger radiation resistance – the radiation resistance increases by a factor of two or more. This is because the volume of the enclosing sphere is used more efficiently. Second, a potentially lower loss is expected since we only need a few turns of a greater radius. The radiation pattern of a small spiralpole antenna is that of a small dipole, so is the first (series) resonance. The Q-factor of the antenna has been verified against the standard curves. The antenna is convenient in construction and is appealing when used in conjunction with passive RFID tags such as SAW temperature sensors.

Acknowledgements

First off, I would like to thank Allah (SWT) for His Blessings, for His Guidance and I continue to ask for His Forgiveness.

I wish to thank the ECE department of WPI for giving me the opportunity to be a student here, accepting me and allowing me to be under the tutelage of its great faculty and guidance of its compassionate staff. I am very grateful for the valuable knowledge and experiences I have gained here and all the great people I have met.

I wish to thank Professor Sergey N. Makarov for being my advisor since my freshman year at WPI and until my final year as a graduate student, for motivating me, for making Maxwell's equations less intimidating, for allowing me to conduct research in his Labs, for allowing me to teach his introductory ECE class, for being a great teacher, for being a guardian to me, for accepting me and being patient with me despite the countless faults I have, for treating my family with so much respect. I would also like to thank his wife Natasha for her kindness, hospitality and warmth (and Masha for being a wonderful and playful dog). My family and I will always keep you all in our prayers.

I wish to thank Professor Reinhold Ludwig for being a part of my thesis committee, for allowing me to take his invaluable RF and EM classes and helping me build my foundation in RF knowledge, and for being such a great Professor to all his students.

I also wish to thank Dr. Sabah Sabah, Dr. Daniel Stevens, and everyone else at Vectron International for allowing me to be a part of Sengenuity, to conduct my research there, allowing me to be a part of the Wireless team, and for all the support that they have provided. This would work not be possible with their generosity, faith and kindness towards me.

Last but never least, I would especially like to thank my mother Syeda Ferdousi Jahan and my father Dr. Abul Kasem Khairulislam for being the most amazing parents any child could ever ask for. This thesis is dedicated to these two irreplaceable people in my life. Without your love, support, motivation, teachings, blessings, and sacrifices that you have made for me, I would be absolutely nothing. You are the most important people in my life, and always will be no matter what.

Table of Figures

Figure 1: Coordinate system showing linear current element with far field components in E and H planes	8
Figure 2: Spiralpole antenna incorporated into wireless food probe design	13
Figure 3: Current distribution at 96MHz (resonance) on a five turns Spiral.....	17
Figure 4: Current distribution on the shaft of the same five turns spiralpole at 96MHz (resonance)	18
Figure 5: Cross section of a given spiralpole configuration in its minimum bounding sphere.....	21
Figure 6: Chu's transformation of a wave problem in space to an equivalent circuit problem at the surface of the sphere. The antenna structure and current distribution is assumed to be arbitrary and thus the fields expressed in terms of <i>TM_{n0}</i> spherical modes	23
Figure 7: Original ladder network depiction from Chu's paper	26
Figure 8: Equivalent circuit of lowest <i>TM₁₀</i> mode. This is also the equivalent circuit for the radiation given by an infinitesimally small dipole	26
Figure 9: Algorithm for generating antenna Q - kr relationship using MATLAB.....	34
Figure 10: Creation of the spiral sheet in Ansoft HFSS	36
Figure 11: Arrangement of the feeding mechanism. The red circular surface is the lumped port or feed	36
Figure 12: Design parameters of three turn spiralpole model	38
Figure 13: Dipole of length 300mm inside enclosing sphere.....	39
Figure 14: Three turn Spiral Pole	40
Figure 15: Three turn spiralpole in Chu Sphere	41
Figure 16: Simulated VS analytical Dipole and 3 turn spiralpole impedances.....	42
Figure 17: Radiation resistance comparison between 3 turn spiralpole and dipole antenna at spiralpole resonance.....	43
Figure 18: Q - kr for 3 turn spiral VS dipole and absolute limit	44
Figure 19: E and H plane radiation patterns for 3 turn spiralpole and dipole.....	45
Figure 20: Four turn spiralpole	45

Figure 21: Four turn spiralpole in Chu Sphere	46
Figure 22: Simulated VS analytical Dipole and 4 turns spiralpole impedances	47
Figure 23: Radiation resistance comparison between 4 turns spiralpole and dipole at spiralpole resonance.....	48
Figure 24: Q - kr for 4 turn spiral VS dipole and absolute limit	49
Figure 25: E and H Plane Pattern for 4 turn spiralpole and Dipole at spiralpole resonance	50
Figure 26: Five turn spiralpole	51
Figure 27: Five turn spiralpole in Chu Sphere.....	52
Figure 28: Simulated VS analytical Dipole and 5 turns spiralpole impedances	53
Figure 29: Radiation resistance comparison of 5 turn spiralpole and dipole antenna at spiralpole resonance.....	54
Figure 30: Q - kr for 5 turn spiral VS dipole and absolute limit	55
Figure 31: E and H Plane radiation pattern overlays for 5 turn spiralpole and dipole antennas at spiralpole resonance.....	56
Figure 32: Six turn Spirapole	57
Figure 33: Six turns spiralpole in Chu Sphere	58
Figure 34: Simulated VS analytical Dipole and 6 turn spiralpole impedances.....	59
Figure 35: Radiation resistance comparison of 6 turns spiralpole and dipole antennas at resonance.....	60
Figure 36: Q - kr for 6 turns spiral VS dipole and absolute limit.....	61
Figure 37: E and H plane radiation plot comparison of 6 turn spiralpole and dipole antennas at spiralpole resonance.....	62
Figure 38: Actual food probe produced by Vectron International, Hudson. NH.....	63
Figure 39: Temperature sensing data acquired with the spiralpole based foodprobe and a wired thermoelement. The spiralpole based wireless solution shows excellent accuracy.	64
Figure 40: 300mm dipole with cubic radiation box of side length 400mm	71
Figure 41: Radiation Pattern in the H plane at 600 MHz. Notice the symmetrical results obtained	72
Figure 42: 300mm dipole within cubic radiation box of side length 2500mm	73
Figure 43: Radiation Pattern in the H plane at 600 MHz. Notice the irregular pattern.	74
Figure 44: Initial disk-dipole hybrid design in Ansoft\ANSYS HFSS.....	75

Figure 45: Impedance of disk-dipole hybrid antenna from 350 MHz to 600 MHz. The antenna reactance is primarily capacitive. 76

Figure 46: Return Loss (S11) in dB from 350 MHz to 600 MHz of the disk-dipole hybrid. The antenna is starting to resonate at higher frequencies. 76

Contents

1	Introduction	1
1.1	Motivation.....	4
1.2	Electrically Small Antennas	5
1.3	Radiation of a small linear current element: Maxwell’s Equations	6
1.4	External Matching and Efficiency.....	10
1.5	Thesis Outline.....	11
2	The Spiralpole	13
2.1	Antenna Description	13
2.2	Similar Designs	14
2.3	Analytical Model: Linear First Resonance Approximate	15
2.4	Analytical Model: Resonant Length Approximate	16
3	Bandwidth, Q and Minimum Bounding Sphere for ESAs.....	19
3.1	Definition of Bandwidth and Q	19
3.2	Spiralpole Minimum Bounding Sphere	20
4	The $Q - kr$ Limit.....	22
4.1	Absolute Limit: Chu Approach	22
4.2	Absolute Limit: McLean approach	27
5	Results:.....	32
5.1	Performance Evaluation Methodology.....	33
5.2	Ansoft HFSS Spiralpole Model.....	35
5.3	Simulated and Analytical Results: 3,4,5 and 6 Turns Spiralpoles.....	38
5.3.1	3 Turns Spiralpole Results	40
5.3.2	4 Turns Spiralpole	45
5.3.3	5 Turn Spiralpole	51
5.3.4	6 Turn Spiralpole	56
6	Hardware Prototype	62
7	Conclusion.....	64
8	Appendix A: MATLAB Codes	66
9	Appendix B: Dipole H – Plane pattern discrepancy in Ansoft HFSS	70
9.1.1	Model 1	70
9.1.2	Model 2	72
10	Appendix C: Disk – dipole hybrid antenna results	75
11	Bibliography	77

1 Introduction

Wireless electronics in today's world have pervaded our lives so immensely that we cannot look around and not notice an electronic device that communicates wirelessly or has some form of wireless communication. From radios, televisions and cell-phones to three-dimensional wireless tracking, wireless-power charging mats and wireless temperature monitoring systems all make use of the radio spectrum for sending and receiving information in some way. For the everyday observer it is impressive to see such intricate, accurate and elegant devices. It is easy to appreciate all the visual aesthetics and tangible utility that such inventions provide. However, it is not so easy to appreciate the most integral part of a system that allows for wireless communications; the antenna.

James Clerk Maxwell delivered his *Treatise* [1] in 1873 and this was one of the first authoritative work on electricity and magnetism that considered radiation of electromagnetic waves. Visionaries such as Marconi and Hertz demonstrated the utility of antenna radiators with experiments done in the late eighteenth century. Heinrich Hertz experimented with wireless propagation and antennas by using an inductive coil to drive a spark generator. The sparks from this generator created electromagnetic waves that were received by a loop antenna. Marconi established communication links over the atlantic [2] by using a conductive pole connected with a set of cables that looked like a tent as an antenna. Even earlier, Micheal Faraday stumbled upon electromagnetic induction, where a changing magnetic field caused deflections on a Galvanometer. An interesting observation was made by Professor Joseph Henry, a Professor of Natural Philosophy at Princeton University in 1842 [3]. He created sparks on a closed loop wire and was able to detect these sparks in a room that was 30ft below where the wire was sparked. He also set up a wire running from the roof of his house to his study room where he could detect lightning flashes that were up to 8 miles away.

The art of antenna design is such that the complexity of the problem increases very drastically with a slight increase in complexity of the operational scenario. Our understanding of antenna radiators has come a long way since these early pioneers, and thanks to the power of today's computers we can solve large order differential and integral equations using numerical methods with significant accuracy [4] in order to solve antenna problems. Nonetheless, the design and construction of antennas is not very simple. It requires patience, a strong mathematical background and substantial understanding of electromagnetic field theory. Antennas are natural electric or magnetic resonators. They emanate electromagnetic energy due to resonance conditions or standing waves developing on the body of the antenna due to a certain source excitation. An simple analogy is that of a flute: when air is blown through the flute at the right rate (excitation at a certain frequency), the longitudinal waves in air bounce back and forth inside the flute in such a way that they reinforce each other to establish *standing waves*. The characteristics of these standing waves will depend on the structural features of the flute, such as the length and the cross section. Similarly, an antenna's radiation characteristics primarily depend on structure of the antenna. Of course, material properties matter as well but antenna geometry dominates design. There are many classes of antennas, such as patch antennas dielectric resonators, wire antennas, loop antennas, frequency independent antennas and antenna arrays to name just a few. This thesis, however, is geared towards a special category of antennas called the *electrically small antenna*. Electrically small antennas are termed as such due to their size, as the name implies. The primary feature of electrically small antennas is that they are not naturally resonant at the operational frequency. A naturally resonant antenna at a certain frequency, just like any naturally resonant structure, has its resonant dimension (along which the standing waves are established) vary inversely in length as the operational frequency. In other words as the frequency increases, the smaller that the length of the dimension supporting the resonance becomes. Electrical length is measured in radians, and is a product of wavenumber and length

$$k = \frac{2\pi}{\lambda} = \frac{\omega}{c_0} \quad (1)$$

$$kl = \frac{2\pi}{\lambda} \times l$$

where λ is the wavelength at the operating frequency and l is the length in the direction of wave travel. ω is the angular frequency and c_0 is the speed of electromagnetic waves in vacuum. Electrically small antennas are operated at frequencies that are below the first natural resonance frequency. The operating wavelength is significantly smaller than the resonant length of the antenna. In other words, these antennas are operated at small values of electrical length. In order to do this, the antenna must be brought to resonance by some method. Generally, this has been done by using passive matching elements, either by lumped or distributed capacitances or inductances.

This section will provide a brief introduction on electrically small antennas and why there is a need for them. A brief introduction to antenna analysis and radiation in view of Maxwell's Equations will also be provided. The design presented is a modification of an electrically small dipole, a hybrid between a dipole antenna and spiral antenna called the Spiralpole. The Spiralpole negates the need for a matching network to bring it to resonance due to its structural modification. The antenna performance is compared to that of an equivalent electrically small dipole and is seen to outperform it in terms of Q for $ka \leq 0.5$ where a is the radius of a sphere that completely and minimally encloses the antenna. The antenna structure is a hybrid between a spiral antenna and one wing of a dipole antenna. It can be tuned by varying the length of the spiral that adds an inductive reactance to the feedpoint impedance.

1.1 Motivation

Electrically small antennas are usually employed in systems where the size of the antenna is critically small and the operating frequency is much lower than the first resonance of the antenna. When the maximum dimension of the antenna needs to be smaller than its operating wavelength, the antenna must be tuned to resonance somehow. When tuned, the resonance that is generated is usually narrowband. Some antenna designs are more narrowband than others. Structural modifications and design enhancements can improve this bandwidth. Electrically small antennas can find use in many commercial and military applications [5]. The reduced size is particularly attractive and can mean reduced visibility of the antenna on military vehicles, conformity for small electronics devices reduced risk of damage due to collision. The electrically small antenna is also becoming popular for use in mobile TV [6] reception on cellular phones. The UHF TV bands at 470 MHz-860MHz require that the antennas be electrically small. Another important and emerging use of electrically small antennas is in the domain of wireless temperature monitoring [7]. The wireless temperature monitoring system employs the RFID technique using patented Surface Acoustic Wave technology. The system consists of a transmitting reader that sends wireless signals to the temperature sensing unit. The sensing unit is passive and is powered by the transmitted signal itself. The receiving unit quite often needs to be physically small due to size restrictions of vendors. This means that the antenna employed by these devices need to be electrically small.

The major obstacle facing electrically small antennas is that of matching efficiency [8] [9]. Matching networks are usually constructed using lumped capacitors and inductors either static or variable. However, these inductors and capacitors are lossy and contribute to the reduction of the efficiency of the overall system. This can affect the realized gain of the antenna and lead to a degradation of performance. In addition, matching using simple lumped elements usually results in a narrowband match. It is thus necessary for antenna designers to design self resonant electrically small

antennas. The spiralpole antenna presented in this thesis overcomes the difficulty of reduced matching efficiency because it is self resonant and can be tuned to different frequencies by varying the length of the spiral.

1.2 Electrically Small Antennas

An electrically small antenna is defined as an antenna whose maximum dimension is less than $\frac{\lambda}{2}$ for dipoles and their likes, $\frac{\lambda}{4}$ for monopoles and monopole like antennas and $\frac{\lambda}{3}$ for loop and loop like antennas [10]. These antennas are usually non resonant and made to resonate by matching, but they can also be self resonant by structure inductive or capacitive loading. These antennas show low radiation resistance at the operating band, thus having the need for impedance transformers for source matching. Electrically small antennas are also characterized by bandwidth and gain tradeoff for a particular electrical size of the antenna. A fundamental limitation of electrically small antennas has been derived by Chu [11] and later confirmed by other authors [12]. A universal limitation on bandwidth by external matching has been developed by Fano over 50 years ago [13]. Hansen [10] explicates that an antenna is a one port network, and using many additional matching networks provide a limiting increase of half power bandwidth by a factor of 3.2. However, any more than two matching networks will provide diminishing returns. Therefore it is important to make use of good antenna design in electrically small antennas to maximize performance. The main kind of electrically small antennas are dipoles, monopoles and patch antennas. These can be optimized using clever design modifications such as [14]. In this design modification, the antenna is made to use the spherical volume efficiently, thus increase bandwidth and lower Q. It is also shown that the antenna can be made self resonant by increasing the wire lengths and sacrificing antenna efficiency to eliminate the antenna reactance at a specified frequency.

There have been clever designs that at first sight seem promising, but in reality do not work well. Hansen [10] describes a few of these. For example, the cross wound toroidal helix antenna has low radiation resistance and tight mechanical tolerance, and is relatively narrowband. The transmission line antenna, which is a wire $\frac{\lambda}{4}$ folded monopole exhibits low radiation resistance due to its low height. Other designs have been made where clever modifications are thought to improve the antennas bandwidth beyond the Chu limit. The evaluation of these antennas was either not carried out correctly or in a fair, impartial manner, or the analysis done was too simple [10]. To date, the fundamental Chu limit has not been surpassed by any ideal resonant or non resonant antenna with passive matching elements. A practical antenna designer's motive should thus be to attempt to come as close as possible to this fundamental limit. Incorporating ferrite core - almost ideal inductors and using non Foster-matching circuits will enable designers to come close to these limits in addition to efficient use of the spherical volume enclosing an antenna by good design.

1.3 Radiation of a small linear current element: Maxwell's Equations

In this section, the fields for a small, finite length dipole antenna will be derived since this is the most simple antenna radiator. Solutions presented in this section will be used later in this thesis. It is customary to start from Maxwell's equations in free space:

$$\begin{aligned}
 \epsilon_0 \frac{\partial \vec{E}}{\partial t} &= \nabla \times \vec{H} - \vec{J} \\
 \mu_0 \frac{\partial \vec{H}}{\partial t} &= -\nabla \times \vec{E} \\
 \nabla \cdot \epsilon_0 \vec{E} &= \rho \\
 \nabla \cdot \mu_0 \vec{H} &= 0 \\
 \frac{\partial \rho}{\partial t} + \nabla \cdot \vec{J} &= 0
 \end{aligned} \tag{2}$$

where \vec{E} is the electric field vector, \vec{H} is the magnetic field vector, ρ is the charge density, \vec{J} is the current density vector, ϵ_0 and μ_0 are the electric permittivity and magnetic permeability of free space respectively.

The magnetic field vector can be written as follows since the curl of any divergence is zero:

$$\mu_0 \vec{H} = \nabla \times \vec{A} \quad (3)$$

where \vec{A} is the magnetic vector potential. Now, we substitute (2) into the first equation in equation (1):

$$\nabla \left[\vec{E} + \frac{\partial \vec{A}}{\partial t} \right] = 0 \quad (4)$$

From here the general solution for the electric field is :

$$\vec{E} = -\nabla\phi - \frac{\partial \vec{A}}{\partial t} \quad (5)$$

where ϕ is the electric scalar potential. This term can be included in the solution since taking the curl of equation (4) and rearranging will give back (3) . Applying the curl to both sides of (2):

$$\mu_0 \nabla \times \vec{H} = \nabla \times \nabla \times \vec{A} = \nabla(\nabla \cdot \vec{A}) - \nabla^2 \vec{A} \quad (6)$$

The curl of the magnetic field relates the electric field by the first equation in (1). Substituting this into (5):

$$\epsilon_0 \mu_0 \frac{\partial \vec{E}}{\partial t} = \nabla(\nabla \cdot \vec{A}) - \nabla^2 \vec{A} - \mu_0 \vec{J} \quad (7)$$

and substituting (4) into (6) gives:

$$\nabla^2 \vec{A} - \epsilon_0 \mu_0 \frac{\partial^2 \vec{A}}{\partial t^2} = -\mu_0 \vec{J} + [\nabla(\nabla \cdot \vec{A}) + \epsilon_0 \mu_0 \nabla \frac{\partial \phi}{\partial t}] \quad (8)$$

In order to simplify (7), a gauge condition will be applied. This particular gauge condition is the Lorentz gauge. A gauge condition is simply an expression that aids in removing redundancies in field expressions.

The Lorentz gauge is:

$$\frac{\partial \phi}{\partial t} = -\frac{1}{\epsilon_0 \mu_0} \nabla \cdot \vec{A} \quad (9)$$

Substitution of (8) into (7) yields:

$$\nabla^2 \vec{A} - \epsilon_0 \mu_0 \frac{\partial^2 \vec{A}}{\partial t^2} = -\mu_0 \vec{J} \quad (10)$$

or in phasor form

$$\nabla^2 \vec{A} - k^2 \vec{A} = -\mu_0 \vec{J} \quad (11)$$

Equation (11) is the Helmholtz wave equation for a travelling wave. The solution to (11) yields an integral equation in space. Assuming, the source is defined (the antenna with excitation), solving for the magnetic vector potential yields in phasor form:

$$\vec{A}(\vec{r}) = \mu_0 \iiint \frac{e^{-jk|\vec{r}-\vec{r}'|}}{4\pi|\vec{r}-\vec{r}'|} \vec{J}(\vec{r}') d\vec{r}' \quad (12)$$

where \vec{r} and \vec{r}' are the observation point vector and source position vector respectively. They are also depicted in Figure 1 below. Note that the integration is with respect to the source position vector.

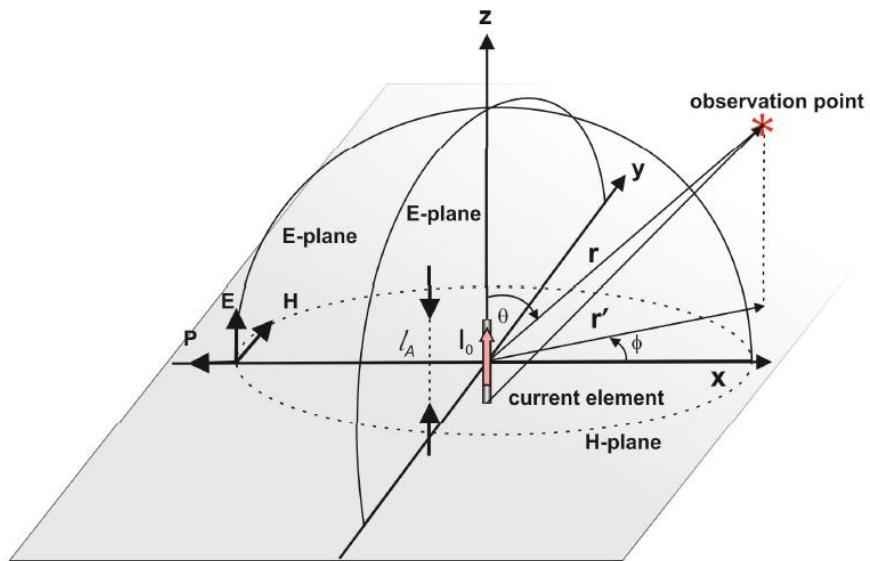


Figure 1: Coordinate system showing linear current element with far field components in E and H planes

Solving the above integral equation for a linear current element, or a small dipole will give us the field expressions. The following assumptions about the linear current element shown in Figure 1 will aid in solving the integral equation for an infinitesimally small dipole:

- The length of the current element $l_a \rightarrow 0$
- The radius of the cylindrical cross section $\rightarrow 0$
- The current distribution is such that it can be thought of as constant
- The current density vector is therefore $\vec{J}(\vec{r}) = \delta(x)\delta(y)I_0\hat{z}$

The integral, after these assumptions, now becomes:

$$A(\vec{r}) = \mu_0 I_0 \hat{z} \int_{-\frac{l_a}{2}}^{\frac{l_a}{2}} \frac{e^{-jk|r-z'|}}{4\pi|r-z'|} dz'$$

as l_a and $z' \rightarrow 0$

(13)

$$= \hat{z} \frac{\mu_0 I_0 l_a}{4\pi|\vec{r}|} e^{-jk|\vec{r}|}$$

This is the solution for the vector potential in Cartesian coordinates. Converting this to spherical coordinates one obtains:

$$\begin{aligned} A_r &= \hat{r} \frac{\mu_0 I_0 l_a}{4\pi|\vec{r}|} e^{-jk|\vec{r}|} \cos(\theta) \\ A_\theta &= \hat{\theta} \frac{-\mu_0 I_0 l_a}{4\pi|\vec{r}|} e^{-jk|\vec{r}|} \sin(\theta) \\ A_\phi &= 0 \end{aligned} \tag{14}$$

We have obtained the vector potential for an infinitesimally small linear current element (dipole) in spherical coordinates. The magnetic field vector can now be obtained from (2) as:

$$\begin{aligned}\vec{H} &= \nabla \times \vec{A} \\ \vec{H}_\phi &= \hat{\phi} \frac{jkI_0 l_a \sin(\theta)}{4\pi r} \left[1 + \frac{1}{jkr} \right] e^{-jkr} \\ \vec{H}_\theta &= 0 \\ \vec{H}_r &= 0\end{aligned}\tag{15}$$

where $|\vec{r}|$ is replaced by r . For the electric field, the second equation in (2) can be used. However, the current density vector is now zero since there are sources in free space. Therefore, the electric field vector is now:

$$\begin{aligned}\vec{E} &= \frac{1}{j\omega\epsilon_0} \nabla \times \vec{H} \\ \vec{E}_r &= \hat{r} \frac{\eta I_0 l_a \cos(\theta)}{2\pi r^2} \left[1 + \frac{1}{jkr} \right] e^{-jkr} \\ \vec{E}_\theta &= \hat{\theta} \frac{j\eta k I_0 l_a \sin(\theta)}{4\pi r} \left[1 + \frac{1}{jkr} - \frac{1}{k^2 r^2} \right] e^{-jkr} \\ \vec{E}_\phi &= 0\end{aligned}\tag{16}$$

The above equations describe the field patterns of an infinitesimally small linear current element (dipole) completely. The electric and magnetic field solutions show a travelling wave behavior, and thus radiating fields are implied. These field solutions will be important in our derivation of the absolute Q-ka limit for small antennas.

1.4 External Matching and Efficiency

Antenna matching is an important factor for small antennas because of their non-resonant nature. The electrically small antenna generally needs to be matched with an inductor or a capacitor in series to

bring it to resonance. However, due to ohmic losses in the matching elements and the antenna itself, matching efficiency becomes very low. In addition, the small antenna reactance at the operating frequency is usually very large, so large capacitances or inductances are needed to perform matching. An example taken from [15] will explain this further.

A 300mm long dipole antenna is chosen. This dipole antenna is seen to have an impedance of $1.96 - j1758$ ohms. The reactance is large and capacitive. An inductor is used to cancel the capacitive reactance of the antenna. A capacitor is used in parallel to this combination to transform the real part of the impedance to match it to the source. In order to cancel the reactance the inductor has a value of $L = 2.8\mu H$ at 100 MHz. An inductor's Q generally ranges from 50 to 200. Assuming the inductor's Q value is about 100 at 100MHz, the Q of the inductor at 100 MHz is given by:

$$Q = \frac{|X_L|}{R_L} \quad (17)$$

where Q_L is the Q of the inductor and X_L is the reactance of the inductor And so the resistive part of the impedance is about 17.58 Ohms. This resistance is added together in series with the antennas impedance. The power lost in delivering power from the source to the antenna now is

$$20 \log\left(\frac{1.96}{(1.96 + 17.58)}\right) = -20dB \quad (18)$$

As per the calculation, most of the power delivered from the load is dissipated in the inductors. Very little power is delivered to the antenna for radiation. In order to mitigate this problem, electrically small antennas are designed in such a way that the antenna is naturally resonant and does not require matching.

1.5 Thesis Outline

The structure of the remainder of this thesis is as follows. The spiralpole antenna will be presented with its structure and geometry in Chapter 2. Similar antenna designs will also be presented where the

respective authors have designed similar antennas, but not in the configuration that is presented here. Approximate models that predict the resonance frequency of the spiralpole antenna will be presented, including a resonant length model and an impedance based model. In Chapter 3, the bandwidth and Q definitions used in the evaluation of small antennas will be presented. The minimum bounding sphere for the spiralpole antenna and the equations governing the spheres dimensions will be presented as well. Chapter 4 details the derivation of the absolute $Q - kr$ limit of an electrically small antenna. This limit is important since it is a benchmark used to see evaluate the bandwidth performance of the electrically small antenna. Results of the simulation and comparisons of performance of the electrically small dipole and spiralpole antennas will be presented in Chapter 5. Hardware prototypes will be described in Chapter 6, along with measured results of a food probe that is designed as a spiralpole antenna. Section 7 concludes with final remarks and future work.

2 The Spiralpole

The spiralpole design was conceived when new solutions were sought for the wireless temperature monitoring systems as described in [7]. The problem was to enclose an antenna inside the protective casing shown in Figure 2 such that the device could work at 433 MHz. In this section the antenna geometry will be described and similar designs will be investigated. Incorporating the spiral as the second wing of the dipole was a good choice given the planar nature of its layout. Two analytical models for the spiralpole antenna that approximate the center frequency of the first series resonance will be presented in this section.

2.1 Antenna Description

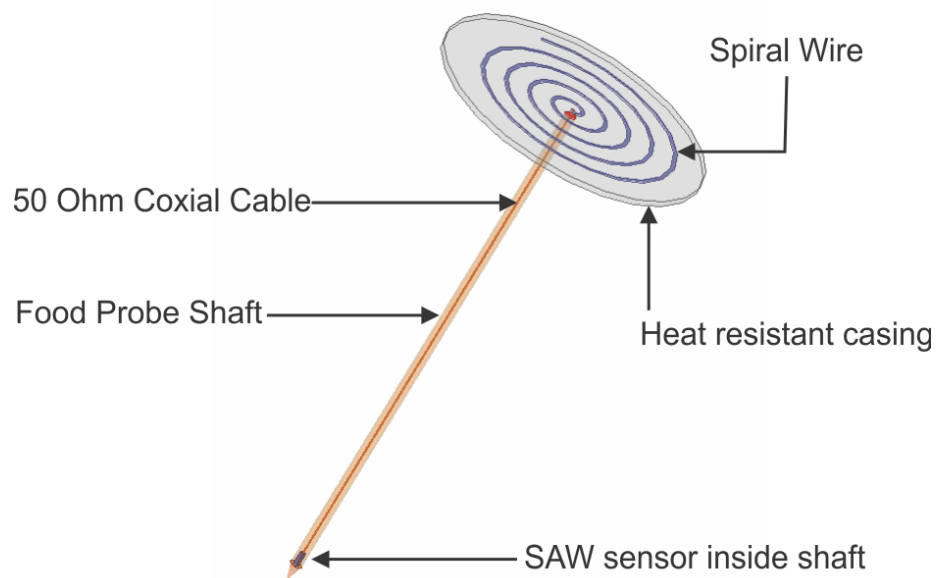


Figure 2: Spiralpole antenna incorporated into wireless food probe design

Figure 2 shows the geometry of the spiralpole antenna as first conceived in context of food probe application. The first wing of the antenna is the conductive food probe shaft. The second wing of the antenna is the Archimedian spiral wire enclosed in the heat resistant casing. The antenna is fed by a 50

Ohm shielded coaxial cable that is connected to a SAW sensor inside the shaft. The SAW sensor acts as the feed and the body of the SAW sensor is in contact with the inside of the shaft as the ground. The inner conductor of the coaxial cable is soldered on to the positive terminal of the SAW sensor. The other end of the inner conductor essentially extends into the spiral at the top of the antenna inside the heat resistant enclosure. Therefore, the antenna is somewhat like a dipole but one wing is modified into a spiral wire. This allows a much longer overall length of the antenna. In addition, the spiral acts like an inductor hybridized with the second dipole wing. This is similar to a matching inductor in series with the dipole antenna.

2.2 Similar Designs

There are a number of designs that incorporate the Spiral antenna. The spiral antenna theory was qualitatively presented in [16]. The theory is based on a current sheet approximation that considers currents on the spiral being in phase at certain locations creating radiation. In [17], a planar rectangular one arm spiral over a dielectric substrate was investigated where the arm lengths are varied to enable beamforming. Another one arm spiral antenna with non uniform spacing between windings (similar to a logarithmic spiral) was investigated in [18]. The non uniform spacing allows for good impedance matching. This antenna is also fabricated on top of a dielectric substrate (FR4) and has a ground plane. It is designed for use in Wireless Body Area Networks, which is a very growing field currently. The antenna is designed for operation at 284 MHz. The use of dielectric, however, for electrically small antennas should be avoided since it can reduce the radiation resistance of the antenna itself. No empirical or analytical model of the antenna is provided. Other single arm designs are presented in [19] [20] [18] [21]. Most of these designs are for UWB applications and for beamforming either with a single antenna or an array. The design that is closest to the spiralpole is that presented in [22]. The author also calls the antenna the Spiral Dipole. The antenna in question comprises of a dipole and two spirals, each loading the end of the dipole wings. Although the design is similar, the antenna is self resonant at about 5.2 GHz and thus cannot be classified as electrically small.

2.3 Analytical Model: Linear First Resonance Approximate

The analytical first resonance model approximates the first series resonance by using the reactance of a dipole antenna with a spiral inductor in series. The well known impedance of a dipole antenna Z_a is given in [23] by:

$$Z_{dipole} = R_{dipole}(z) - j[120(\ln\left(\frac{l_{dipole}}{2a} - 1\right) \cot(z) - X_{dipole}(z)) \quad (19)$$

$$R_{dipole}(z) \approx -0.48787 + 7.3246z + 0.3963z^2 + 15.6131z^3$$

$$X_{dipole}(z) \approx -0.4456 + 17.0082z - 8.6793z^2 + 9.6031z^3$$

where l_{dipole} is the antenna length, $z = kl_{dipole}$ and a is the radius of the dipole wire. The above equation is valid for $0.05 \leq \frac{f_c}{f_{res}} \leq 1.2$ where f_c is the center frequency of the band being considered and f_{res} is the ideal half wavelength dipole resonant frequency.

The spiral inductance is given in [24]. Of the three inductance models presented, the *current sheet* approximation is used since this approximation allows for the circular spiral. The inductance is calculated based on the arithmetic mean distance and geometric mean distance between current sheets and the fact that orthogonal currents do not contribute to the mutual inductance of the spiral. The resulting expression is:

$$L_{gmd} = \frac{\mu n^2 d_{avg} c_1}{2} (\ln\left(\frac{c_2}{\rho}\right) + c_3 \rho + c_4 \rho^2) \quad (20)$$

where n is the number of turns, d_{avg} is the inner and outer diameter average, ρ is the fill ratio given by $\frac{d_{out} - d_{in}}{d_{out} + d_{in}}$ and c_1 , c_2 and c_3 are spiral layout dependent (square, hexagonal or circular) constants. The constants are 1, 2.46 0 and 0.2 respectively for our circular spiral.

With this expression, the spiralpole antenna's first order series resonance frequency can be approximated as the frequency at which the reactance goes to zero due to the matching inductor in series from:

$$X_{spiral} = X_{dipole} + j\omega L_{gmd} \quad (21)$$

where X_{spiral} is the approximated reactance of the spiralpole antenna. The addition of the spiral inductance to the regular dipole impedance implies a match with a series inductor. Note that this is a linear first order approximate. For the results presented in the results section, the antenna used to calculate the dipole impedance in our calculations is the fixed 150mm dipole used for our evaluation of the spiralpole. The spiral parameters used for the inductance calculation are changed according to each spiralpole configuration.

2.4 Analytical Model: Resonant Length Approximate

The resonant length model for approximating the spiralpole resonant frequency for a given configuration is based on the current distribution of the simulated spiralpole at resonance. The current distribution for a five turns spiralpole at resonance is shown in Figure 3 from the Ansoft HFSS simulation. The current density is almost zero at the ends of the spiralpole, and the distribution is somewhat like a dipole. This is the distribution for the first natural resonance for the spiralpole, and is half a wavelength long sinusoidally. Note that the scale used is a logarithmic scale. Based on this observation, the spiralpole's resonant frequency can be approximated using a resonant length model similar to that of a dipole antenna. It will be considered that the total length of the spiralpole antenna is half wavelength at resonance. However, as the results section will show, the prediction seems to be about 80 MHz off with every scenario. Thus in the model, the 80 MHz is subtracted. The resonant length model can be summarized as

$$f_c = \frac{c_0}{2(l_{shaft} + l_{spiral})} - 80\text{MHz} \quad (22)$$

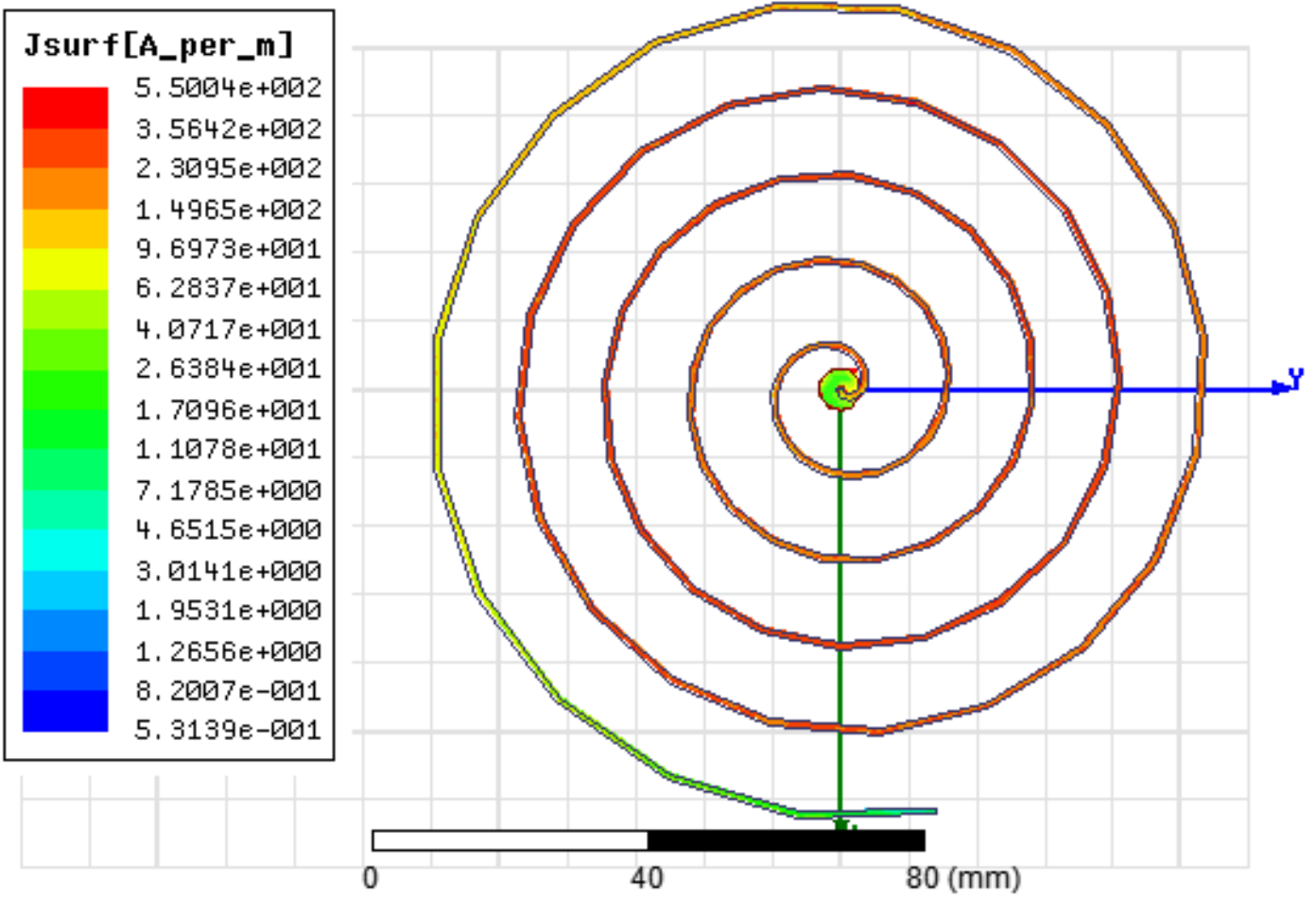


Figure 3: Current distribution at 96MHz (resonance) on a five turns Spiral

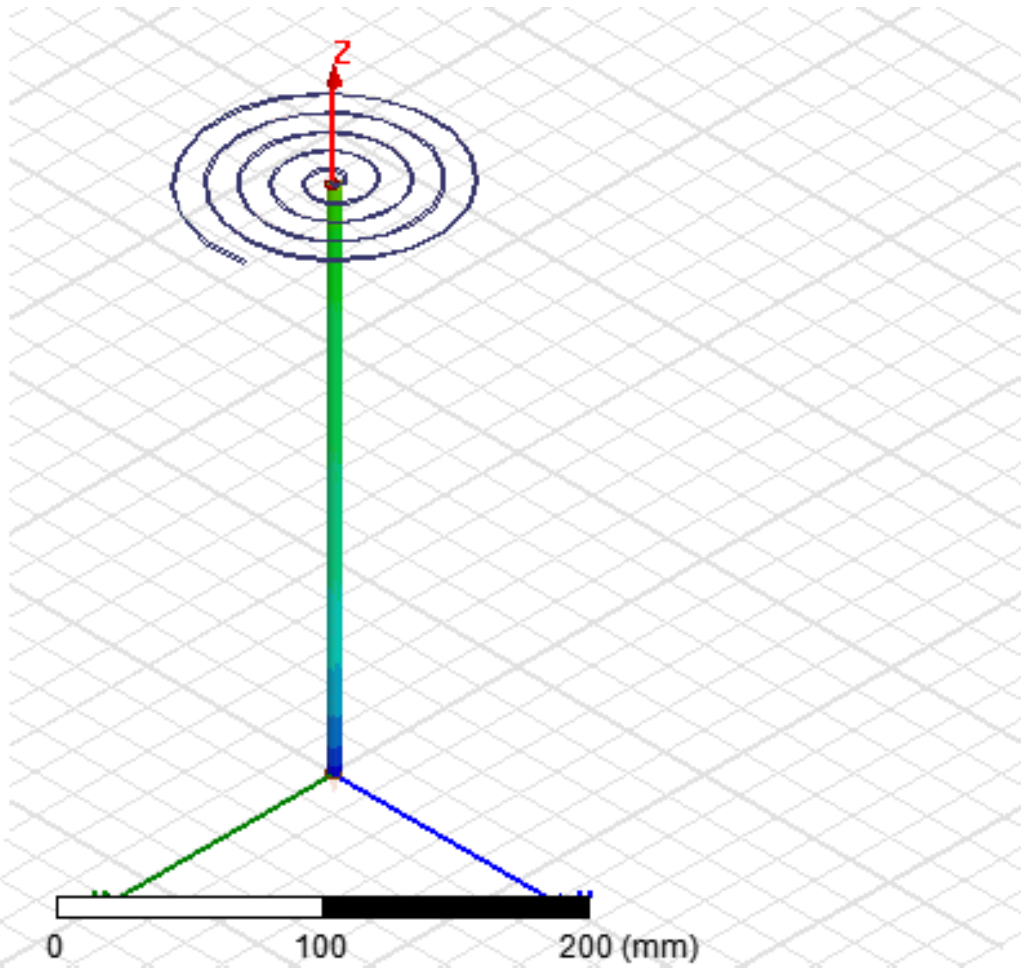
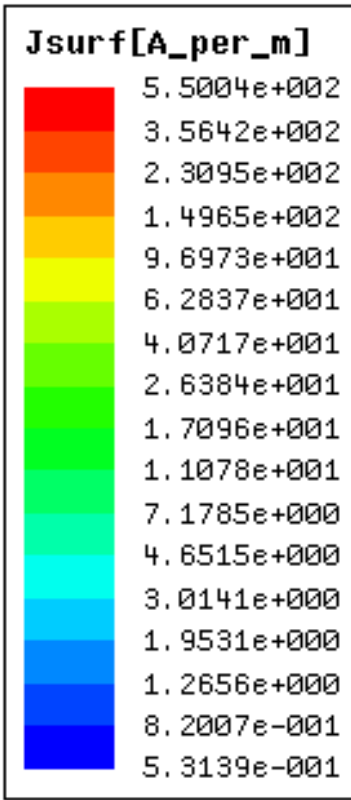


Figure 4: Current distribution on the shaft of the same five turns spiralpole at 96MHz (resonance)

Current density on the shaft also decays to zero at the end as expected. Of particular note however, is the magnitude of the current on the spiral. The spiral seems to have a higher current density overall than the shaft. Therefore, it can be concluded that the sinusoidal distribution is not evenly distributed as it is for a dipole antenna.

3 Bandwidth, Q and Minimum Bounding Sphere for ESAs

The bandwidth of a tuned antenna and its relation to Q for electrically small antennas will be presented here. These definitions are standard and are used in our methodology for evaluating the spiralpole against the dipole antenna. The standard definition of a tuned antenna bandwidth, or fractional VSWR bandwidth, will be described.

A simple derivation of the spiralpole dimensions that allow the antenna to fit inside a fixed bounding sphere will be provided. This will allow design constraints to be established in our Ansoft HFSS model such that, if the spiralpole dimensions are changed, the antenna will still fit inside the sphere fixed radius. Essentially, the idea is to allow both the spiralpole and dipole antennas to occupy the same volume and compare their performances. This method is in agreement with the Chu methodology for electrically small antennas [11].

3.1 Definition of Bandwidth and Q

The definition of bandwidth and Q of an electrically small antenna used in the evaluation of the spiralpole antenna and the dipole antenna are taken from [25]. The paper describes a universal definition for bandwidth and Q for any tuned electrically small antenna. The most suited bandwidth metric, as prescribed by the authors is the *fractional matched VSWR bandwidth*. This is the difference in frequencies on either side of the matching frequency at which the magnitude squared of the reflection coefficient is of a certain fixed value. The authors use the definition of the reflection coefficient and squared as a function of angular frequency, along with a Taylor's series expansion about the matching frequency to obtain an expression for the fractional matched VSWR bandwidth, given by

$$FBW_v(\omega_0) = \frac{\omega_+ - \omega_-}{\omega_0} \approx \frac{4\sqrt{\beta}R_0(\omega_0)}{\omega_0|Z'_0(\omega_0)|} \quad (23)$$

where ω_+ and ω_- are the two frequencies at which the FBW_v attains a certain value about the matching frequency ω_0 . $|Z'_0(\omega_0)|$ is the magnitude of the derivative of the **matched** impedance at the center frequency and $R_0(\omega_0)$ is the real part of this matched impedance. β is given by $\frac{\alpha}{1-\alpha}$ where α is the value that the FBW_v attains at either side of the matching frequency. α is chosen to be $\frac{1}{2}$.

The Q of a tuned antenna is defined as the ratio of the stored electric and magnetic energies at the resonance to the power radiated by the antenna per cycle at the resonant frequency. The Q for a tuned small antenna is given by

$$Q(\omega_0) \approx \frac{\omega_0}{2R_0(\omega_0)} |Z'_0(\omega_0)| \quad (24)$$

Comparing this to the expression for FBW_v , the Q is then related by

$$Q(\omega_0) = \frac{2\sqrt{\beta}}{FBW_v} \quad (25)$$

In our analysis, we find the FBW_v using $\alpha = \frac{1}{2}$ (-3dB) about the center frequency and then relate it to Q using the above expression.

3.2 Spiralpole Minimum Bounding Sphere

In order to perform a fair evaluation of the spiralpole antenna against the small dipole and generate the right $Q - kr$ curves, the spiralpole antenna must be enclosed in the same bounding volume as the small dipole. Given a fixed spherical volume the small dipole and spiralpole configurations should be bounded completely and minimally by this spherical volume. It is desired to be able to change the physical dimensions of the spiralpole and still be able to fit it inside the same fixed spherical volume. For example, if the radius of the spiral wing is increased then height of the vertical wing should be decreased and vice versa. Figure 5 shows the spiralpole inside one such minimal bounding sphere. r is

the fixed radius of the sphere. z is the height of the shaft and x_0 is the final radius of the spiral itself. We can write a simple Pythagorean relationship with these quantities in this configuration. This allows us to change one parameter, say the probe height and the sphere radius is fixed so the spiral radius will now be changed as well.

$$\begin{aligned}
 r^2 &= x_0^2 + (z - r)^2 \\
 r^2 &= x_0^2 + z^2 - 2rz + r^2 \\
 2rz &= x_0^2 + z^2 \\
 r &= \frac{1}{2} \left(\frac{x_0^2}{z} + z \right)
 \end{aligned}
 \tag{26}$$

Note that when $z = x_0$ then $r = x_0 = z$. This equation is programmed into the Ansoft\ANSYS HFSS base model and 3,4,5 and 6 turn spiralpole antennas that fit in a fixed 150mm radius sphere are created.

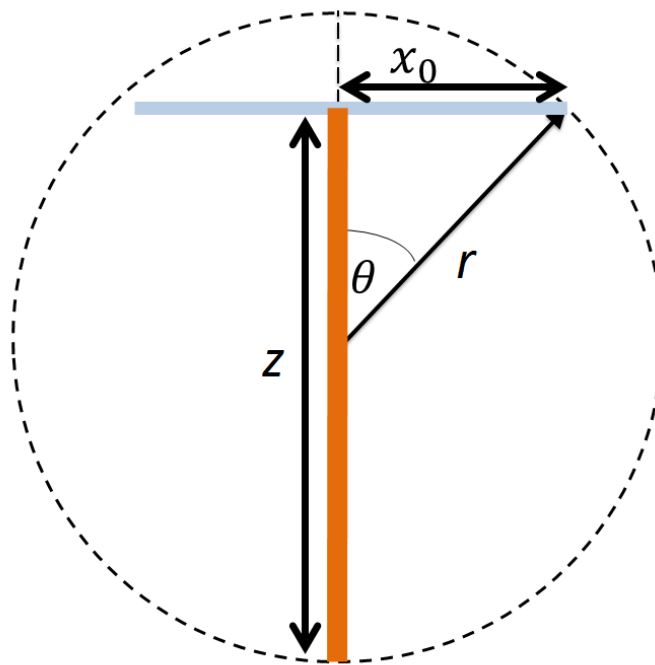


Figure 5: Cross section of a given spiralpole configuration in its minimum bounding sphere

4 The $Q - kr$ Limit

In his paper [11] Chu devises a methodology to determine the fundamental limitations of small antennas using spherical mode theory for an arbitrary antenna enclosed in a spherical volume. In this section, Chu's fundamental limit will be summarized and his derivation succinctly presented. In 1997, another paper [12] was published by Mclean where a fields approach was taken to calculate the absolute limit for antenna Q in terms of electrical length. This approach will also be presented in this section. The absolute $Q - kr$ limit is of importance since it can be used as a benchmark to compare a small antenna's performance to this limit. Of particular interest is the electrical length range $kr \leq 0.5$ as this is where the antenna is generally considered electrically small.

4.1 Absolute Limit: Chu Approach

In 1948, Chu published a paper that attempts to find a fundamental limitation to omnidirectional, small antennas. A few authors around the time have realized on paper current distributions that produce higher gain than expected for antennas of a certain size. However, this meant that high currents and thus high amount of stored energy would be present on the antenna. Therefore, there had to be some sort of trade off between bandwidth and gain of an antenna. Chu set out to find the optimum 'operating point' of given antenna given this trade off. He starts out by enclosing an arbitrary antenna structure or source distribution inside a sphere. The antenna's maximum dimension can be as large as the diameter of the sphere or less. He then uses omnidirectional field expressions derived by Stratton [26] in the form of orthogonal spherical vector wave functions. The fields outside of the sphere do not uniquely determine the source distribution or antenna structure inside the sphere that can give rise to such fields [11]. To simplify the problem, a vertically polarized radiator or dipole antenna is used and it is assumed that there is no reactive energy stored within the sphere.

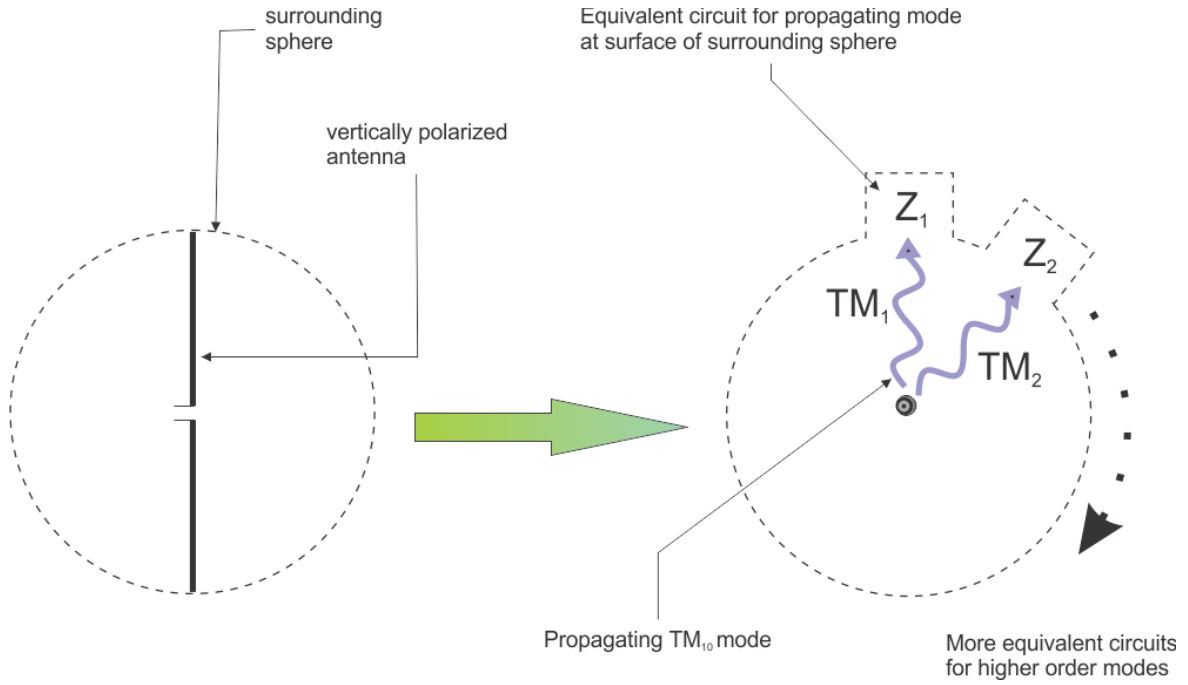


Figure 6: Chu's transformation of a wave problem in space to an equivalent circuit problem at the surface of the sphere. The antenna structure and current distribution is assumed to be arbitrary and thus the fields expressed in terms of TM_{n0} spherical modes

Figure 6 shows a vertically polarized antenna (dipole) enclosed in a sphere. The exact antenna structure is assumed arbitrary and therefore the fields of the vertically polarized radiator are written in terms of TM_{n0} spherical modes as [11]:

$$\begin{aligned}
 H_{\phi} &= \sum_n A_n P_n^l \cos(\theta) h_n(kr) \\
 E_r &= -j \sqrt{\frac{\mu}{\epsilon}} \sum_n A_n n(n+1) P_n \cos(\theta) \frac{h_n(kr)}{kr} \\
 E_{\theta} &= j \sqrt{\frac{\mu}{\epsilon}} \sum_n A_n P_n^l \cos(\theta) \frac{1}{kr} \frac{d}{dr} [r h_n(kr)]
 \end{aligned} \tag{27}$$

where

$h_n(kr) \rightarrow$ spherical hankel function of the second kind

$P_n^l \rightarrow$ associated legendre polynomial of order n

$P_n \rightarrow$ legendre polynomial of order n

$A_n \rightarrow$ coefficients of field solution. These coefficients are found from boundary conditions

k is the wavenumber previously defined and r is the radius of an enclosing sphere. The radial electric field can be seen to decay much more quickly as $r \rightarrow \infty$. The following assumptions are made about the antenna enclosed in the sphere:

- No electric or magnetic energy is stored within the sphere, but only outside of it.
- The antenna is lossless
- The only form of electric energy or magnetic energy found inside the sphere will be that which is radiating outwards from the antenna

Based on these assumptions, the focus is then on the surface of the sphere. The total instantaneous power carried by the fields at the surface of the sphere is obtained by integrating the complex Poynting vector over the surface of the sphere S :

$$\begin{aligned}
 P(r) &= \iint_S \vec{E} \times \vec{H}^* \cdot d\vec{S} = \iint_S (\vec{E}_\theta + \vec{E}_r) \times \vec{H}_\phi^* \cdot d\vec{S} \\
 &= \iint_S (\vec{E}_\theta \times \vec{H}_\phi^* + \vec{E}_r \times \vec{H}_\phi^*) \cdot d\vec{S} \\
 &= \iint_S \vec{E}_\theta \times \vec{H}_\phi^* \cdot d\vec{S} \\
 &= j2\pi \sqrt{\frac{\mu}{\epsilon}} \sum_n \frac{2n(n+1)}{2n+1} kr h_n(kr) [kr h_n(kr)]'
 \end{aligned} \tag{28}$$

From here, the problem is transformed from a spatial to a 'circuit' problem by

- Recognizing that each orthogonal spherical mode has a power associated with it that is carried out of the sphere.
- Defining voltage and current expressions proportional to the electric and magnetic field expressions at the surface of the sphere

The voltage and current of each mode at the surface of the sphere are then defined as

$$V_n = \sqrt[4]{\frac{\mu}{\epsilon}} \frac{A_n}{k} \sqrt{4\pi \frac{n(n+1)}{2n+1} j[krh_n(kr)]'} \quad (29)$$

$$I_n = \sqrt[4]{\frac{\mu}{\epsilon}} \frac{A_n}{k} \sqrt{4\pi \frac{n(n+1)}{2n+1} krh(kr)}$$

The impedance of each mode is then given by

$$Z_n = \frac{V_n}{I_n} = j \frac{[krh_n(kr)]'}{krh_n(kr)} \quad (30)$$

Equation (29) reveals that the impedance of each mode is essentially a Ricatti-Bessel function in log-derivative form. The Ricatti-Bessel functions in log derivative form are shown in [27] to follow the recurrence relation

$$C_n = -\frac{n}{x} + \frac{1}{\frac{n}{x} - C_{n-1}} \quad (31)$$

This relationship can now be expanded as a continued fraction

$$C_{n-1} = -\frac{n-1}{x} + \frac{1}{\frac{(n-1)}{x} - C_{n-2}} \quad (32)$$

Thus ,

$$C_n = -\frac{n}{x} + \frac{1}{\frac{2n-1}{x} - \frac{1}{\frac{2n-3}{x} - \dots}}$$

The impedance of each spherical mode can therefore also be written as

$$Z_n = j \left[-\frac{n}{kr} + \frac{1}{\frac{2n-1}{kr} - \frac{1}{\frac{2n-3}{kr} - \dots}} \right] \quad (33)$$

Or

$$Z_n = \frac{n}{jkr} + \frac{1}{\frac{2n-1}{jkr} + \frac{1}{\frac{2n-3}{jkr} - \dots}}$$

From this, it can be seen that the wave impedance of the spherical modes at the surface can be interpreted as a cascaded ladder network of series capacitors and shunt inductors. Figure 7

below from [11] depict this network. For the lowest mode, TM_{10} the circuit simple becomes that shown in Figure 8.

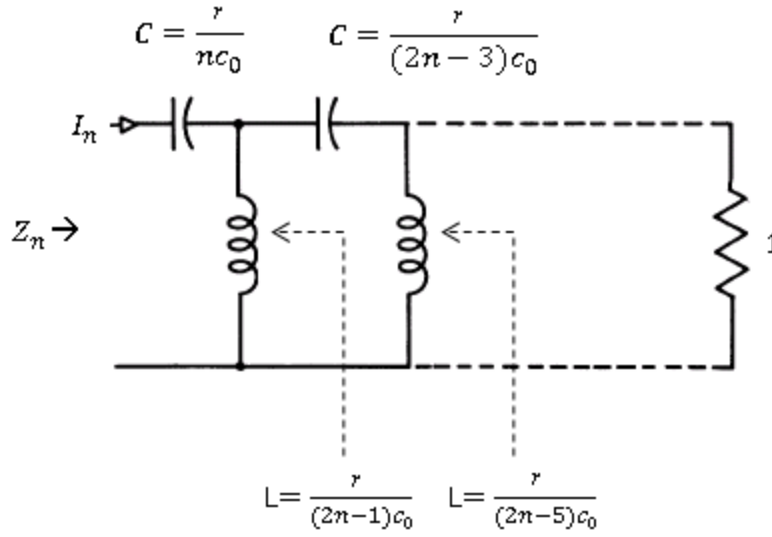


Figure 7: Original ladder network depiction from Chu's paper

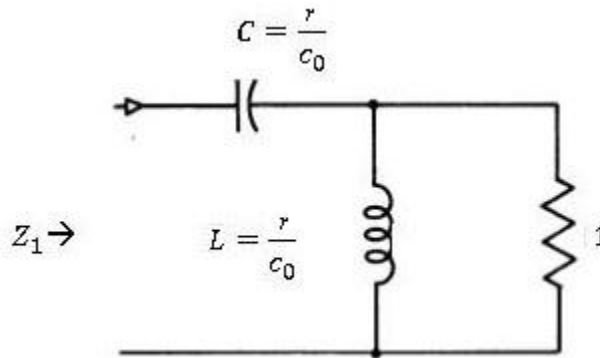


Figure 8: Equivalent circuit of lowest TM_{10} mode. This is also the equivalent circuit for the radiation given by an infinitesimally small dipole

For $n = 1$, the impedance is then

$$\begin{aligned}
 Z_1 &= \frac{1}{jkr} + \frac{1}{\frac{1}{jkr} + 1} = \frac{1}{jkr} + \frac{jkr}{1 + jkr} \\
 &= \frac{1}{jkr} + \frac{jkr(1 - jkr)}{1 + (kr)^2} = \frac{1}{jkr} + \frac{jkr + (kr)^2}{1 + (kr)^2}
 \end{aligned} \tag{34}$$

Now, assuming the stored energy is primarily electric in nature in consideration of an electric dipole, the Q is calculated as

$$\begin{aligned}
Q_{min} &= \frac{|X_c|}{\text{Re}\{Z_1\}} = \frac{1}{kr} \times \frac{1 + (kr)^2}{(kr)^2} \\
&= \frac{1}{kr} + \frac{1}{(kr)^3}
\end{aligned} \tag{35}$$

4.2 Absolute Limit: McLean approach

Chu's derivation had employed the equivalent circuit model for the wave impedance at the surface of the sphere for each orthogonal spherical mode. In [12] a fields approach is take to derive the absolute $Q - kR$ limit. This will briefly be presented in this section. The tuned antenna Q is defined in the paper as

$$\begin{aligned}
Q &= \frac{2\omega W_e}{P_{rad}} & W_e > W_m \\
Q &= \frac{2\omega W_m}{P_{rad}} & W_m > W_e
\end{aligned} \tag{36}$$

An infinitesimally small electric dipole is considered therefore $W_e > W_m$. The electric and magnetic fields of a n infinitesimally small dipole were derived in Chapter 1. These fields will now be used to derive the Chu limit. Assuming an infinitesimally small electric dipole, the first definition in (38) is used. Therefore, the non-radiating or stored energy is primarily electric. First, the field equations for the infinitesimally small electric dipole are normalized and rearranged

$$\vec{E}_r = \hat{r} \frac{\eta I_0 l_a \cos(\theta)}{2\pi r^2} \left[1 + \frac{1}{jkr} \right] e^{-jkr} \tag{37}$$

normalize by $-\frac{j\eta I_0 l_a k}{4\pi}$

$$\begin{aligned}
&\rightarrow \hat{r} \frac{\eta}{k} \frac{2 \cos(\theta) e^{-jkr}}{-jr^2} \left[1 + \frac{1}{jkr} \right] \\
&= \hat{r} \frac{2}{\omega\epsilon} \cos(\theta) e^{-jkr} \left[\frac{1}{-jr^2} + \frac{1}{kr^3} \right]
\end{aligned} \tag{38}$$

$$= \hat{r} \frac{2}{\omega \epsilon} \cos(\theta) e^{-jkr} \left[\frac{j}{r^2} + \frac{1}{kr^3} \right]$$

where we have made the substitution $\frac{\eta}{k} = \frac{1}{\omega \epsilon}$. The θ component of the electric field can be also

rearranged with normalization by the same factor as

$$\begin{aligned} \vec{E}_\theta &= -\hat{\theta} \eta \sin(\theta) \left[\frac{1}{r} + \frac{1}{jkr^2} - \frac{1}{k^2 r^3} \right] e^{-jkr} \\ &= -\hat{\theta} \frac{\eta}{k} \sin(\theta) \left[\frac{k}{r} + \frac{1}{jr^2} - \frac{1}{kr^3} \right] e^{-jkr} \\ &= \hat{\theta} \frac{1}{j\omega \epsilon} \sin(\theta) e^{-jkr} \left[-\frac{1}{r^2} - \frac{jk}{r} + \frac{j}{kr^3} \right] \end{aligned} \quad (39)$$

Similarly the ϕ component of the magnetic field is written as

$$\begin{aligned} H_\phi &= -\hat{\phi} \frac{\sin(\theta)}{r} \left[1 + \frac{1}{jkr} \right] e^{-jkr} \\ &= \hat{\phi} \sin(\theta) e^{-jkr} \left[\frac{j}{kr^2} - \frac{1}{r} \right] \end{aligned} \quad (40)$$

The total electric energy density is given by

$$\begin{aligned} w_e^{total} &= \frac{1}{2} \epsilon \vec{E} \cdot \vec{E}^* = \\ &= \frac{1}{2} \epsilon (\vec{E}_\theta \cdot \vec{E}_\theta^* + \vec{E}_\theta \cdot \vec{E}_r^* + \vec{E}_r \cdot \vec{E}_\theta^* + \vec{E}_r \cdot \vec{E}_r^*) = \frac{1}{2} \epsilon (|E_\theta|^2 + |E_r|^2) \\ &= \frac{1}{2} \epsilon \left(\frac{1}{\omega^2 \epsilon^2} b \sin^2(\theta) \left[\frac{1}{r^4} + \left(-\frac{k}{r} + \frac{1}{kr^3} \right)^2 \right] \right. \\ &\quad \left. + \frac{4}{\omega^2 \epsilon^2} \cos^2(\theta) \left[\frac{1}{k^2 r^6} + \frac{1}{r^4} \right] \right) \end{aligned} \quad (41)$$

replacing the $\frac{1}{\omega \epsilon}$ by $\frac{\eta}{k}$ and bringing the outer ϵ inside get

$$w_e = \frac{1}{2} \left(\frac{\eta}{\omega} \sin^2(\theta) \left[\frac{k}{r^2} - \frac{1}{kr^4} + \frac{1}{k^3 r^6} \right] + \frac{4\eta}{\omega} \cos^2(\theta) \left[\frac{1}{k^3 r^6} + \frac{1}{kr^4} \right] \right) \quad (42)$$

The electric energy density associated with the travelling wave is obtained from the θ component as r becomes large (the $\frac{1}{r^2}$ and $\frac{1}{r^3}$ terms become negligible). Therefore, the radiating electric field can be

written as

$$\begin{aligned} E_{\theta}^{rad} &= -\frac{1}{\omega\epsilon} k \sin(\theta) \frac{e^{-jkr}}{r} \\ &= -\eta \sin(\theta) \frac{e^{-jkr}}{r} \end{aligned} \quad (43)$$

Therefore the radiating or propagating electric energy density w_e^{prop} is given by

$$\begin{aligned} w_e^{prop} &= \frac{1}{2} \epsilon \frac{\eta^2}{r^2} \sin^2(\theta) = \frac{1}{2} \epsilon \frac{\eta}{r^2} \frac{k}{\omega\epsilon} \sin^2(\theta) \\ &= \frac{1}{2} \frac{\eta}{\omega} \sin^2(\theta) \frac{k}{r^2} \end{aligned} \quad (44)$$

Now the non-propagating electric energy density is found by subtracting the propagating electric energy from the total electric energy density

$$\begin{aligned} w_e &= w_e^{total} - w_e^{prop} \\ &= \frac{1}{2} \left(\frac{\eta}{\omega} \sin^2(\theta) \left[-\frac{1}{kr^4} + \frac{1}{k^3 r^6} \right] + \frac{4\eta}{\omega} \cos^2(\theta) \left[\frac{1}{k^3 r^6} + \frac{1}{kr^4} \right] \right) \end{aligned} \quad (45)$$

The total non-propagating energy W_e is therefore given by integrating (45) over an infinite volume excluding the volume of the enclosing sphere (since Chu's assumption was that no energy is stored inside the bounding sphere). Assuming the bounding sphere has a radius of a

$$W_e = \int_0^{2\pi} \int_0^{\pi} \int_a^{\infty} w_e \sin(\theta) r^2 dr d\theta d\phi \quad (46)$$

$$\begin{aligned}
&= \int_0^{2\pi} \int_0^\pi \int_a^\infty \frac{1}{2} \left(\frac{\eta}{\omega} \sin^3(\theta) \left[-\frac{1}{kr^2} + \frac{1}{k^3r^4} \right] \right. \\
&\quad \left. + \frac{4\eta}{\omega} \sin(\theta) \cos^2(\theta) \left[\frac{1}{k^3r^4} + \frac{1}{kr^2} \right] \right) dr d\theta d\phi \\
&= \frac{\pi\eta}{\omega} \int_a^\infty \frac{4}{3} \left[-\frac{1}{kr^2} + \frac{1}{k^3r^4} \right] + \frac{8}{3} \left[\frac{1}{kr^2} + \frac{1}{k^3r^4} \right] dr \\
&= \frac{4\pi\eta}{3\omega} \left[\frac{1}{ka} + \frac{1}{(ka)^3} \right]
\end{aligned}$$

Note that the integration limits with respect to r starts from a , the radius of the sphere. Otherwise the integral would be non convergent. The *total radiated power* can be obtained by integrating the real part of the complex Poynting vector over the surface of the sphere of radius R

$$\begin{aligned}
P_{rad} &= \int_0^{2\pi} \int_0^\pi \operatorname{Re}(\vec{E} \times \vec{H}^*) \cdot \hat{r} \sin(\theta) r^2 d\theta d\phi \\
&= \int_0^{2\pi} \int_0^\pi \operatorname{Re}(\vec{E}_\theta \times \vec{H}_\phi^*) \cdot \hat{r} \sin(\theta) r^2 d\theta d\phi \\
&= \int_0^{2\pi} \int_0^\pi \operatorname{Re} \left(\hat{\theta} \frac{1}{j\omega\epsilon} \sin(\theta) e^{-jkr} \left[-\frac{1}{r^2} - \frac{jk}{r} + \frac{j}{kr^3} \right] \right. \\
&\quad \left. \times \hat{\phi} \sin(\theta) e^{+jkr} \left[\frac{-j}{kr^2} - \frac{1}{r} \right] \right) \cdot \hat{r} \sin(\theta) r^2 d\theta d\phi \\
&= \int_0^{2\pi} \int_0^\pi \operatorname{Re} \left(\frac{1}{j\omega\epsilon} \sin^3(\theta) \left[-\frac{1}{r^2} - \frac{jk}{r} + \frac{j}{kr^3} \right] \left[\frac{-j}{kr^2} - \frac{1}{r} \right] \right) r^2 \cdot d\theta d\phi \quad (47) \\
&= \int_0^{2\pi} \int_0^\pi \operatorname{Re} \left(\frac{1}{j\omega\epsilon} \sin^3(\theta) \left[\frac{j}{kr^2} + \frac{1}{r} - \frac{1}{r} + jk + \frac{1}{k^2r^3} - \frac{j}{kr^2} \right] \right) \cdot d\theta d\phi \\
&= \int_0^{2\pi} \int_0^\pi \operatorname{Re} \left(\frac{1}{\omega\epsilon} \sin^3(\theta) \left[k + \frac{1}{jk^2r^3} \right] \right) \cdot d\theta d\phi \\
&= \int_0^{2\pi} \int_0^\pi \left(\frac{1}{\omega\epsilon} \sin^3(\theta) k \right) \cdot d\theta d\phi \\
&= \frac{4}{3} \times 2\pi \times \frac{k}{\omega\epsilon} = \frac{8\pi}{3} \eta
\end{aligned}$$

Based on the first equation in (36) the Q of the infinitesimally small dipole is then given by

$$\begin{aligned} Q_{min} &= \frac{2\omega W_e}{P_{rad}} \\ &= \frac{2\omega \frac{4\pi\eta}{3\omega} \left[\frac{1}{ka} + \frac{1}{(ka)^3} \right]}{\frac{8\pi}{3}\eta} \\ &= \frac{1}{ka} + \frac{1}{(ka)^3} \end{aligned} \tag{48}$$

This is in agreement with Chu's derivation.

5 Results:

The simulated and analytical results of the spiralpole and dipole will be presented in this section. The purpose is to evaluate the performance of both antennas relative to each other. A fair evaluation can be performed by choosing a fixed spherical volume that encloses or bounds both antennas minimally. This idea of enclosing the antenna structure within a bounding sphere again stems from Chu's paper [11] where inherent physical limitations of antenna Q and Gain are analyzed using spherical radiating modes. This becomes an important metric in evaluating electrically small antennas, as the closer the performance of the antenna to the absolute limit the better the antenna performance. The antenna structures are simulated in HFSS for full wave solutions for the antenna impedances. Analytical solutions are also generated using MATLAB and, where appropriate, compared to the Ansoft HFSS full wave results. In the case of the dipole antenna, established results are available [23] for use and can be verified using Ansoft HFSS. However, for radiation resistance comparison purposes the Ansoft HFSS results are used for accuracy. The sphere chosen to be used as a bounding sphere is one of diameter 300mm. This choice is somewhat arbitrary, although it closely reflects dimensions of actual fabricated spiralpole antennas used in integrated food probe designs. Analytical results will also be presented for the spiralpole antenna and compared to simulated results to evaluate the accuracy of the analytical models. All antennas and matching elements are assumed as lossless to place more emphasis on design efficiency of the antennas themselves.

5.1 Performance Evaluation Methodology

Once the size of the antenna is determined by the enclosing sphere of fixed radius, the antenna configurations are evaluated using two primary metrics:

- $Q - kr$ relationship
- Radiation resistance
- Directivity in E and H planes

The definition used for antenna Q is in accordance with [23] [25]. In order to calculate this $Q - kr$ relationship for a particular antenna configuration the structure is simulated first to extract impedance data. The impedance data is then read into MATLAB and interpolated with the built in **interp1** function by about 500 times to increase the resolution of the data. High Q resonances may not be detected or misleading due to too few data points. Once this data is interpolated the antenna is matched to a certain frequency f_c by a series ideal inductor or capacitor. If the reactance of the antenna $X_A(f_c) > 0$, then an ideal capacitor of equal and opposite reactance is used to tune the antenna to resonance. Similarly, if the antenna reactance $X_A(f_c) < 0$ then an ideal inductor of equal and opposite reactance is used to tune the antenna to resonance. However, if the antenna's reactance $X_A(f_c) = 0$ then it does not need to be matched since it is naturally resonant. Once matched, the antennas return losses is calculated and the fractional (3dB) VSWR bandwidth [25] is found about f_c . The radiation Q [23] [25] at this frequency (or electrical length) is then calculated to be $\frac{2}{FBW_V}$. This process is repeated for all frequencies to generate a smooth $Q - kr$ curve for the antenna configuration. Since a lossless lumped inductor or capacitor is used for matching the antenna, the radiation resistance will not change using this method. Thus, the radiation resistance values are simply identified for each frequency of interest independent of matching. The radiation pattern in the E and H planes are extracted from Ansoft HFSS simulations.

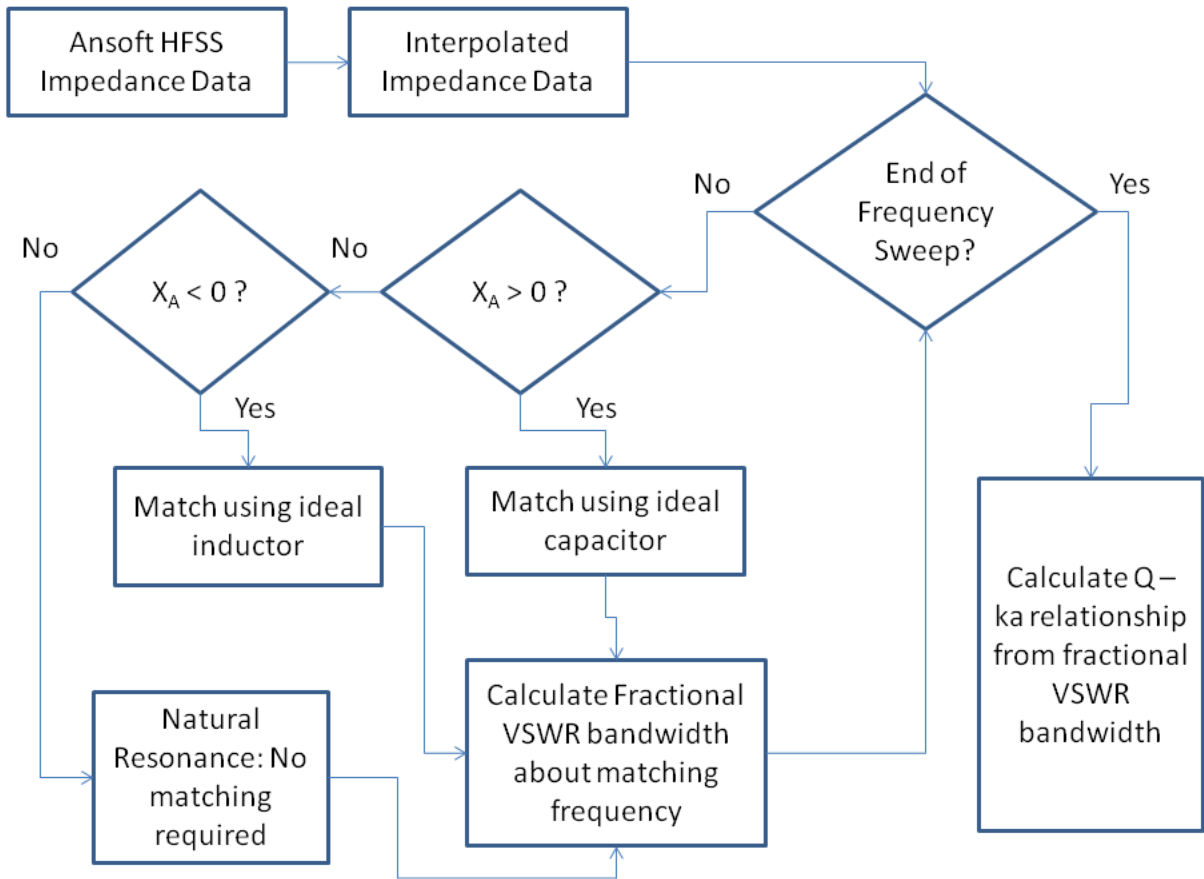


Figure 9: Algorithm for generating antenna Q - kr relationship using MATLAB

Figure 9 summarizes the $Q - kr$ curve generation process in a flowchart. The next important performance metric used to evaluate each spiralpole configuration is the radiation resistance. A higher radiation resistance indicates better radiation performance. The radiation resistance of electrically small antennas is usually very small, so any increase in radiation resistance is a significant performance enhancement. In addition, it is usually easier to match to this higher radiation resistance than to a very small radiation resistance.

5.2 Ansoft HFSS Spiralpole Model

The Ansoft HFSS spiralpole model will be described in this section. As mentioned, a base spiralpole model was created from which spiralpoles of 3,4,5 and 6 turns were then created. Construction of the spiralpole is three-fold in Ansoft HFSS. First the first wing or the shaft is created as a cylindrical perfect electrical conductor. Next, the second wing or the Archimedean spiral wing is created. The parametric equations for an Archimedean spiral is given by

$$x(t) = bt \cos(at) \quad (49)$$

$$y(t) = bt \sin(at) \quad (50)$$

The variable t is a parametric variable in radians and determines the number of turns. The variable a is a frequency term, and is set to 1. The variable b is an amplitude term and is set to 2. A planar spiral curve is first drawn using these parametric equations, and a surface is created by sweeping a straight line that is perpendicular to any of this curve's endpoints, along the curve. This creates a spiral sheet with the width being the length of the initial perpendicular straight line. The width of the line or of the spiral sheet was chosen to be 1mm.

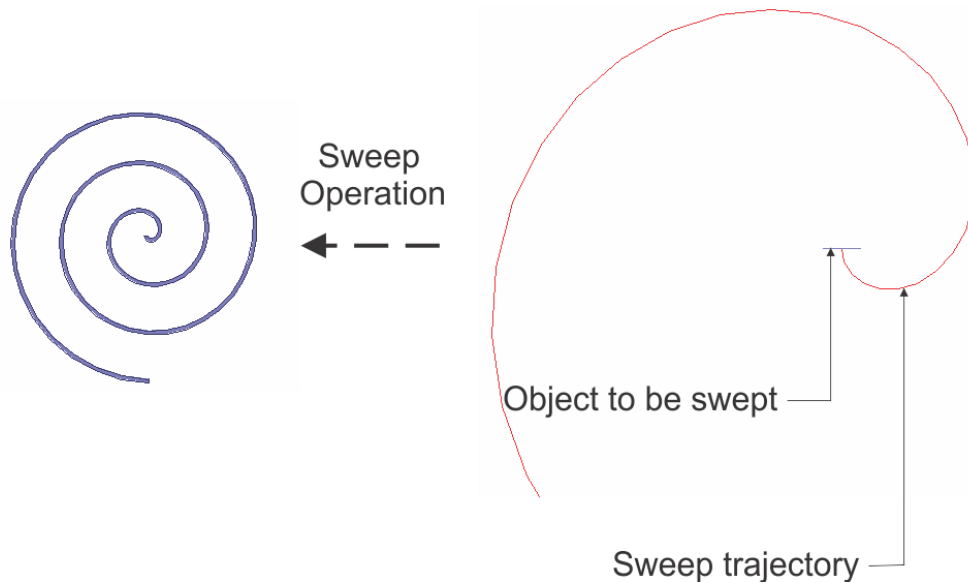


Figure 10: Creation of the spiral sheet in Ansoft HFSS

The feed is finally created between spiral wing and the cylindrical shaft wing. The spiral wing is connected to the feed using a small 1mm long feeding cylinder with a diameter of 1mm. This arrangement is shown in Figure 11. The red circular surface is the feed or lumped port.

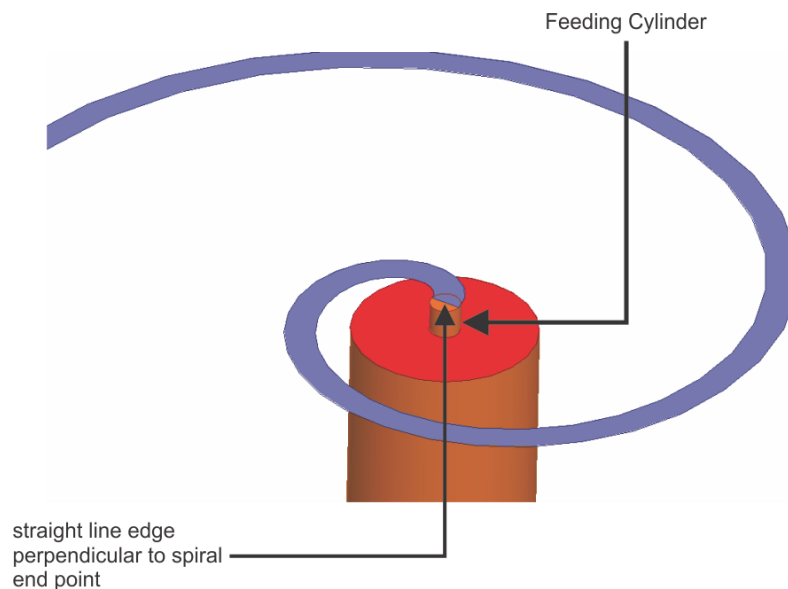


Figure 11: Arrangement of the feeding mechanism. The red circular surface is the lumped port or feed

Finally, a 2.5m x 2.5m x 2.5m box was created from which the perfectly matched layer or PML boundary was created. Once the model objects are created, the next critical step is to parameterize the model

such that the spiral would fit in a sphere with a fixed diameter of 300mm. This is accomplished by setting the sphere radius as a fixed, independent parameter. The relationships between the spiralpole dimensions and the sphere were presented in Section 3.2. These relationships are used to define the model in order to impose the constraint that the spiralpole be bound by this sphere. As such, the parameter of variation was chosen to be the probe height. As an example, if the probe height were to be reduced, the spiral radius would increase and thus the number of turns would increase as well. The final length of the spiral is given by:

$$l_{spiral}(t) = \frac{1}{2}a (t \sqrt{1 + t^2} + \ln(t + \sqrt{1 + t^2})) \quad (51)$$

where a is the frequency of rotation of the spiral, and t is the parametric variable in radians previously defined. The length of the spiral is needed since our half wave resonator approximate makes use of this. Figure 12 shows a snapshot of the design equations and variables for the three turn spiralpole model that has been extracted from this base model.

Properties: three_turns_3mm_1_300 - HFSSDesign1

Local Variables

Value
 Optimization
 Tuning
 Sensitivity
 Statistics

Name	Value	Unit	Evaluated Value	Type	Description
radius_probe	3	mm	3mm	Design	radius of the shaft/probe
height_probe	284.175	mm	284.175mm	Design	height of the probe without the bottom cone
radius_inner	0.5	mm	0.5mm	Design	radius of the feeding cylinder and the hole in the feed
feeding_cyl_h...	1	mm	1mm	Design	height of the feeding cylinder
thickness	1	mm	1mm	Design	width of the spiral wire
b	2	mm	2mm	Design	amplitude of the spiral
a	1		1	Design	frequency of the spiral
end_of_param...	spiral_radius/b		18.8694155646...	Design	No. of turns is end_of_parameter/(2*pi)
height_cone	10	mm	10mm	Design	
sphere_radius	150	mm	150mm	Design	
z0	height_probe+height_co...		295.175mm	Design	
spiral_radius	sqrt(2*sphere_radius*z0-...		0.03773883112...	Design	
Turns	end_of_parameter/(2*pi)		3.003160760363	Design	
xbox	2500	mm	2500mm	Design	

Figure 12: Design parameters of three turn spiralpole model

5.3 Simulated and Analytical Results: 3,4,5 and 6 Turns Spiralpoles

In this section the $Q - kr$ relationship, impedance and directivity for the dipole and 3,4,5,6 turns spiralpoles will be presented and analyzed. The first candidate is the simple dipole antenna in the Chu sphere of radius 150mm. The results for the dipole will be presented with each candidate spiralpole antenna results for comparison.

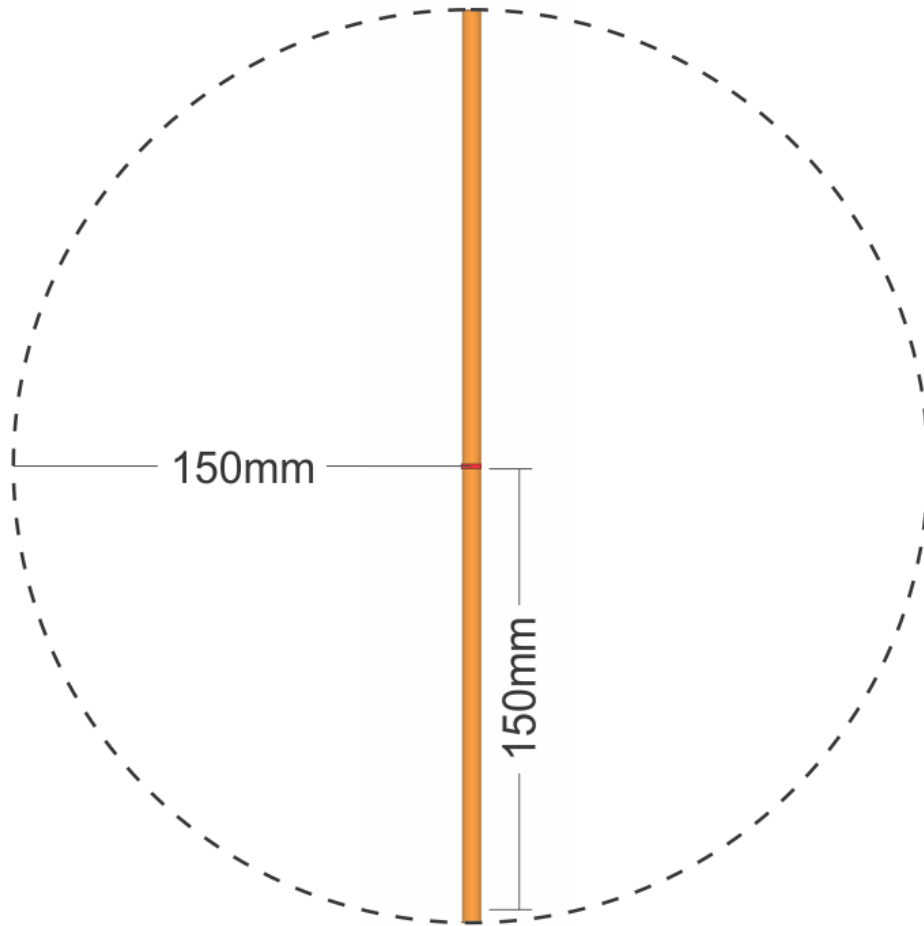


Figure 13: Dipole of length 300mm inside enclosing sphere

. Figure 13 shows the 300mm long dipole inside the bounding Chu sphere. The dipole has a wire radius of 3mm and therefore the ratio of *half length* to wire radius is 50. This was done to maintain consistency between Hansen's study [28] and this work. Taking the same sphere shown in Figure 13, we place a spiralpole antenna within the sphere and vary the number of turns of the spiral wing. Our aim is to validate the performance of the spiralpole using the $Q - kr$ curves for different spiral configurations inside the same sphere against the $Q - kr$ curves of the 300mm long dipole. Since the spiralpole uses up the volume in inside the sphere more efficiently, it is expected that the performance will be better than the dipole.

5.3.1 3 Turns Spiralpole Results

Our first spiralpole candidate is the three turns spiralpole. The number of turns in this configuration is still relatively small, so the antenna performance is expected to be close to the dipole performance. The width of the spiral sheet is 1mm.

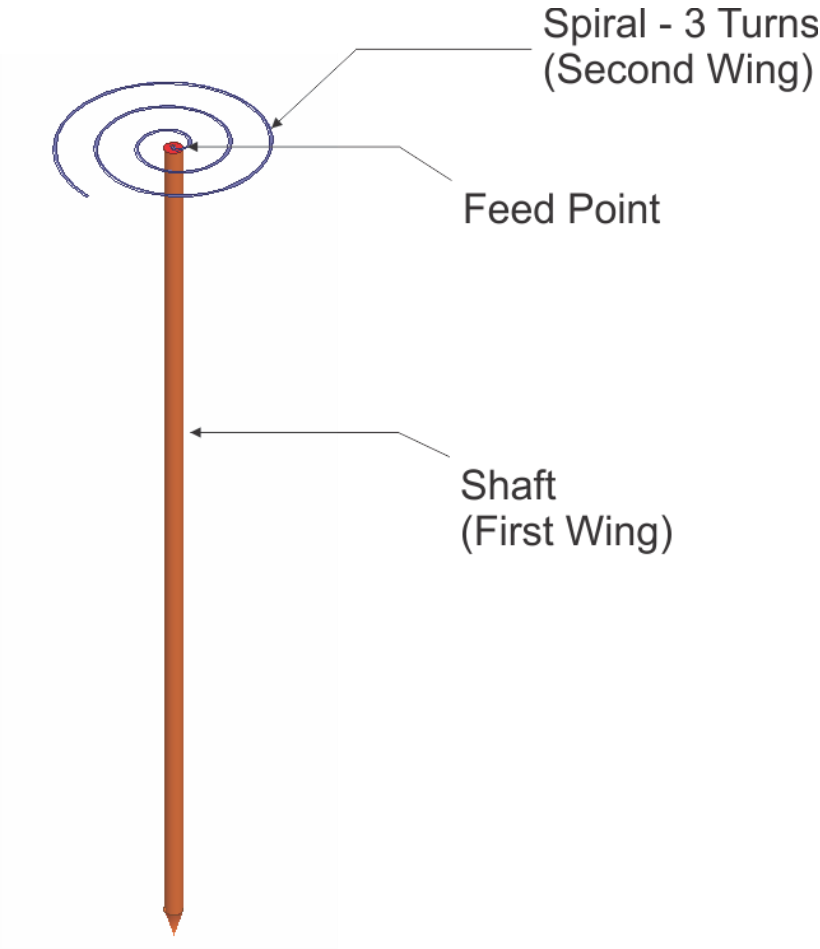


Figure 14: Three turn Spiral Pole

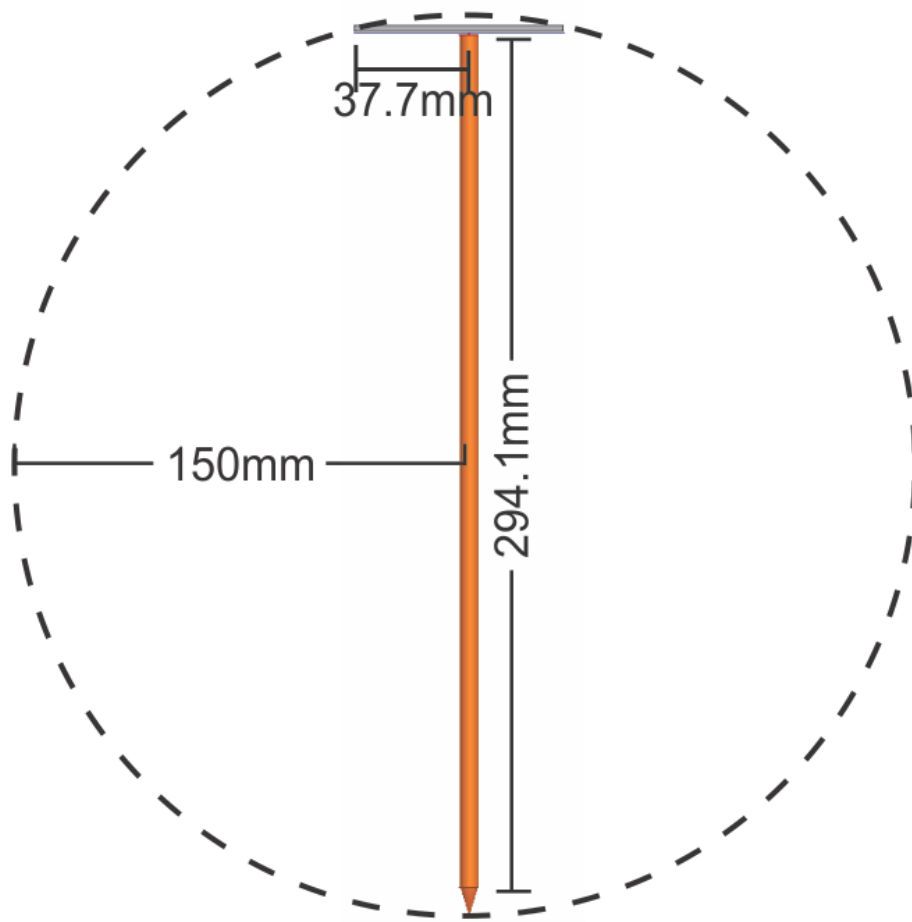


Figure 15: Three turn spiralpole in Chu Sphere

Figure 14 shows the three turn spiralpole antenna, the feed point and the shaft. Figure 15 shows the same spiralpole antenna enclosed within the same 150mm radius bounding sphere. Notice that the total antenna height is reduced due to the introduction of the spiral wing. The total antenna height is 294.1mm and the spiral radius is 37.7mm. The total length of spiral is 179.7mm. The total length of the antenna structure is therefore 473.8mm.

Spiral-pole impedance comparison- Theory vs Simulation

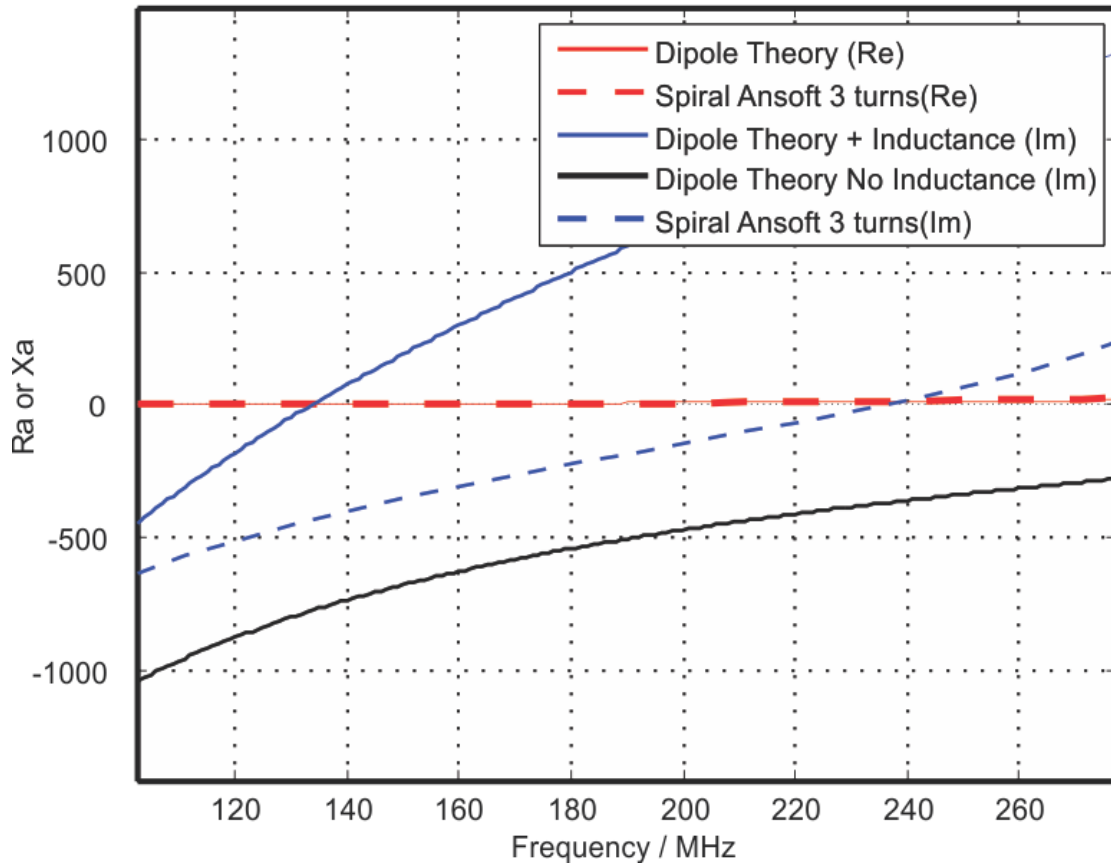


Figure 16: Simulated VS analytical Dipole and 3 turn spiralpole impedances

The linear impedance approximate model in Figure 16 predicts the resonance to be around 137 MHz. As per the analytical resonant length model the antenna resonance is expected to be at $f_0 = \frac{c_0}{\lambda} = \frac{c_0}{2 \times 0.4741} - 80 \text{ MHz} = 236.3 \text{ MHz}$. The true resonance as seen in Figure 16 is around 235 MHz. Figure 17 shows that the radiation resistance of the spiralpole antenna at 235.9 MHz is 12.4 Ohms. The radiation resistance of the dipole antenna at the same frequency is seen to be 10.14 Ohms. This represents a 23% increase in radiation resistance as compared to the dipole antenna. The $Q - kr$ relationship for the dipole and 3 turns spiralpole is shown in Figure 18. Notice that the spiralpole with three turns is better than the dipole antenna as the curve is closer to the absolute limit, although not by much in this case. It seems that the spiralpole is starting to outperform the dipole antenna. Figure 19 shows the radiation pattern of the dipole antenna and spiralpole antenna at the spiral resonance. Note that these patterns

are extracted from Ansoft HFSS simulations and are raw pattern data. There was no external matching applied to either antenna. The dipole antenna is seen to have a gain of about 1.7 dB symmetrically in the H-plane. This is the well known gain for a small non-resonant dipole. The spiralpole shows pattern symmetry as well in the H-plane, however with a higher gain overall. The maximum gain is about 2.7 dB. The E-plane pattern shows almost identical characteristics between the dipole and the spiralpole as expected. The overall pattern is a ‘donut’ for both antennas.

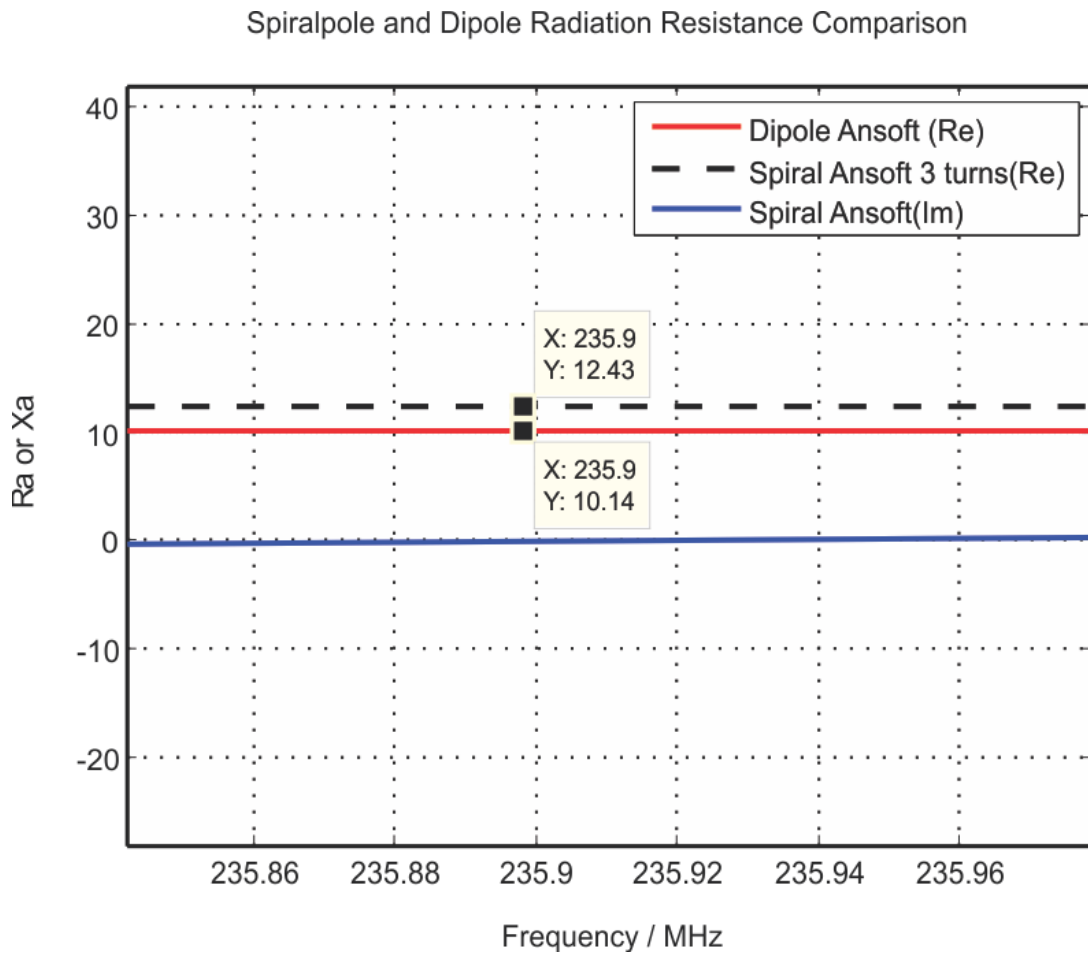


Figure 17: Radiation resistance comparison between 3 turn spiralpole and dipole antenna at spiralpole resonance

Q vs kr

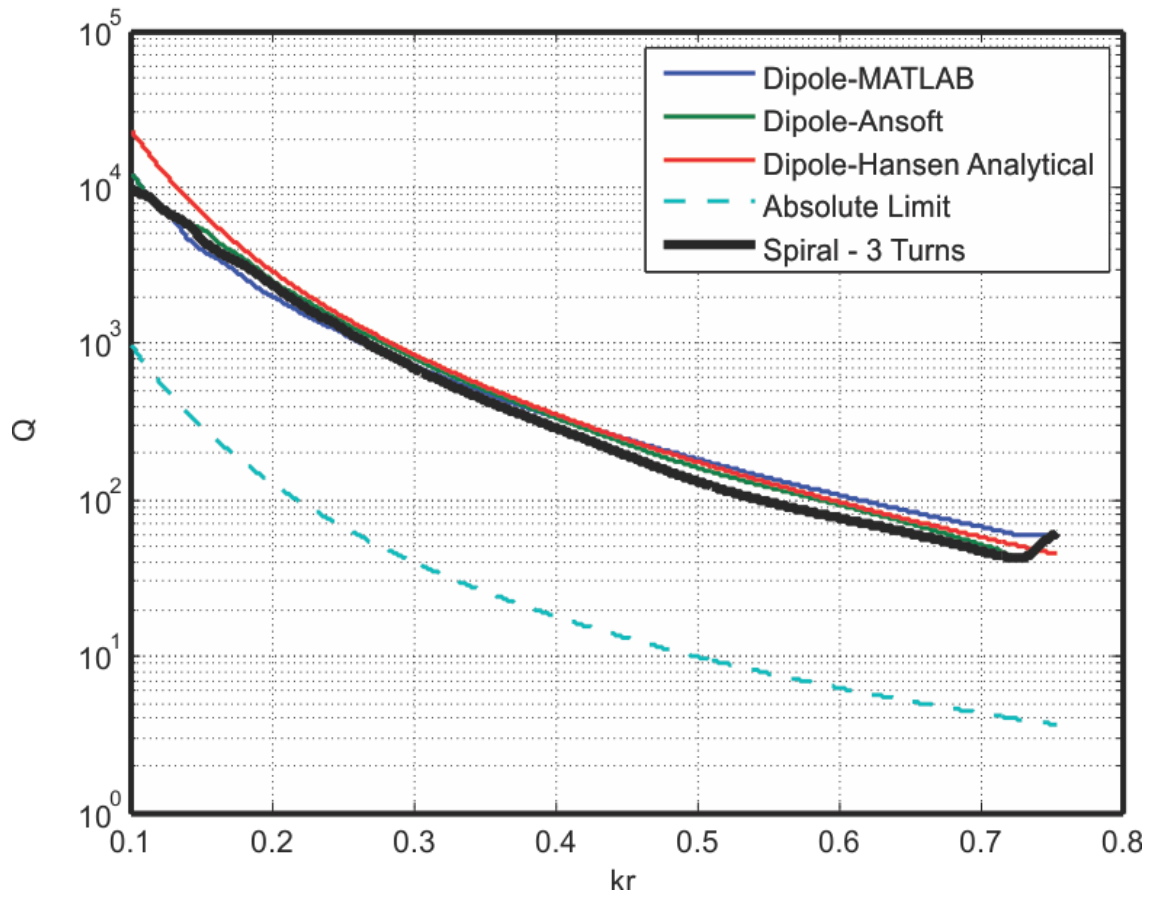
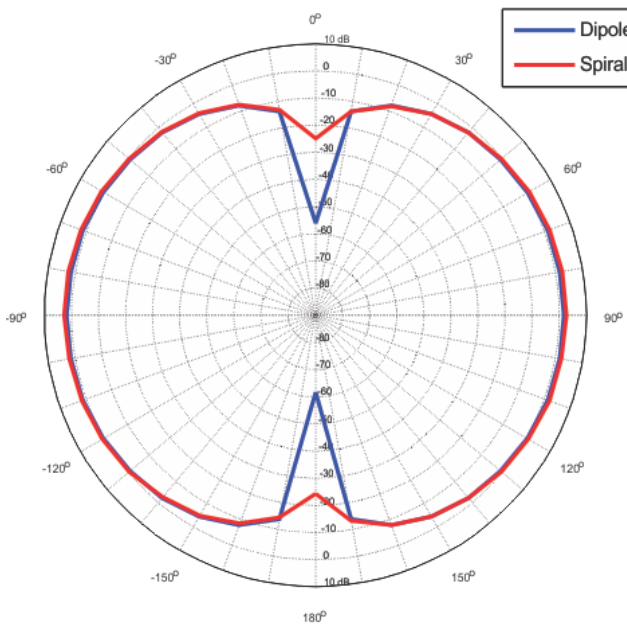


Figure 18: Q - kr for 3 turn spiral VS dipole and absolute limit

3 turn spiral VS Dipole Pattern: E Plane @231 MHz



3 turn spiral VS Dipole Pattern: H Plane @231 MHz

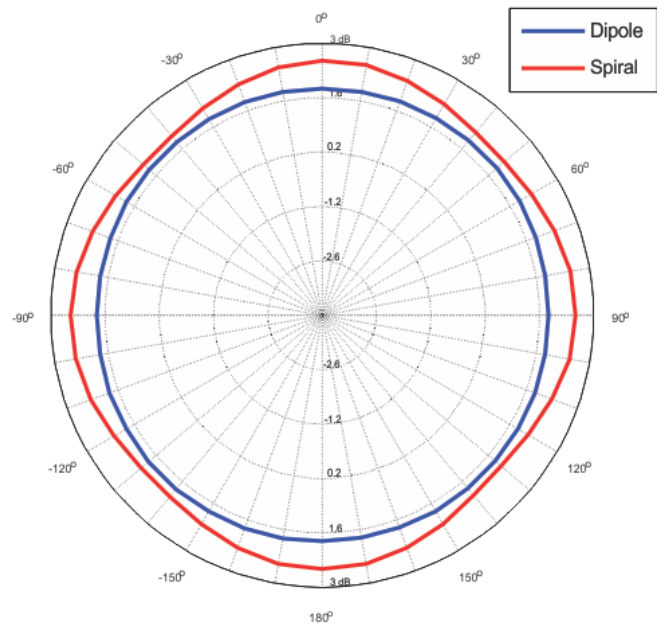


Figure 19: E and H plane radiation patterns for 3 turn spiralpole and dipole

5.3.2 4 Turns Spiralpole

Our next spiralpole candidate is the four turns spiralpole shown in Figure 20. The number of turns for the spiralpole has increased therefore to fit in the Chu sphere the height of the shaft decreased. Figure 21 shows the same spiralpole in the Chu sphere. Since there are more turns now, the spiralpole performance is expected to improve.

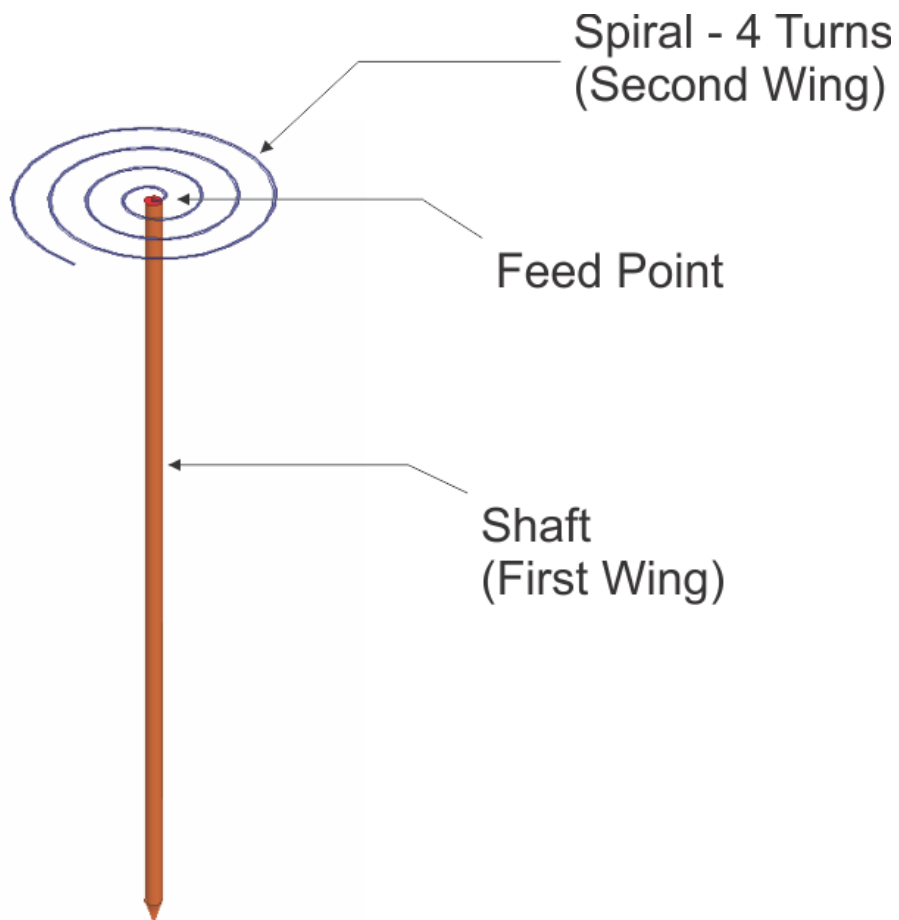


Figure 20: Four turn spiralpole

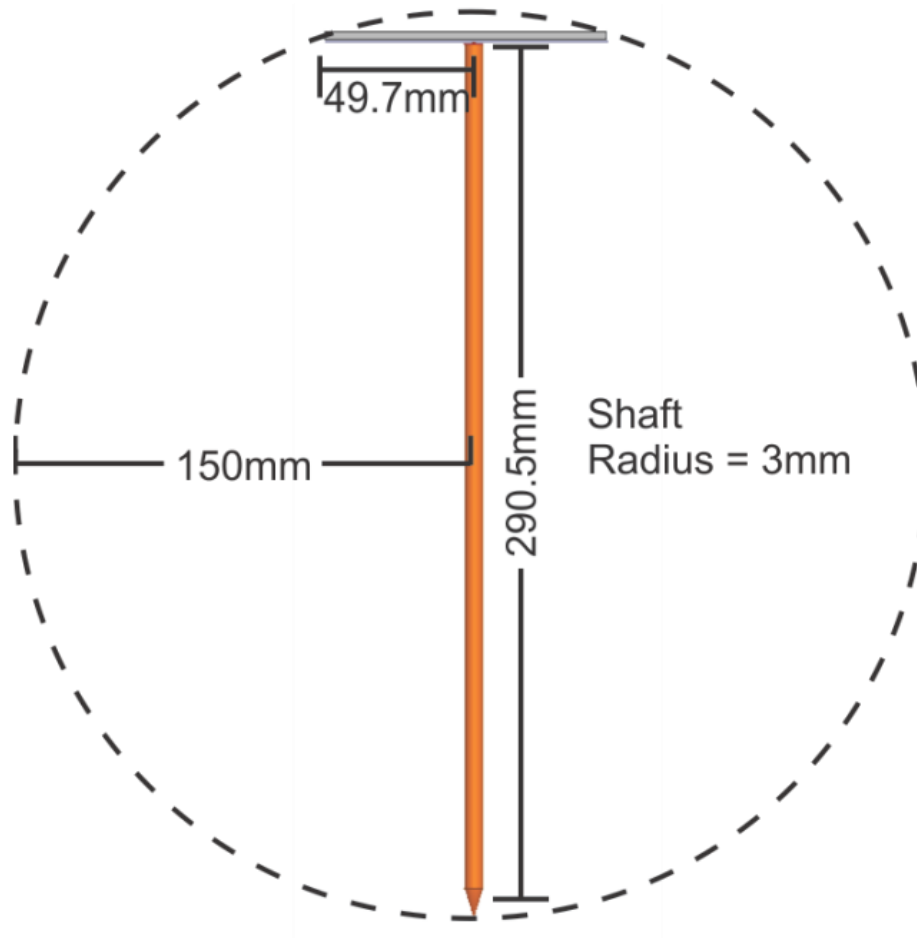


Figure 21: Four turn spiralpole in Chu Sphere

The final radius of the spiral on top is 49.7mm and the shaft height is reduced to 290.5mm. The shaft radius is 3mm and spiral sheet width is 1mm. The total length of the spiral is 318mm. The total length of the antenna is therefore 608.5mm. The resonant length model predicts the resonance to occur at $f_c = 166$ MHz. The analytical impedance model predicts the resonance at 100 MHz.

Spiral-pole impedance comparison- Theory vs Simulation

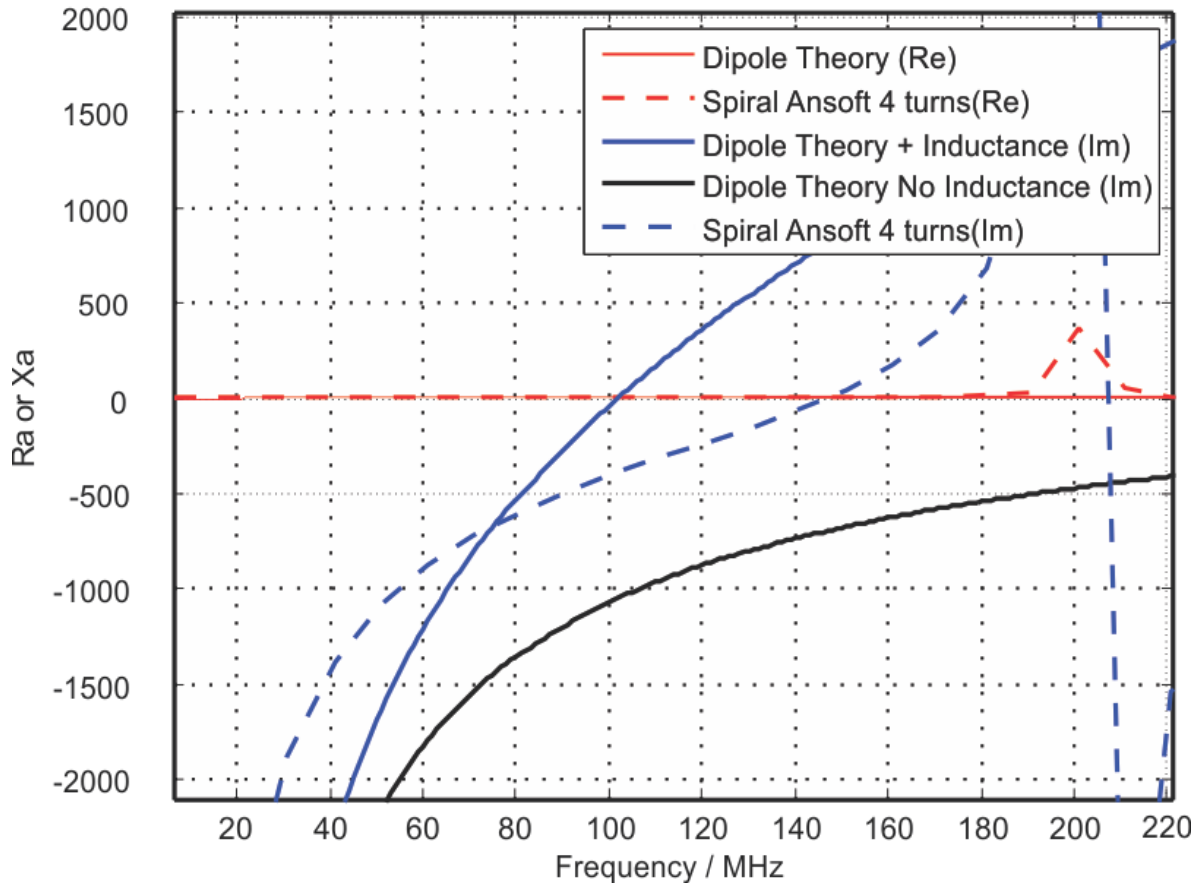


Figure 22: Simulated VS analytical Dipole and 4 turns spiralpole impedances

Figure 22 shows the true resonance to be around 143 MHz. The error between the two predictions is getting smaller since the spiral contribution is becoming more and more prominent. Figure 23 shows the radiation resistance at resonance of the spiralpole antenna and the dipole resistance at the same frequency. The results were obtained from Ansoft HFSS simulations of both the 4 turns spiralpole and dipole antennas. The radiation resistance of the spiralpole is 3.83 Ohms and the dipole radiation resistance is seen to be 2.501 Ohms.

Spiralpole and Dipole Radiation Resistance Comparison

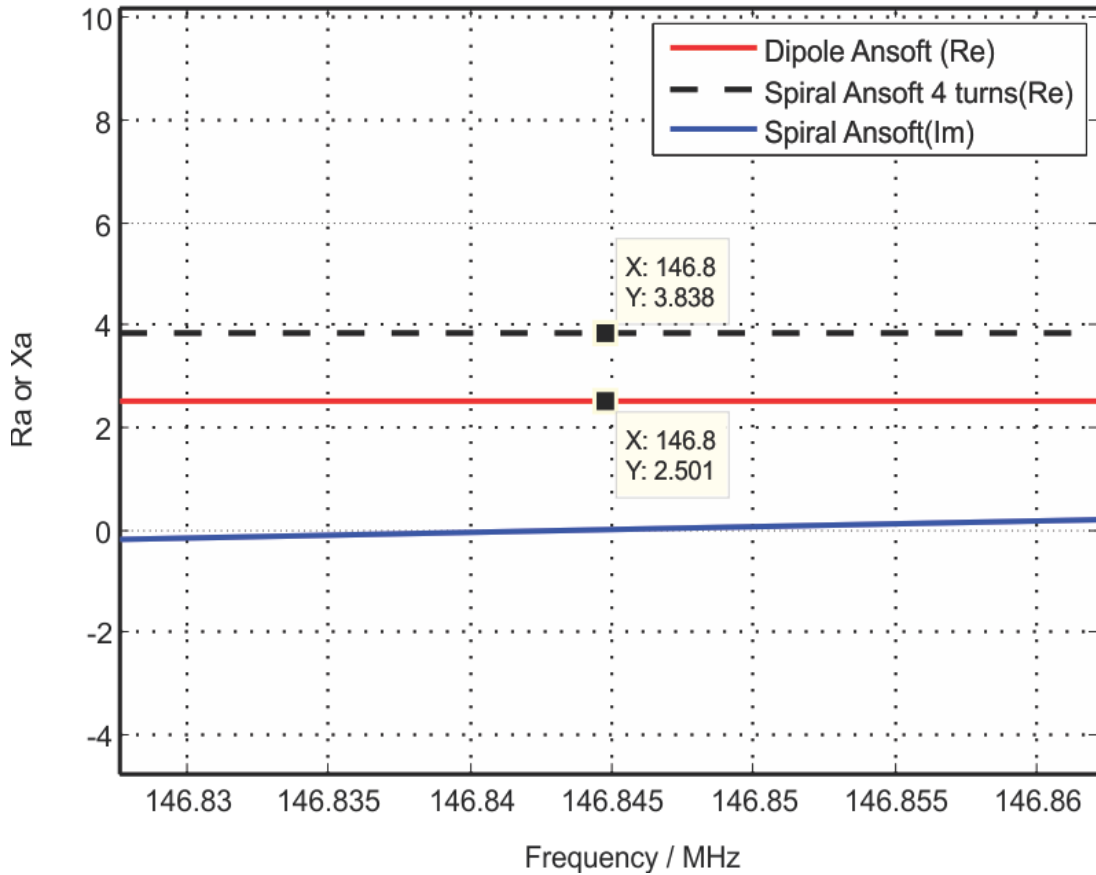


Figure 23: Radiation resistance comparison between 4 turns spiralpole and dipole at spiralpole resonance

The spiralpole antenna’s radiation resistance is about 53 % higher than that of the dipole antenna. This is expected since the spiralpole antenna is using the volume of Chu sphere more effectively. The $Q - kr$ curves are shown in Figure 24 for the dipole from the analytical impedance, Ansoft HFSS simulation and Hansen’s analytical Q expression. All three are in close agreement. The spiralpole antennas $Q - kr$ behavior is shown by the black curve. It can be seen that the spiral outperforms the dipole as the $Q - kr$ curve rests below all three dipole $Q - kr$ curves. Figure 25 shows the directivity in the E and H planes for the spiralpole antenna and the dipole antenna at 143 MHz (at the resonance). It can be seen the spiralpole directivity in the H plane is the same as that of the dipoles with a max gain of 1.7dB. In the E plane, the spiralpole’s null at azimuth is less pronounced than the dipole’s null.

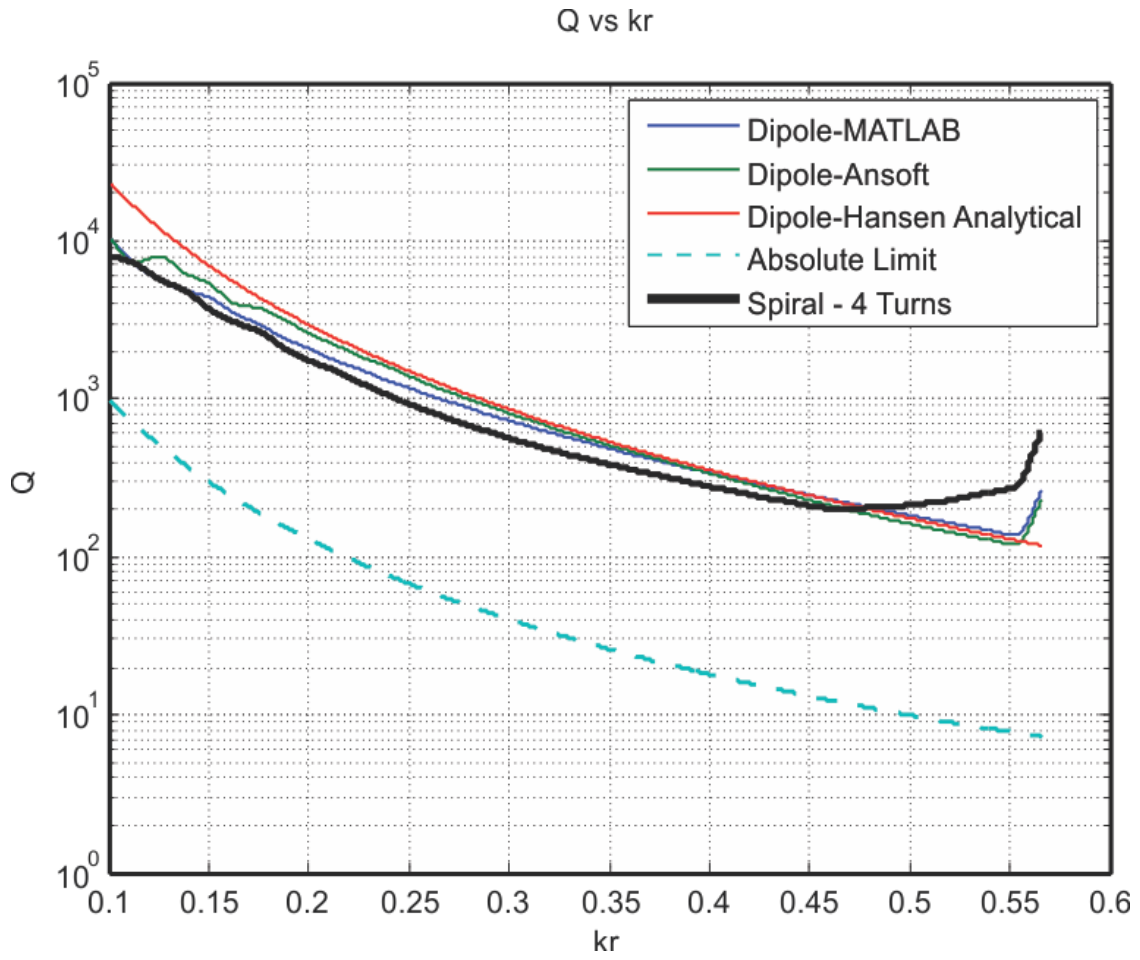
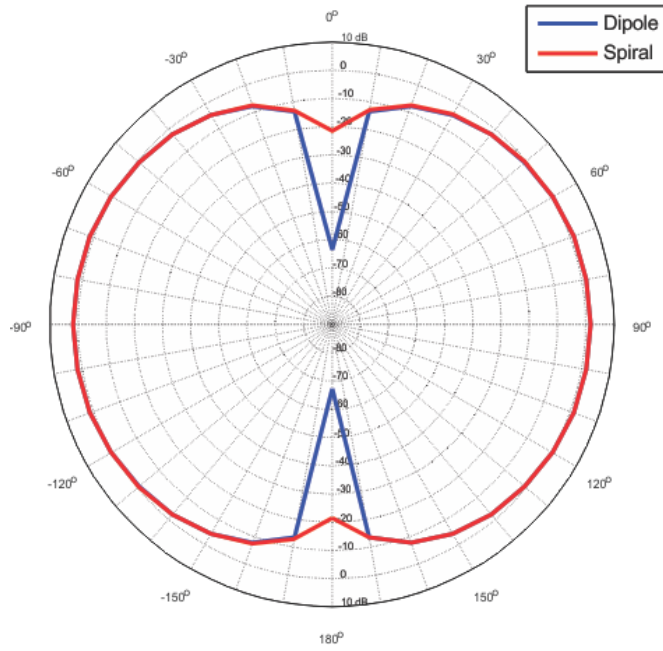


Figure 24: Q - kr for 4 turn spiral VS dipole and absolute limit

4 turn spiral VS Dipole Pattern: E Plane @143 MHz



4 turn spiral VS Dipole Pattern: H Plane @143 MHz

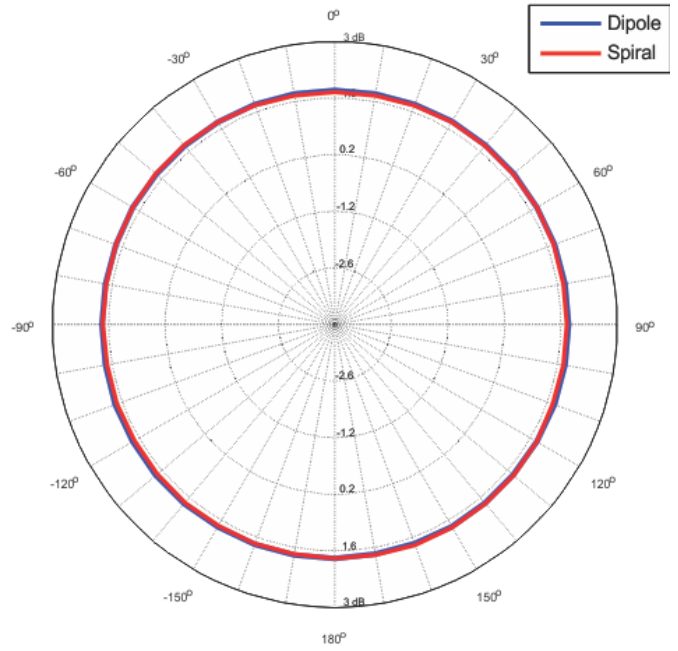


Figure 25: E and H Plane Pattern for 4 turn spiralpole and Dipole at spiralpole resonance

5.3.3 5 Turn Spiralpole

The next configuration of the spiralpole antenna is the 5 turns spiralpole antenna. Figure 26 shows the 5 turns spiralpole antenna as modeled in Ansoft HFSS. The number of turns is more and the spiralpole antenna is expected to resonant at a lower frequency due to the increased inductance of the spiral wing. The size of the shaft is now shorter due to the increased spiral radius in order to fit in the Chu sphere.

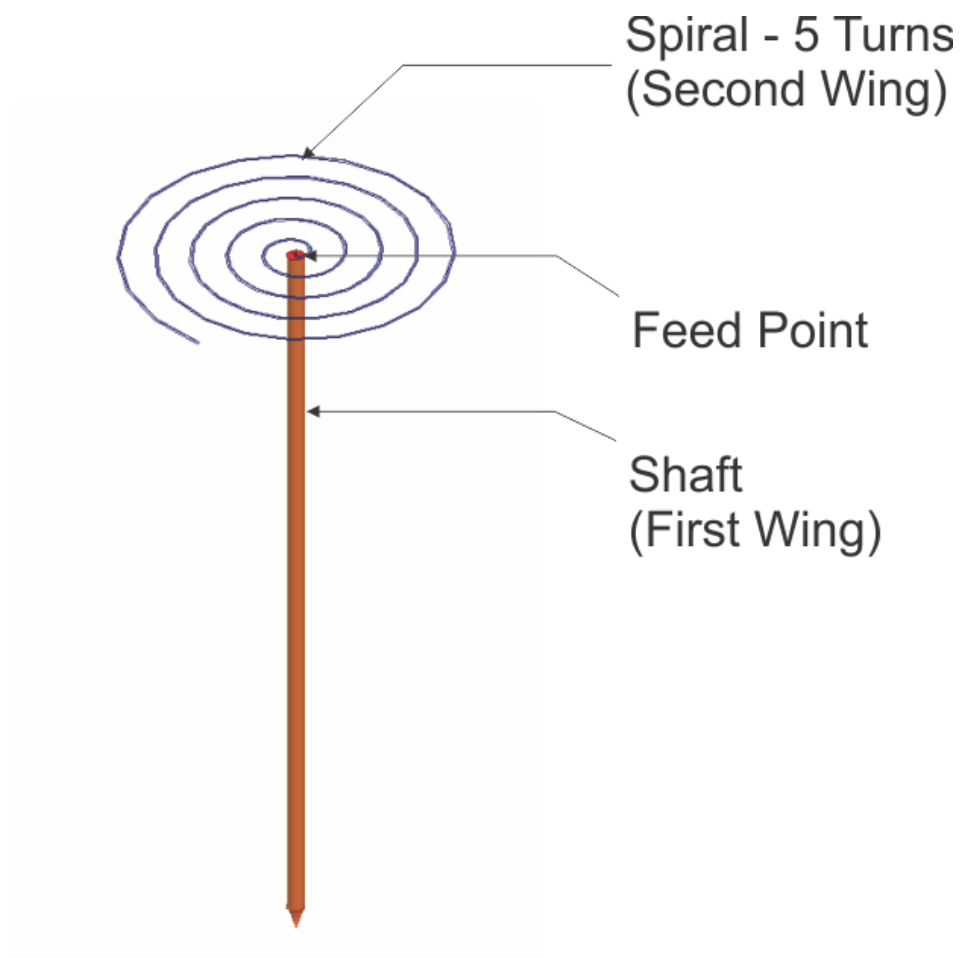


Figure 26: Five turn spiralpole

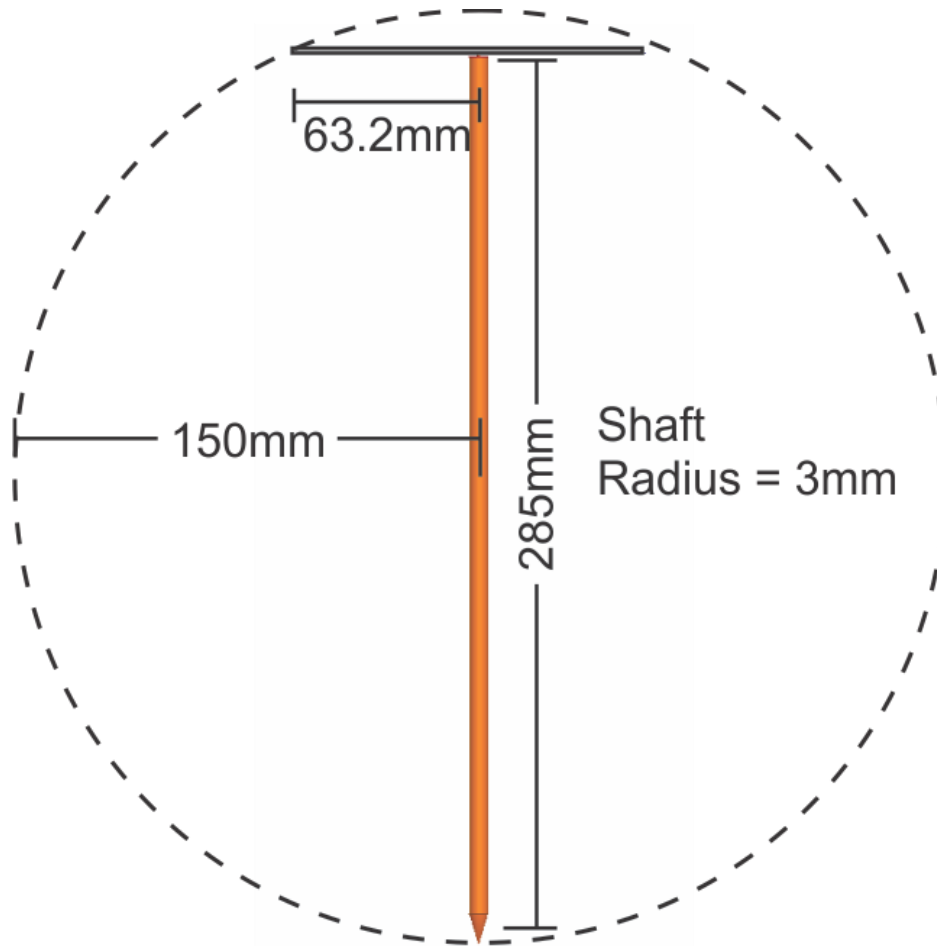


Figure 27: Five turn spiralpole in Chu Sphere

Figure 27 shows the 5 turns spiralpole antenna in the Chu sphere. The final radius of the spiral is 63.2mm and the shaft height is 285mm. The shaft radius is 3mm long and the spiral width is 1mm. The sphere radius is 150mm. The total spiral length is 495.8mm. The total length of the spiralpole is therefore 780.8mm. The analytical resonant length model predicts the resonance to be at 111.9 MHz. The analytical first order impedance model predicts the resonance to be at 82 MHz.

Spiral-pole impedance comparison- Theory vs Simulation

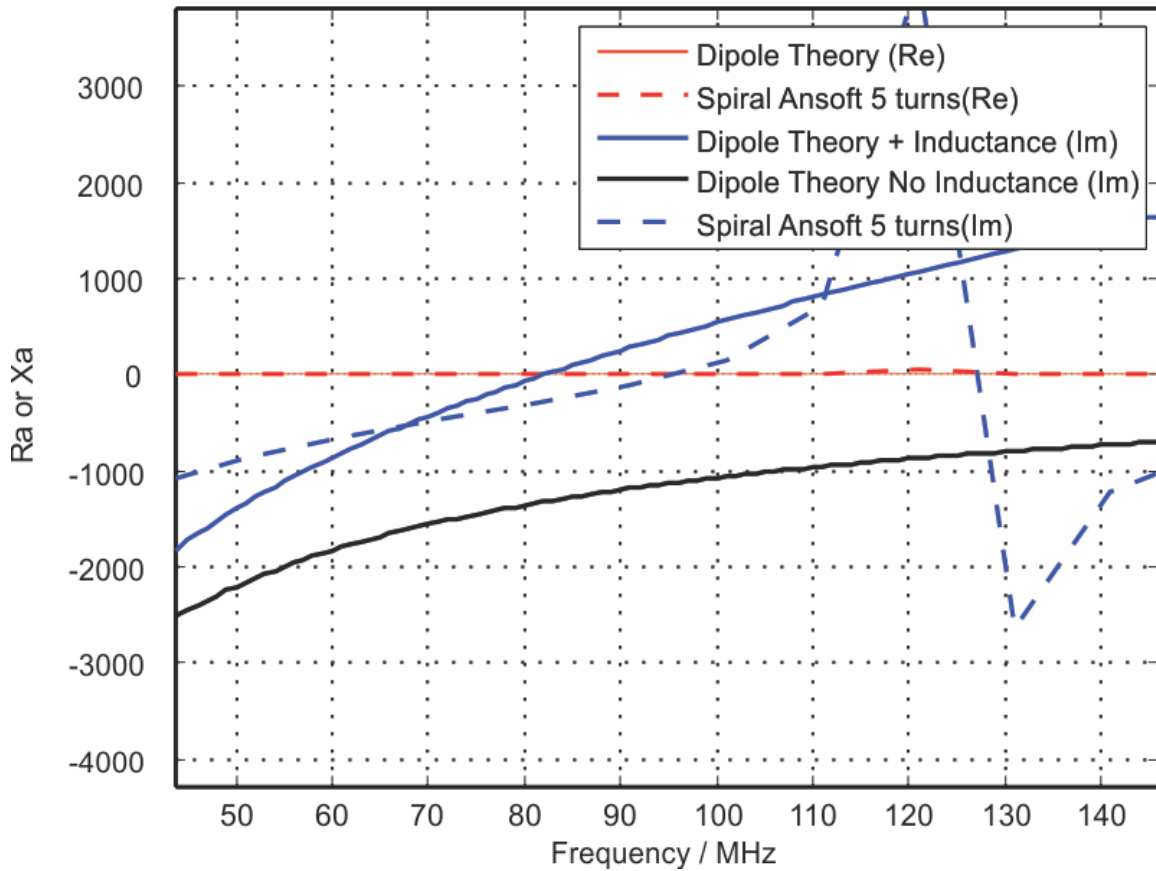


Figure 28: Simulated VS analytical Dipole and 5 turns spiralpole impedances

Figure 28 shows the simulated Ansoft HFSS impedance of the spiralpole antenna in dashed lines. The analytical MATLAB generated dipole impedance is shown, along with the analytical impedance model of the spiralpole antenna using this dipole impedance and the spiral inductance. The true resonance can be seen to occur at about 95 MHz. Again, the analytical length and impedance models predict the resonance frequency quite well since the spiral wing is now more prominent.

Spiralpole and Dipole Radiation Resistance Comparison

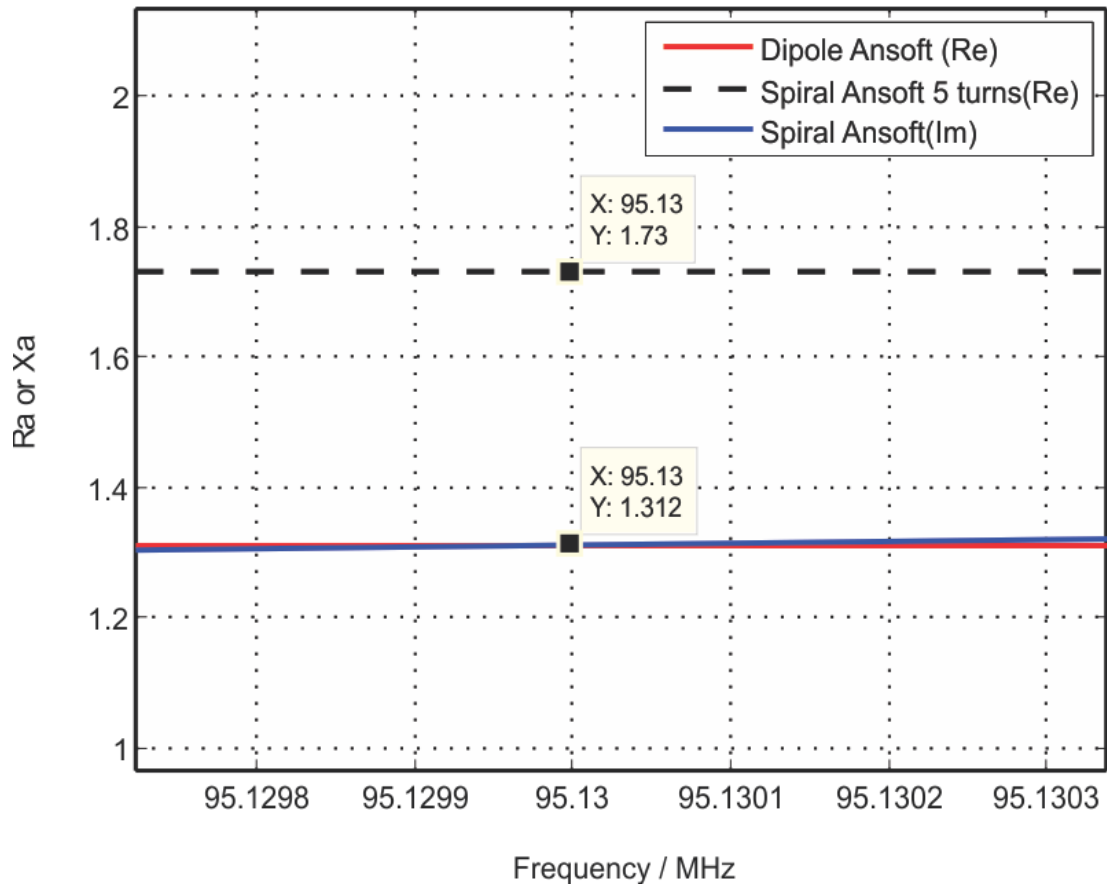


Figure 29: Radiation resistance comparison of 5 turn spiralpole and dipole antenna at spiralpole resonance

Figure 29 shows the radiation resistance of the spiralpole antenna obtained from Ansoft HFSS at resonance and the radiation resistance of the dipole from Ansoft HFSS at the same frequency. As can be seen the dipole radiation resistance is about 1.3 Ohms. The spiralpole antenna radiation resistance at this resonance is about 1.7 Ohms. This represents an increase of about 31 % in radiation resistance as compared to the dipole antenna. Figure 30 shows the $Q - kr$ curves for the spiralpole antenna and the dipole antenna. From the graph, it can be seen the spiralpole antenna performs significantly better than the dipole for values of kr less than 0.3 (at which resonance occurs). The first resonance now occurs at a lower frequency of about 95 MHz due to the increased inductance of the spiral. The E and H plane patterns are shown in Figure 31. Once again, the pattern is almost identical to the dipole pattern, with the azimuthal null being marginally less pronounced.

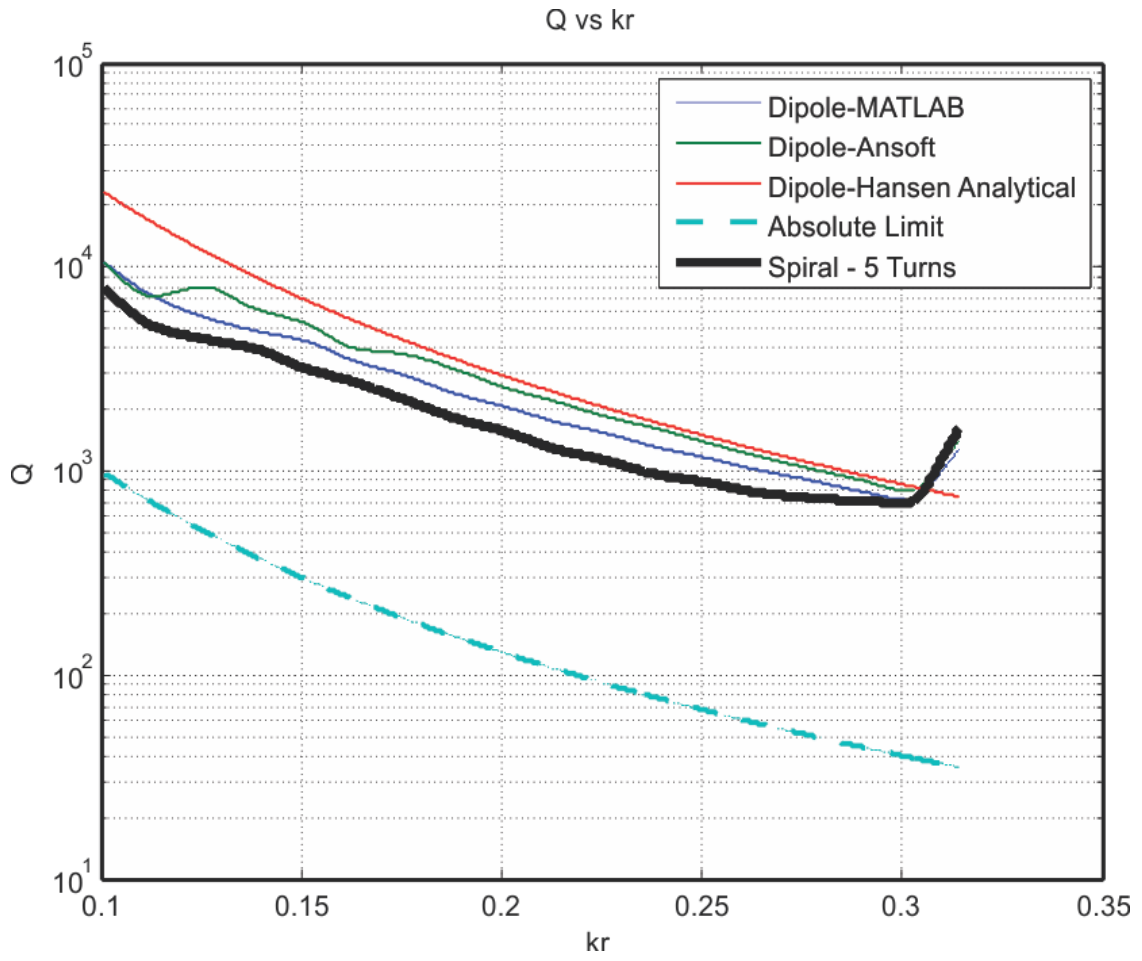
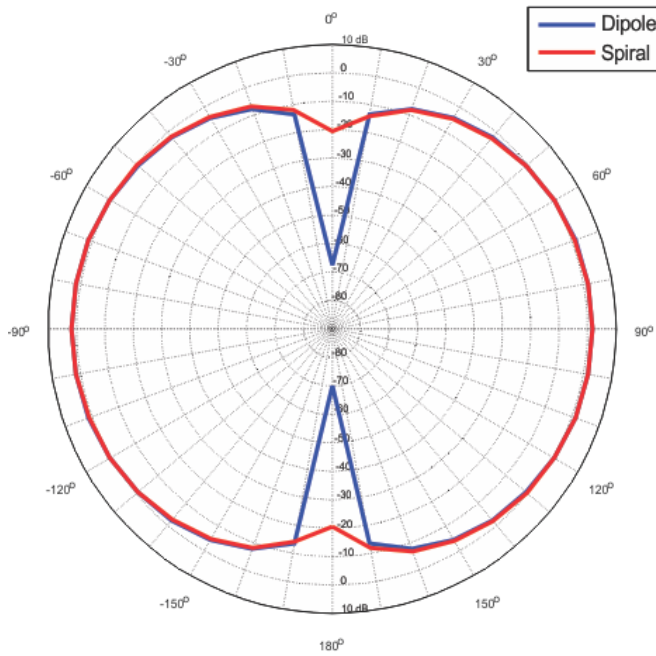


Figure 30: Q - kr for 5 turn spiral VS dipole and absolute limit

5 turn spiral VS Dipole Pattern: E Plane @95 MHz



5 turn spiral VS Dipole Pattern: H Plane @95 MHz

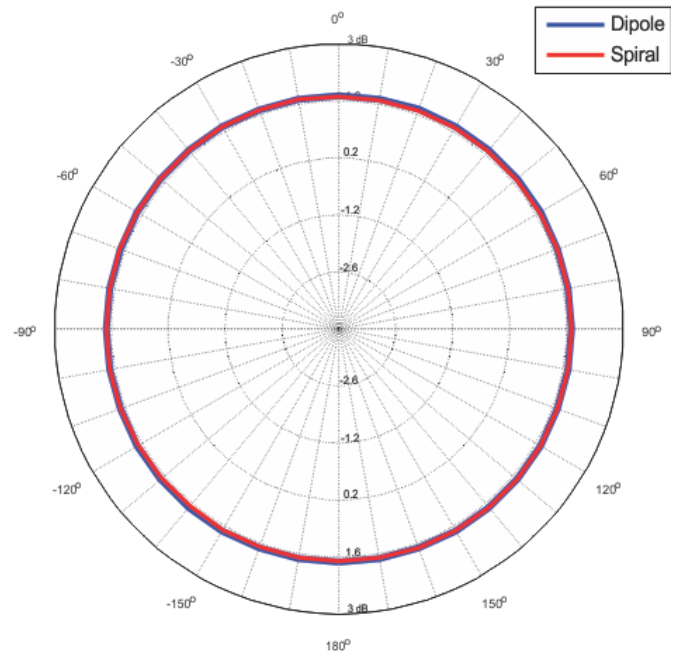


Figure 31: E and H Plane radiation pattern overlays for 5 turn spiralpole and dipole antennas at spiralpole resonance

5.3.4 6 Turn Spiralpole

The final candidate in our comparison is the 6 turns spiralpole antenna. The antenna configuration is shown in Figure 32. The number of turns is now very significant. The shaft length is now much smaller to accommodate for the increased spiral radius.

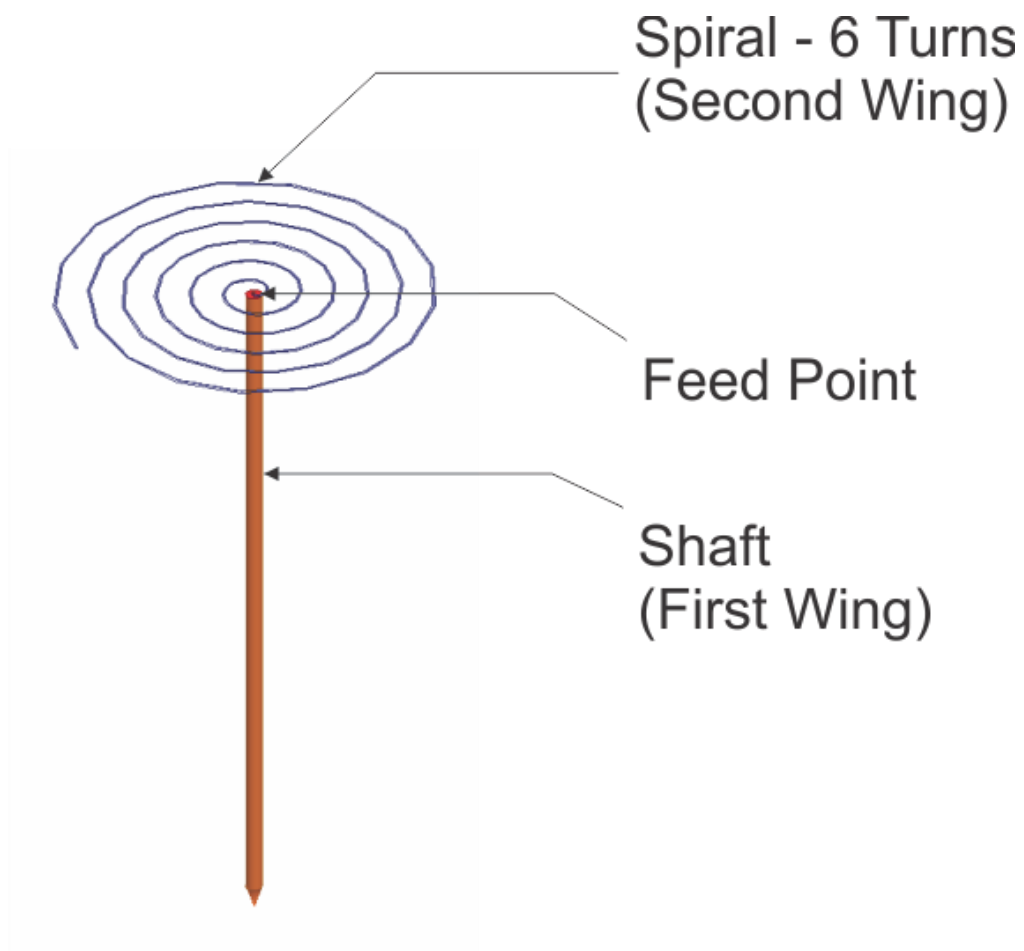


Figure 32: Six turn Spirapole

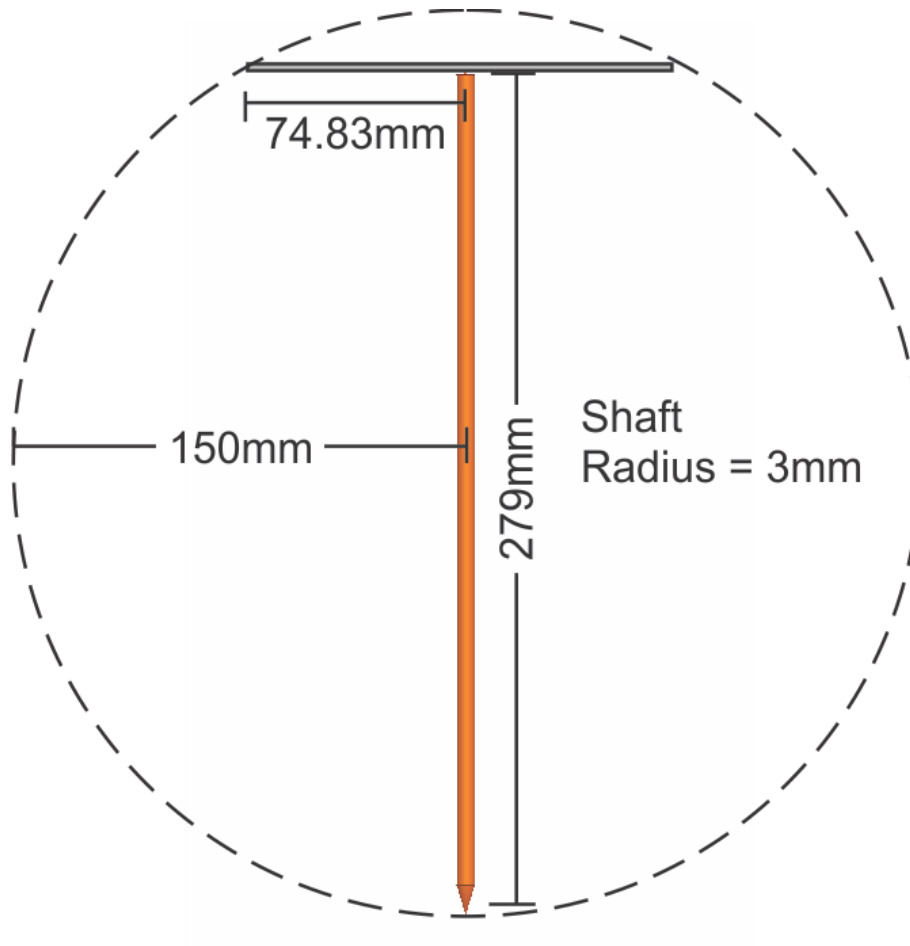


Figure 33: Six turns spiralpole in Chu Sphere

The six turns spiralpole antenna in the Chu sphere is shown in Figure 33. The final spiral radius is now 74.83mm and the shaft height is 275mm. The total length of the spiral is 713mm. The total spiralpole antenna length is therefore 988mm. The analytical resonant length model predicts the resonance to be at 71.7 MHz and the analytical first order impedance approximate predicts the resonance to occur at 69 MHz.

Spiral-pole impedance comparison- Theory vs Simulation

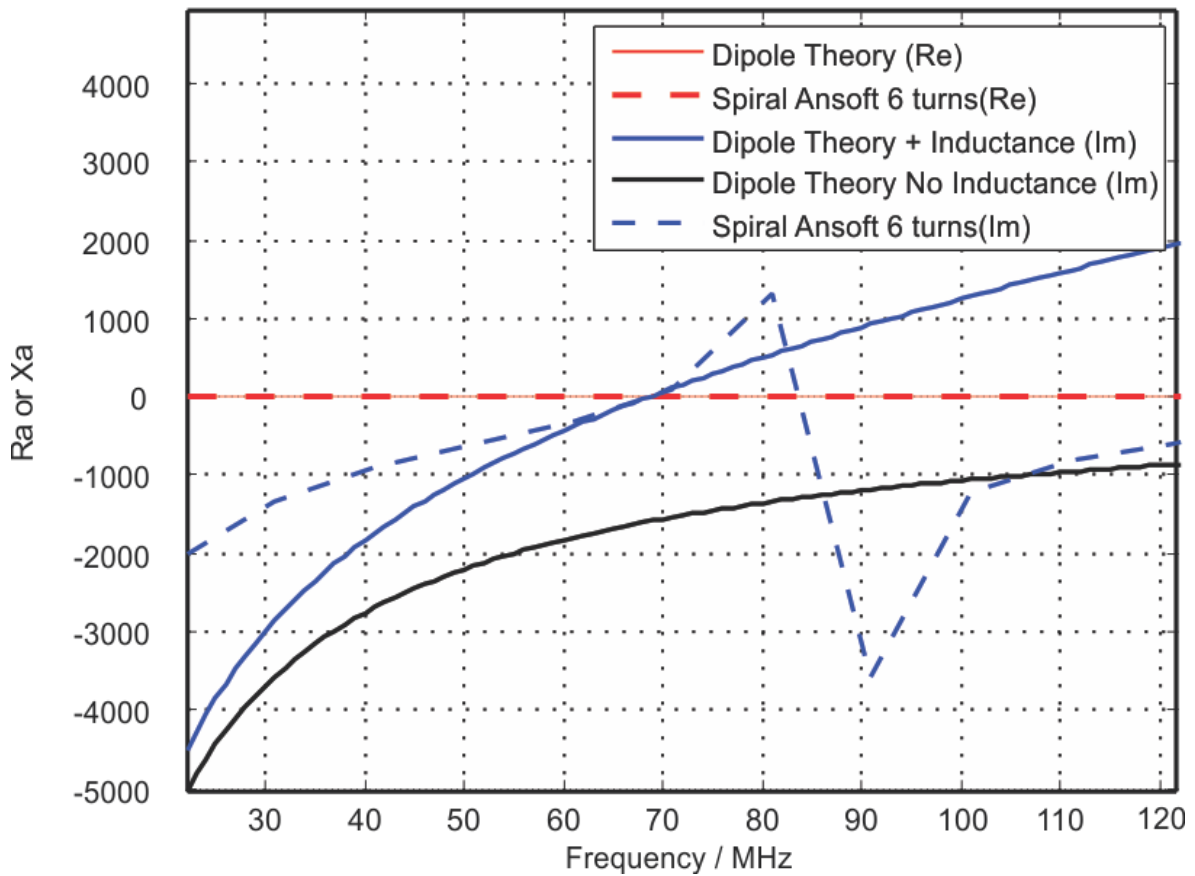


Figure 34: Simulated VS analytical Dipole and 6 turn spiralpole impedances

The true resonance is seen to occur at 69 MHz as well. Both the analytical models predict the antenna resonance quite accurately. This is due to the spiral contribution now being very significant. Figure 35 shows the radiation resistance of the spiralpole antenna compared to the dipole antenna at the spiralpole resonance. The spiralpole radiation resistance is 1.15 Ohms where as the dipole radiation resistance is about 0.65 Ohms. This represents an increase of 76.92 % in radiation resistance as compared to the dipole.

Spiralpole and Dipole Radiation Resistance Comparison

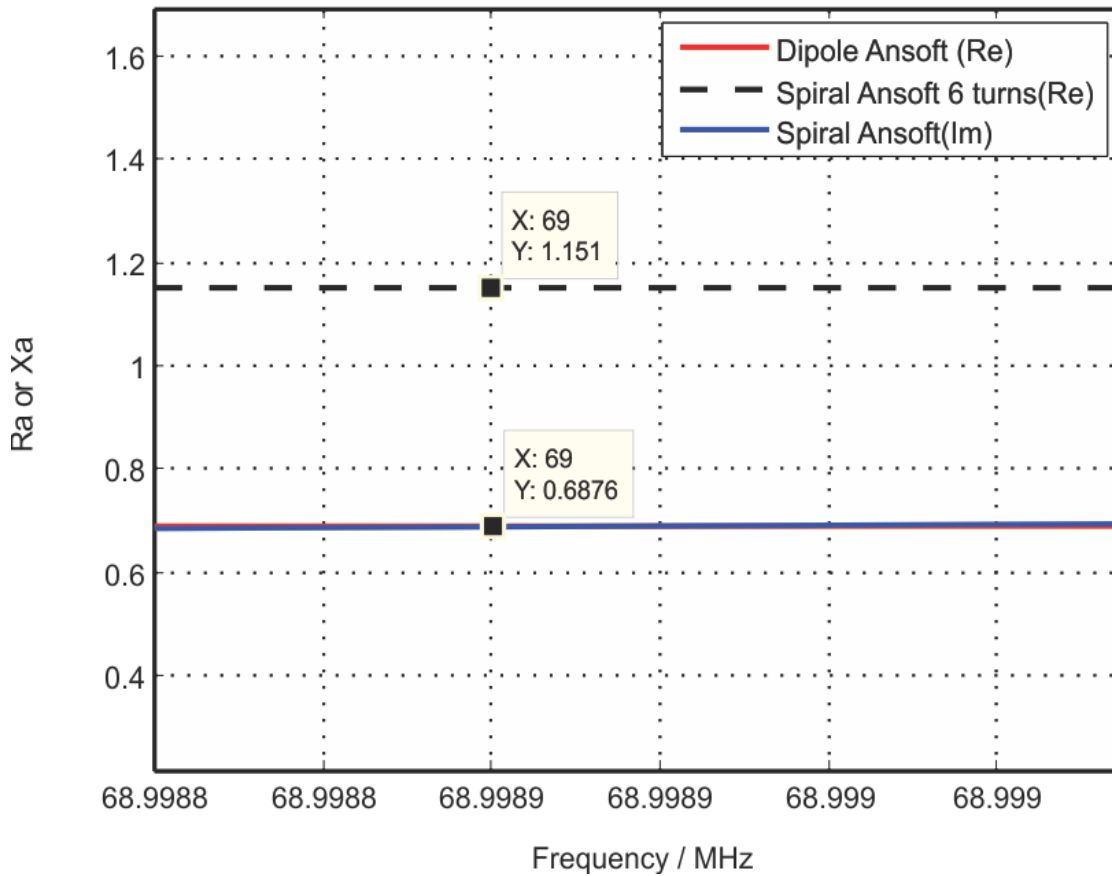


Figure 35: Radiation resistance comparison of 6 turns spiralpole and dipole antennas at resonance

Figure 36 shows the $Q - kr$ relationship of the dipole antenna and the spiralpole antenna up to the resonance at $kr \cong 0.22$. Due to the large spiral size, the antenna uses the volume in the Chu sphere very efficiently and thus the spiralpole antenna outperforms the dipole antenna by quite significantly. Figure 37 shows the E and H plane radiation patterns obtained from Ansoft HFSS simulations for the dipole and spiralpole antenna at resonance. Once again, the radiation pattern mimics that of the small dipole, with a maximum azimuthal gain of about 1.7 dB.

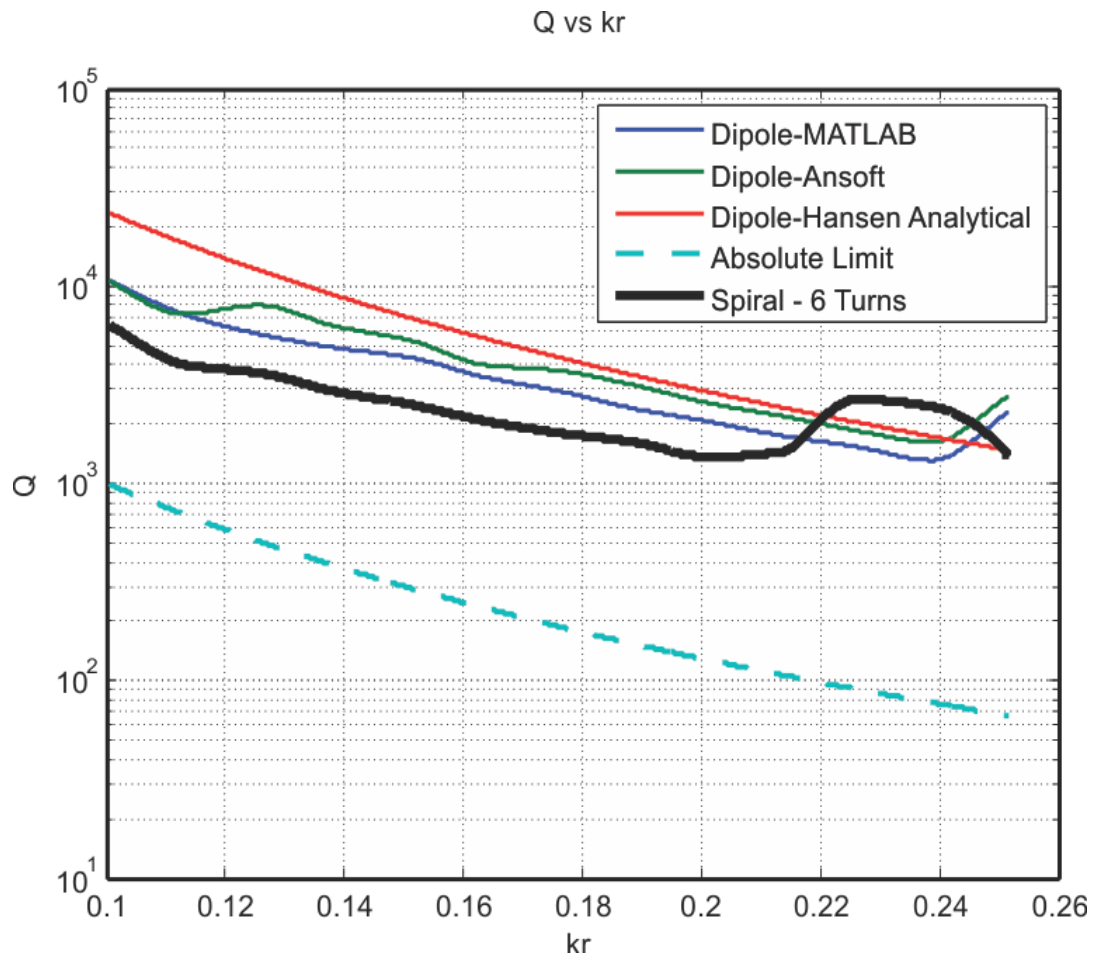
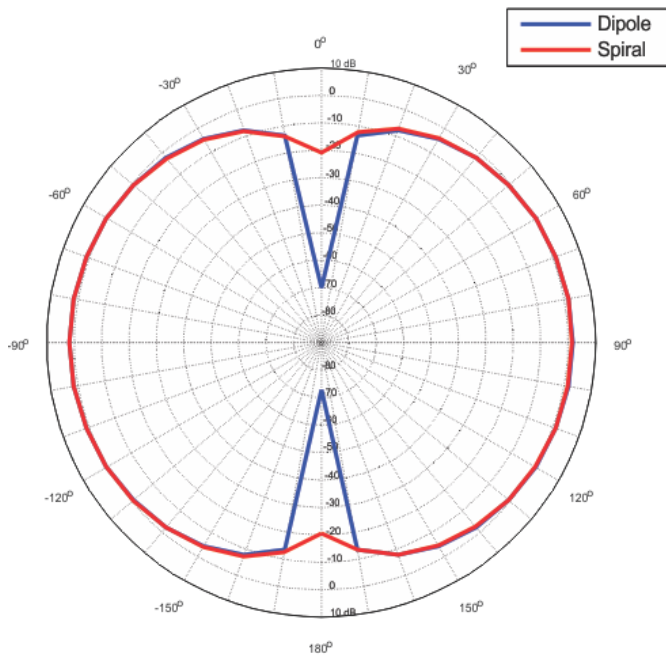


Figure 36: Q - kr for 6 turns spiral VS dipole and absolute limit

6 turn spiral VS Dipole Pattern: E Plane @68MHz



6 turn spiral VS Dipole Pattern: H Plane @68MHz

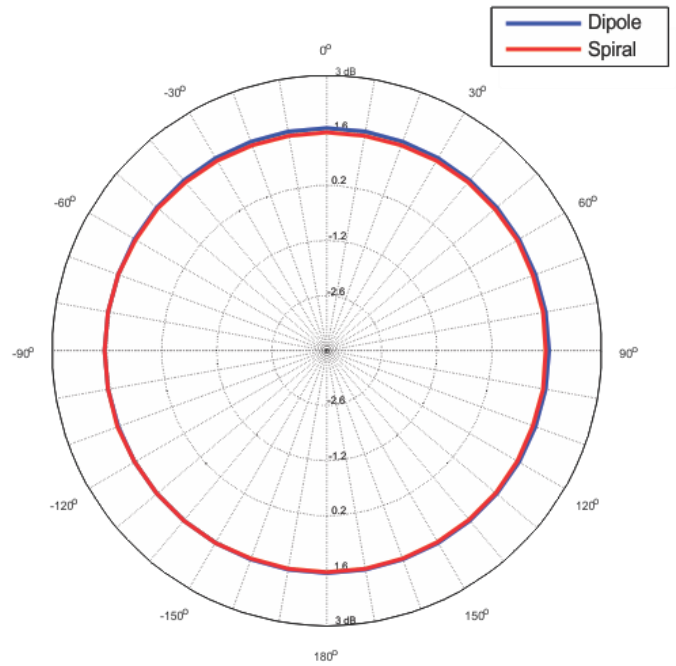


Figure 37: E and H plane radiation plot comparison of 6 turn spiralpole and dipole antennas at spiralpole resonance

6 Hardware Prototype

The spiralpole antenna structure is well suited for deployment as a food probe used for wireless temperature sensing. The spiral is enclosed in a casing that can be conveniently held in one's hand, enabling the probe to be placed in the object whose temperature is to be measured. Since, the sensor and the spiral are within the shaft and the protective casing, no chemical damage can be caused to the contents. The shaft is also made of stainless steel and is free from corrosion and other chemical attacks. Figure 38 shows two versions of the wireless food probe, courtesy of Vectron International, Hudson, NH. The spiral and the SAW sensor are enclosed inside.

The temperature is monitored wirelessly using this device. As the temperature around the shaft changes, the properties of the SAW sensor also change. The reader (transmitter) transmits a signal and the passive RFID – like SAW sensor responds with a signal that reflects the properties of the SAW sensor. These property changes in the SAW sensor are translated at the reader into temperature metrics. The

temperature was increased from 20 °C to 100 °C gradually. Figure 39 shows the results obtained when measuring the temperature of a turkey that is cooking in an oven. Both spiralpole based and wired probes were measuring simultaneously.

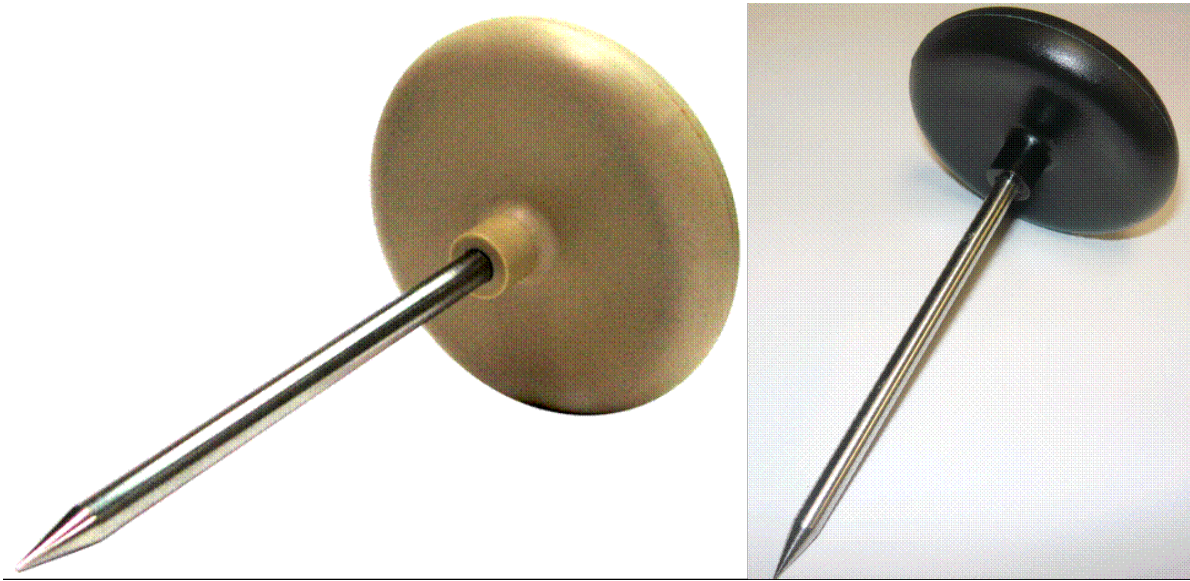


Figure 38: Actual food probe produced by Vectron International, Hudson, NH

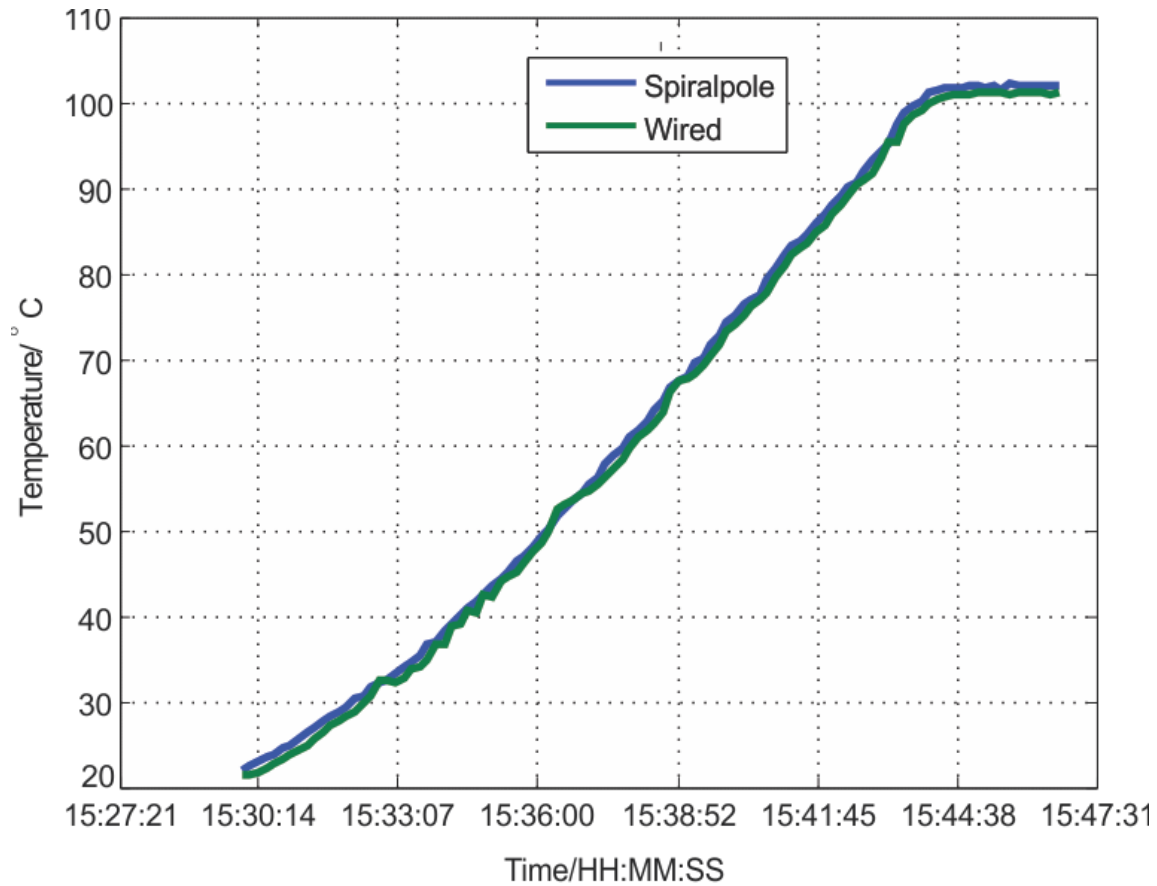


Figure 39: Temperature sensing data acquired with the spiralpole based foodprobe and a wired thermoelement. The spiralpole based wireless solution shows excellent accuracy.

7 Conclusion

A novel electrically small spiralpole antenna that is a hybrid between a dipole antenna and a spiral antenna has been described in this thesis. Two analytical models for the spiralpole antenna have been developed and shown to agree with numerical results. The first model uses a reactance approximation where the resonant frequency is deduced from approximating the reactance of the spiralpole as the reactance of a small dipole with a spiral inductor in series. The second model uses a resonant length approximation, assuming the combined length of the spiral and the shaft is half-wavelength long. The spiralpole antenna was compared to the small dipole using $Q - kr$ relationships, radiation resistance and radiation patterns. Of most importance is the $Q - kr$ relationship since this is essentially the “business card” of the small antenna. The relationship between bandwidth and Q of a small tuned

antenna was briefly discussed. Using this definition of bandwidth and Q , the $Q - kr$ relationship for a dipole antenna with half-length to wire radius ratio of 50 was obtained using MATLAB and ANSOFT\ANSYS HFSS. Hansen's analytical $Q - kr$ expression for the same dipole was also used for comparison and all three $Q - kr$ curves for the small dipole were shown to agree. The absolute Chu $Q - kr$ limit was also presented. The spiralpole $Q - kr$ for three, four, five and six turns were then obtained using the same methodology used for the dipole. The spiralpole antenna is shown to outperform the small dipole quite significantly with increasing number of turns for decreasing values of kr . The radiation resistance of the spiralpole antenna is higher than that of the equivalent small dipole for all spiralpole configurations. The highest increase in radiation resistance for the spiralpole was 77% when compared to the small dipole. The reason for this improved performance is that the spiralpole antenna used the volume of the enclosing Chu sphere much more effectively. The radiation pattern (directivity) of the spiralpole antenna was shown to be almost identical to the equivalent electrically small dipole. The spiralpole antenna was shown to be naturally resonant and thus does not require any external matching circuitry. This leads to lower ohmic losses and increased efficiency of the spiralpole antenna, as external matching circuits introduce further ohmic losses.

8 Appendix A: MATLAB Codes

Q – *kr* curve calculation:

```
%Author: ISHRAK KHAIR
% LAST UPDATED: 5/9/11

% Description:
% This script calculates the Q-kr relationship of a dipole antenna
% for 100% efficiency and h/a = 50, where 'h' is the half length and a is
% the dipole radius. The frequency is varied from 31.8 MHz to 477 MHz and
% the dipole length is fixed at 300mm. The half length to wire radius ratio
% is 50. The result is compared with ANSOFT and HANSEN's analytical Q
% expression

clear all; clc; close all;
%% Initialization

epsilon = 8.85418782e-012; % vacuum, F/m
mu = 1.25663706e-006; % vacuum, H/m
c = 1/sqrt(epsilon*mu); % vacuum, m/s
params.delta_f=(1e6);
params.delta_f_interp = .1e6/6;
params.sweep_start = 32e6;
stopVals = [1e9 1e9 240e6 180e6 100e6 80e6];
turns = 4;
params.sweep_stop = stopVals(turns);
params.freq =params.sweep_start:params.delta_f:params.sweep_stop; %
frequency in Hz =
params.freq_interp
params.sweep_start:params.delta_f_interp:params.sweep_stop;
k = 2*pi*params.freq_interp/c;
thick_ratio = 150;
hlA = 150e-3; % dipole half length
r = hlA; % radius of the surrounding sphere
lA = 2*hlA; % dipole total length
a = hlA/thick_ratio; % wire radius

%% Impedances

Za_analytical = dipole(params.freq,lA,a);
Data_in = csvread('dipole_1_to_300.csv',1,0);
freq_an = (1e6)*Data_in(:,1);
Ra = Data_in(:,3);
Xa = Data_in(:,2);
Za_ansoft = Ra + 1i*Xa;
Za_analytical_interp = interp1(params.freq,Za_analytical, params.freq_interp,
'cubic');
Za_ansoft_interp = interp1(freq_an, Za_ansoft, params.freq_interp, 'cubic');

Data_in = csvread(['spiral_' num2str(turns) 'turns_1_to_300.csv'],1,0);
freq_an = (1e6)*Data_in(:,1);
Ra = Data_in(:,3);
Xa = Data_in(:,2);
Za_spiral = Ra+1i*Xa;
Za_spiral_interp = interp1(freq_an, Za_spiral, params.freq_interp, 'cubic');

for i =1:(length(params.freq_interp))
```

```

params.i = i;
params.Za = Za_analytical_interp;
[f_lower, f_upper, f_c] = find_3dB(params);
Analytical_FBW_mat = (f_upper-f_lower)/f_c;
Q_mat(i) = 2./Analytical_FBW_mat;
params.Za = Za_ansoft_interp;
[f_lower, f_upper, f_c] = find_3dB(params);
Analytical_FBW_ansoft = (f_upper-f_lower)/f_c;
Q_ansoft(i) = 2./Analytical_FBW_ansoft;
params.Za = Za_spiral_interp;
[f_lower, f_upper, f_c] = find_3dB(params);
Analytical_FBW_ansoft = (f_upper-f_lower)/f_c;
Q_spiral(i) = 2./Analytical_FBW_ansoft;

stopBar= progressbar(i/length(params.freq_interp),0);

if (stopBar)
    break;
end

end

if (~stopBar)
kr = k*r;
figure(2)
skip =1;
Q_mat_s = Q_mat(1:skip:end);
Q_ansoft_s = Q_ansoft(1:skip:end);
Q_spiral_s = Q_spiral(1:skip:end);
Q_mat_smooth = pchip(kr(1:skip:end), Q_mat_s, kr);
Q_ansoft_smooth = pchip(kr(1:skip:end), Q_ansoft_s, kr);
Q_spiral_smooth = pchip(kr(1:skip:end), Q_spiral_s, kr);
Q_hansen = (6*(log(hlA/a)-1))./((k.^2).*(hlA^2).*tan(k*hlA));
Q_abs = (1./kr + 1./(kr.^3));
semilogy(kr,Q_mat_smooth, kr, Q_ansoft_smooth, kr, Q_hansen, kr, Q_abs, '--
');hold on;
semilogy(kr, Q_spiral_smooth, 'k','linewidth', 3);
legend({'Dipole-MATLAB','Dipole-Ansoft', 'Dipole-Hansen Analytical',
'Absolute Limit', ['Spiral - ' num2str(turns) ' Turns']});
grid on; title('Q vs kr');
xlabel('kr'); ylabel('Q');
end

```

Analytical Impedance Model

```

% AUTHOR: Ishrak Khair
% Script to compare theoretical spiral pole impedance to linear first order
% impedance approximate
clear all; close all; clc;
%% Initialization
epsilon = 8.85418782e-012; % vacuum, F/m
mu = 1.25663706e-006; % vacuum, H/m
c = 1/sqrt(epsilon*mu); % vacuum, m/s
params.delta_f=(1e6);
params.sweep_start = 1e6;
params.sweep_stop = 300e6;
params.freq =params.sweep_start:params.delta_f:params.sweep_stop; %
frequency in Hz

```

```

thick_ratio = 50;
hlA = 150e-3; % dipole half length
r = hlA; % radius of the surrounding sphere
lA = 2*hlA; % dipole total length
a = hlA/thick_ratio; % wire radius
DipoleData = csvread('../..'/Chu_Limit/dipole_1_to_300.csv', 1,0);
w = 2*pi*DipoleData(:,1)*1e6;
turns = 3;
%% Inductance approximate from paper
% emperical coefficients
c1 = 1.07;
c2 = 2.29;
c3 = 0;
c4 = 0.19;
K1 = 2.34;
K2 = 2.75;
beta = 1.33e-3;
a1 = -1.21;
a2 = -0.163;
a3 = 2.43;
a4 = 1.75;
a5 = -0.049;

width = 1e-3;
spacing = 12e-3;
n = turns; % number of turns
d_out = (2*74.83)*1e-3; % outer diameter
d_in = 0; % inner diameter
d_avg = d_out; % average diameter
rho = (d_out - d_in)/(d_out + d_in); % fill ratio 1

L_gmd = 0.5*mu*(n^2)*d_avg*c1*(log(c2/rho) + c3*rho + c4*(rho^2));
L_mw = K1*mu*(n^2)*d_avg/(1+K2*rho);
L_mon = beta*(d_out^a1)*(width^a2)*(d_avg^a3)*(n^a4)*(spacing^a5);
reactance_spiral = w*L_mw;

%% Theory Spiral pole Impedance

% Za_analytical = DipoleData(:,3) + 1i*DipoleData(:,2);
Za_analytical = dipole(1e6*DipoleData(:,1), lA,a);
Za_approximate = real(Za_analytical) + (1i*imag(Za_analytical) +
1i*reactance_spiral);

%% Ansoft Spiral pole Impedance
Data_in = csvread(['../..'/Chu_Limit/spiral_' num2str(turns)
'turns_1_to_300.csv'], 1,0);
freq_an = (1e6)*Data_in(:,1);
Xa = Data_in(:,2);
Ra = Data_in(:,3);
Za_spiral = Ra+1i*Xa;

%% Graphics
plot(freq_an/1e6, real(Za_analytical), '-r', freq_an/1e6, Ra, '--r');hold on;
plot(freq_an/1e6, imag(Za_approximate), '-b', freq_an/1e6,
imag(Za_analytical), 'k',freq_an/1e6, Xa, '--b');
grid on; ylim([-2e4 1e4]);

```

```

legend('Dipole Theory (Re)', ['Spiral Ansoft ' num2str(turns) ' turns(Re)'],
'Dipole Theory + Inductance (Im)', 'Dipole Theory No Inductance (Im)',
['Spiral Ansoft ' num2str(turns) ' turns(Im)']);
title('Spiral-pole impedance comparison- Theory vs Actual');
xlabel('Frequency / MHz'); ylabel ('Ra or Xa');

```

Analytical Resonant Length model

```

%AUTHOR: Ishrak Khair
%Analytical Resonant Length Model
% This script calculates the length of the spiral wing and
% calculates the resonance frequency of the spiralpole using
% the half-wavelength resonant length model

epsilon = 8.85418782e-012; % vacuum, F/m
mu = 1.25663706e-006; % vacuum, H/m
c0 = 1/sqrt(epsilon*mu);
turns = 6;
theta=turns*2*pi;
s=0.5*(theta*sqrt(1+theta^2)+log(theta + sqrt(1+theta^2)))*1e-3;
probe_height = 290.5*1e-3;
total_length = s+probe_height;
lambda = 2*(total_length);
f0 = c0/lambda

```

Dipole Analytical Impedance

```

function [Za] = dipole(f, lA, a);
% This script calculates the analytical impedance of a dipole antenna
% with length lA, wire radius a and over the band prescribed by f

epsilon = 8.85418782e-012; % vacuum, F/m
mu = 1.25663706e-006; % vacuum, H/m
c = 1/sqrt(epsilon*mu); % vacuum, m/s
eta = sqrt(mu/epsilon); % vacuum, Ohm
l = lA/2; % dipole half length
k = 2*pi*f/c; % wavenumber
z = k*l; % electrical length corresponding to l
R = -0.4787 + 7.3246*z + 0.3963*z.^2 + 15.6131*z.^3;
X = -0.4456 + 17.0082*z - 8.6793*z.^2 + 9.6031*z.^3;
Za = R - j*( 120*(log(l/a)-1)*cot(z)-X ); % Antenna impedance

```

Plotting Temperature Curves for Wireless and Wired Food Probes

```

% 08/10/2011
% This script simply reads the recorded data temperatyre data and plots its
% against time. The data is courtesy of Vectron International
% AUTHOR: Ishrak Khair
clear all; close all; clc;
data = csvread('data00.csv', 1,1);
wireless = data(:,1);
wired = data(:,2);
fid = fopen('data00.csv');
t = textscan(fid, '%s %s %s', 'delimiter', ',');

```

```

t1 = t{:};
t1(1) = [];
d1 = datenum(t1, 'HH:MM:SS');
fclose(fid);
figure(1)
plot(d1,wireless, d1,wired); legend('Spiralpole', 'Wired');
datetick('x', 'HH:MM:SS', 'keepticks'); xlabel('Time/HH:MM:SS');
ylabel('Temperature/ ^\circ C'); grid on;

```

9 Appendix B: Dipole H - Plane pattern discrepancy in Ansoft

HFSS

An interesting discrepancy has been observed when plotting the H-plane pattern of a dipole in HFSS 12.

The dipole, which is essentially a linear wire antenna of resonant length $\frac{\lambda}{2}$ should have a symmetrical pattern about its axis (H-plane). At the resonant frequency especially, the dipole pattern should be almost the same throughout. This is the case when a $\sim \frac{\lambda}{2}$ length cube is used as a radiation box for the simulation. The radiation pattern in the H-plane significantly changes when the size of the radiation box is increased dramatically. In our case, the length of the antenna is 300mm. This means the wavelength is 600mm long at resonance and corresponds to a frequency of 500MHz. The plots below and their respective model details show the discrepancy described at 600 MHz.

9.1.1 Model 1

<i>Paramater</i>	<i>Value</i>
Dipole Length	300mm
Radiation Box Size	400mm by 400mm by 400mm
Number of Passes	9
Delta S	1e-006

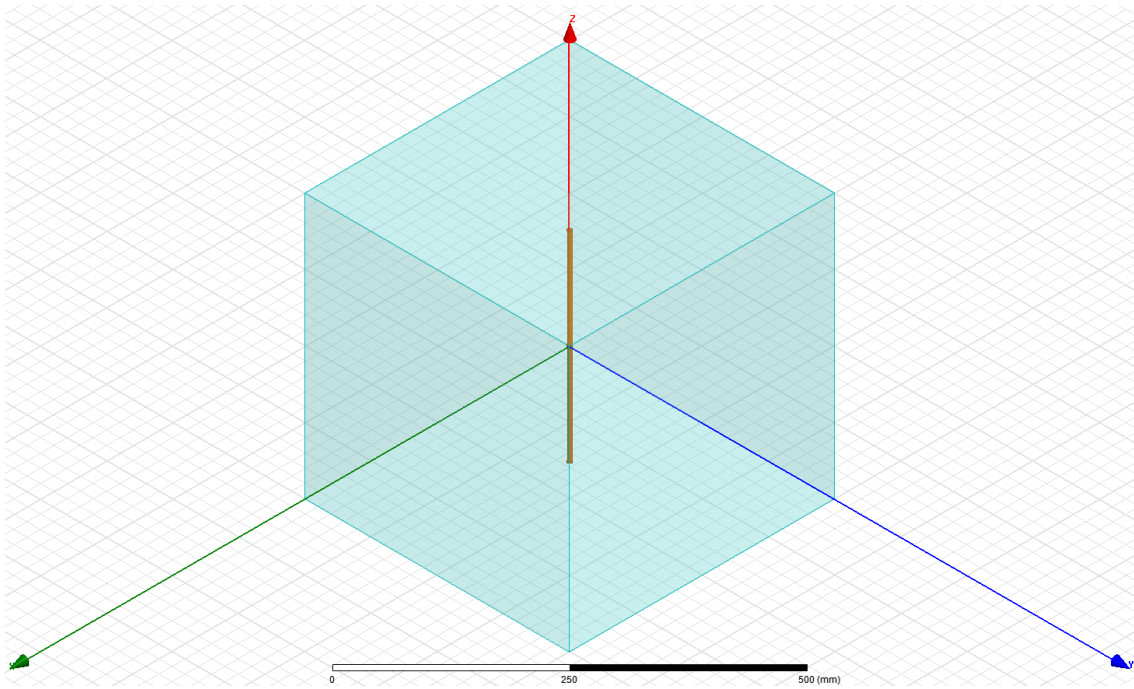


Figure 40: 300mm dipole with cubic radiation box of side length 400mm

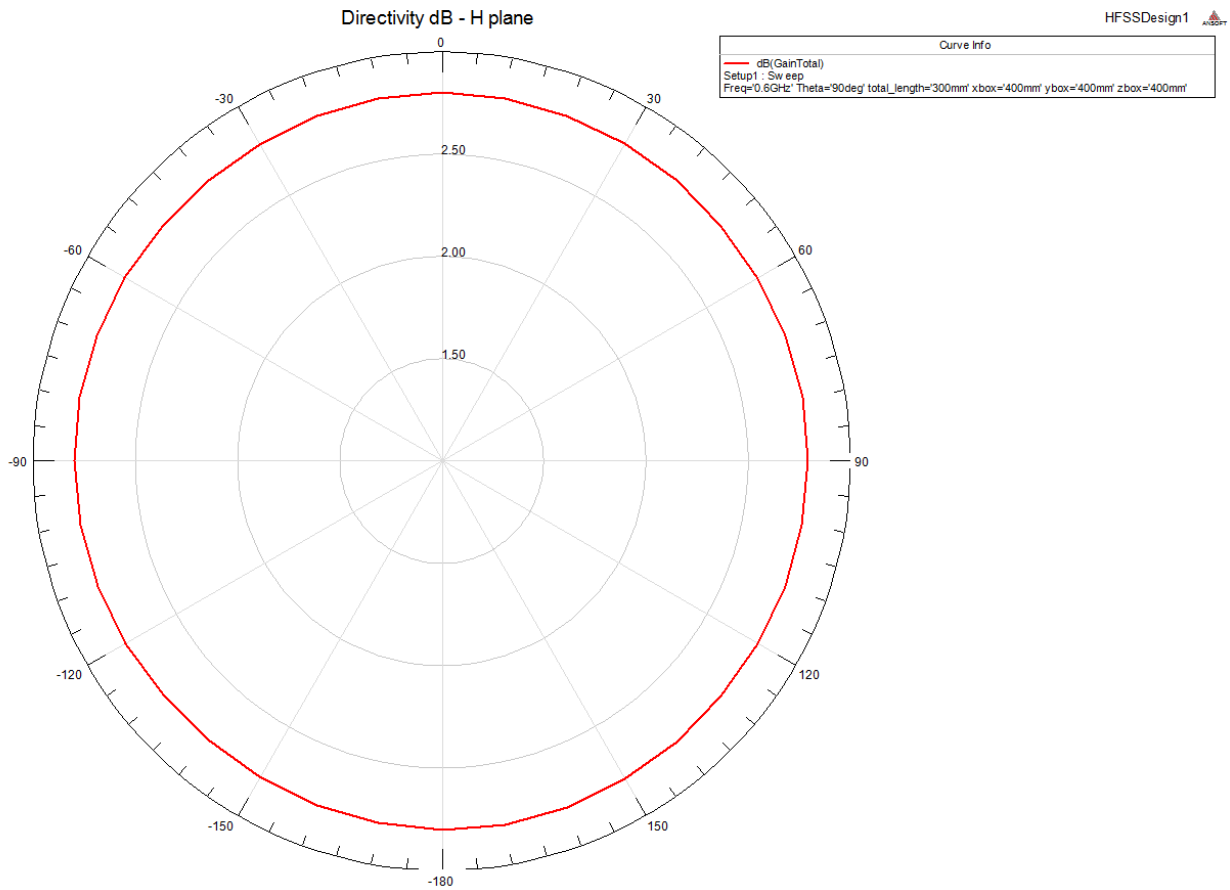


Figure 41: Radiation Pattern in the H plane at 600 MHz. Notice the symmetrical results obtained

9.1.2 Model 2

<i>Parameter</i>	<i>Value</i>
Dipole Length	300mm
Radiation Box Size	2500mm by 2500mm by 2500mm
Number of Passes	9
Delta S	1e-006

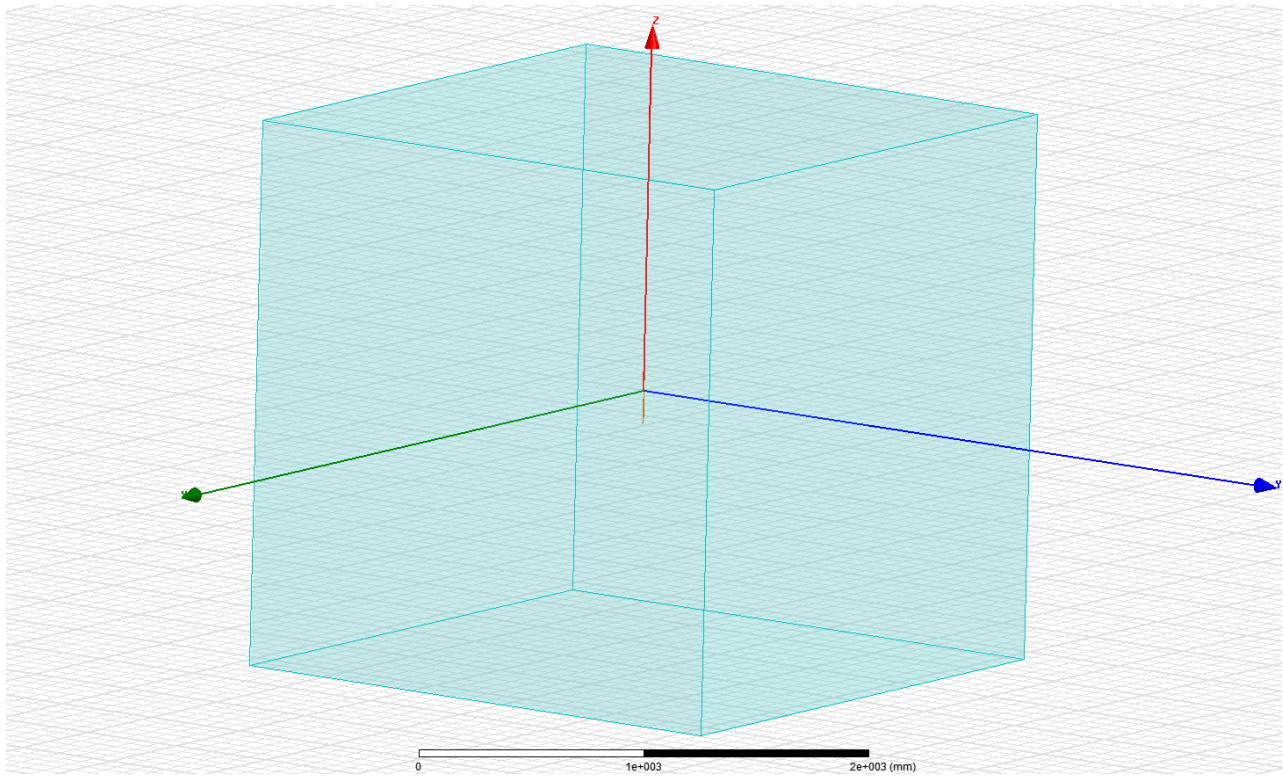


Figure 42: 300mm dipole within cubic radiation box of side length 2500mm

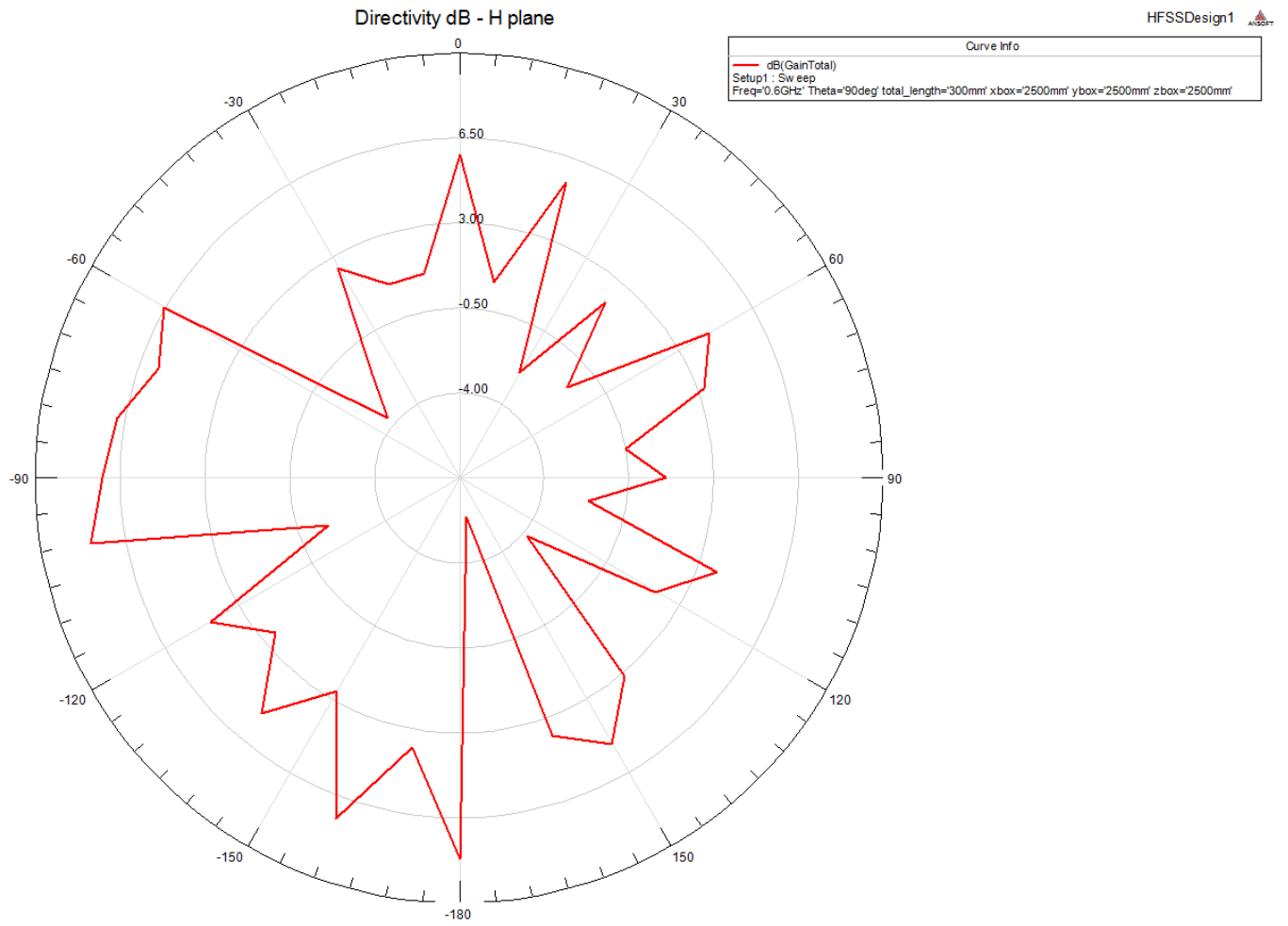


Figure 43: Radiation Pattern in the H plane at 600 MHz. Notice the irregular pattern.

10 Appendix C: Disk – dipole hybrid antenna results

Before the spiralpole antenna design, a disk based dipole hybrid was investigated in the attempts to create a resonant antenna at 433 MHz. The disk antenna design was simple enough and fit well into the wireless food probe design adopted by Vectron Intl. Simulation results however showed that the antenna was not resonant at the desired frequency, given the required antenna size. Figure 44 shows the antenna design in Ansoft/ANSYS HFSS. The design consists of a probe or shaft as one wing. The second wing of the antenna is the top disk. The disk is surrounded by a dielectric of $\epsilon_r = 3.2$ that corresponds to the heat resistant PEEK material used in manufacturing food probes. The feed arrangement is the same as the spiralpole antenna. Figure 45 shows the impedance from 350 MHz to 600 MHz. The reactance is mostly capacitive. As such, the logical approach was to replace the disk with a spiral which would increase the reactance and bring the resonance to the lower frequencies (433 MHz). However, this comes at a compromise with radiation resistance since the spiral aperture is less than the solid disk. Figure 46 shows the return loss (S11) in dB of the disk-dipole hybrid from 350 MHz to 600 MHz. Once again, it is seen from this figure that the antenna is not resonant at these frequencies, but is approaching resonance at higher frequencies.

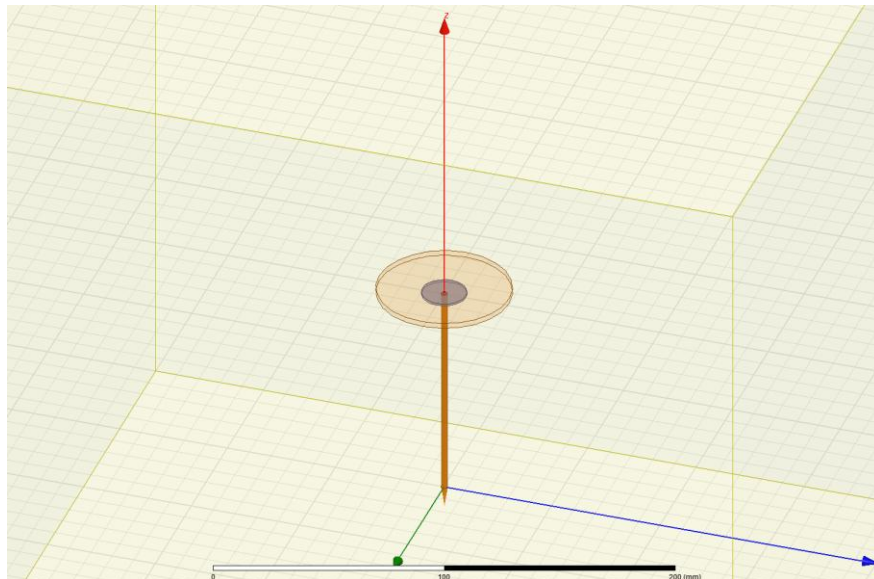


Figure 44: Initial disk-dipole hybrid design in Ansoft\ANSYS HFSS.

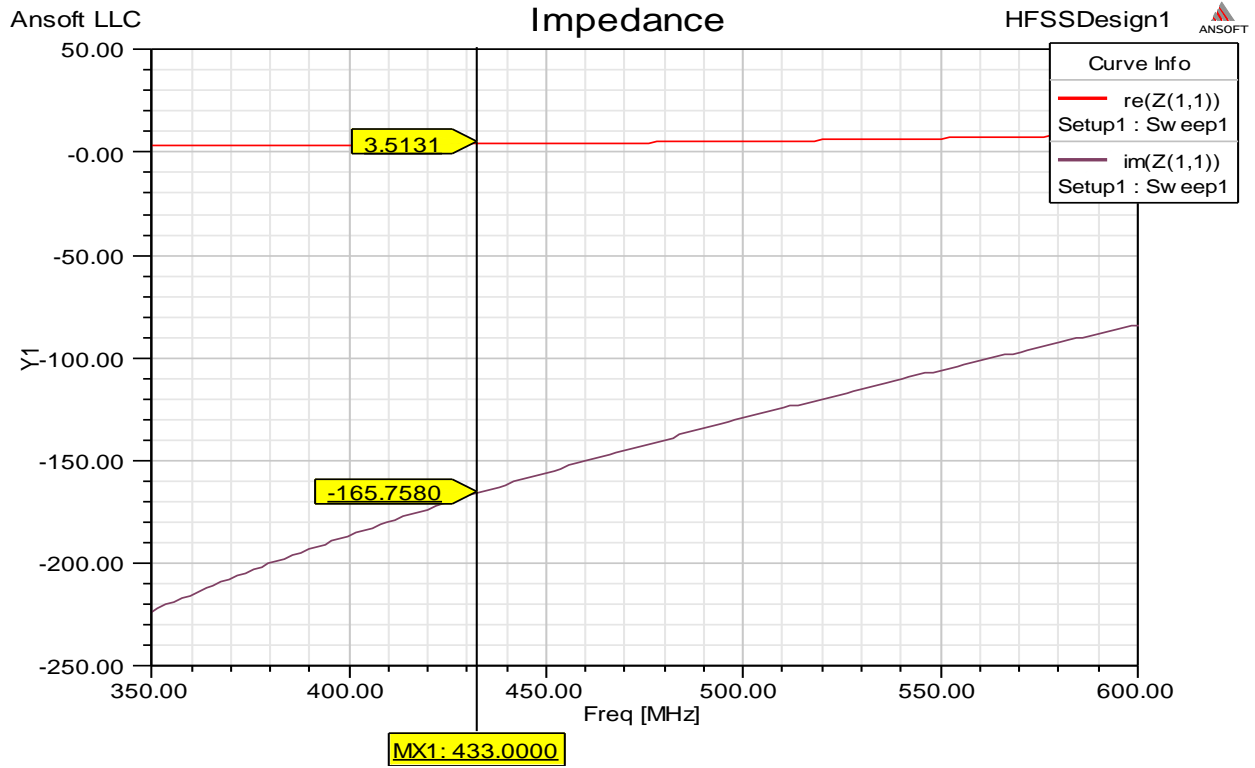


Figure 45: Impedance of disk-dipole hybrid antenna from 350 MHz to 600 MHz. The antenna reactance is primarily capacitive.

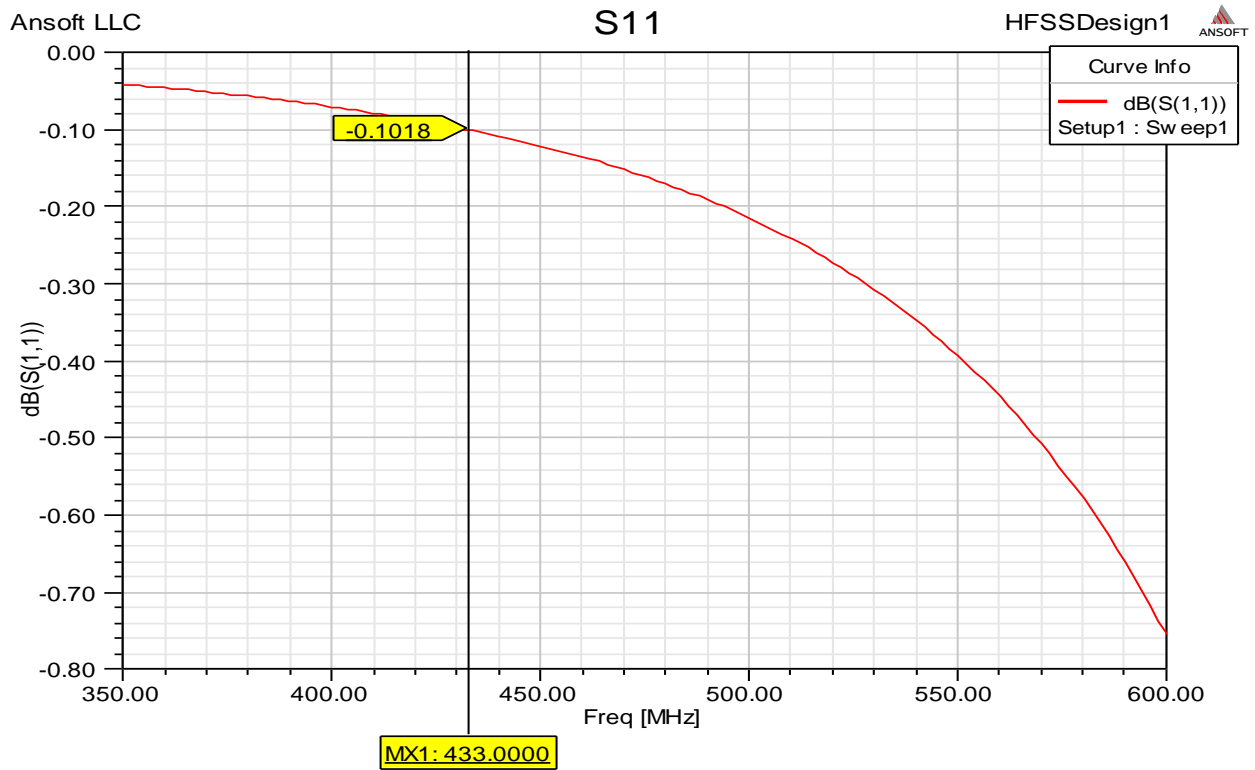


Figure 46: Return Loss (S11) in dB from 350 MHz to 600 MHz of the disk-dipole hybrid. The antenna is starting to resonate at higher frequencies.

11 Bibliography

- [1] James Clerk Maxwell, *A Treatise on Electricity and Magnetism*. London, United Kingdom: Clarendon Press, 1873.
- [2] Constantine Balanis, *Antenna Theory Analysis and Design*. Hoboken, New Jersey, United States: Wiley Interscience, 2005.
- [3] Jack Ramsay, "Highlights of Antenna History," *IEEE Antennas and Propagation Society Newsletter*, pp. 8-20, December 1981.
- [4] Sergey N. Makarov, *Antenna and EM Modelling with MATLAB*. New York, United States and Canada: Wiley Interscience, 2002.
- [5] Electrical Small Antennas: A Review, "R.A Burberry," *IEE Colloquim on Electricall Small Antennas*, pp. 1-5, October 1990.
- [6] Brian S. Collins, "Small Antennas for the Reception of Future Mobile Television Services," Antenova Ltd, Cambridge, UK,.
- [7] Daniel Stevens and Sabah Sabah, "Applications of Wireless Temperature Using SAW Resonators," Vectron International, Hudson, NH,.
- [8] Glenn S. Smith, "Efficiency of Electrically Small Antennas Combined with Matching Networks," *IEEE Transactions on Antennas and Propagation*, pp. 369-373, May 1977.
- [9] Gary Breed, "Basic Principles of Electrically Small Antennas," *High Frequency Electronics*, pp. 50-53, 2007.
- [10] R.C Hansen, *Electrically Small, Superdirective and Superconducting Antennas*. Hoboken, New Jersey, USA: Wiley Interscience, 2006.
- [11] L. J. Chu, "Physical Limitations of Omnidirectional Antennas," Massachusetts Institute of Technology, Research Laboratory of Electronics, Boston, Technical Report MAg 1948.
- [12] James S. McLean, "A Re-Examination of the Fundamental Limits on the Radiation Q of Electrically Small Antennas," *IEEE Transactions on Antennas and Propagation*, vol. 44, no. 5, MAY 1996.
- [13] R.M. Fano, "Theoretical Limitations of the Broadband Matching of Arbitrary Impedances," Massachusetts Institute of Technology, Boston, Technical 1948.
- [14] S.R Best, "The Radiation Properties of Electrically Small Folded Spherical Helix Antennas," *IEEE Transactions on Antennas and Propagation*, vol. 52, no. 4, p. 953, April 2004.
- [15] Gary Breed, "Basic Principles of Electrically Small Antennas," *High Frequency Electronics*, pp. 50-53,

2007.

- [16] R. Bawer and J.J. Wolfe, "The Spiral Antenna," Alexandria, VA,.
- [17] Chan Won Jung and Franco De Flaviis, "Tilt Beam Characteristic by Changing Length of Finite-Sized Square Dielectric Substrate of One Arm Rectangular Spiral Antenna," *Proc. IEEE Asia Pacific Microwave Conference*, 2003.
- [18] J.H.Choi, K.B. Kong, H.S. Lee and S.O Park M.H. Jeong, "A Non-uniform One-Arm Spiral Antenna for WBAN Communication," *IEEE Antennas and Propagation Society International Symposium* , pp. 1-4, 2009.
- [19] "A Monofilar Spiral Antenna Excited Through A Helical Wire," *IEEE Transactions on Antennas and propagation*, pp. 661-664, 2003.
- [20] Yasuhiro Shinma, and Junji Yamauchi Hisamatsu Nakano, "A Monofilar Spiral Antenna and Its Array Above A Ground Plane - Formation of a Circularly Polarized Tilted Fan Beam," *IEEE Transactions on Antennas and propagation*, pp. 1506-1511, 1997.
- [21] and Shaofang Gong Magnus Karlsson, "An integrated spiral antenna system for UWB," *Microwave Conference, 2005 European* , p. 4, 2005.
- [22] Jee-Hoon Lee, Rashid Ahmad Bhatti, and Seong-Ook Park Yun-Taek Im, "A Spiral-Dipole Antenna for MIMO Systems," *IEEE Antennas and Wireless Propagation Letters*, pp. 803-806, 2008.
- [23] Sergey N. Makarov, *Selected Lectures - Antennas*. Worcester, MA, United States, 2010.
- [24] Maria del Mar Hershenson, Stephen P. Boyd, and Thomas H. Lee Sunderarajan S. Mohan, "Simple Accurate Expressions for Planar Spiral Inductances," *IEE Journal of Solid-State Circuits*, pp. 1419-1424, 1999.
- [25] Steven R. Best and Arthur D. Yaghjian, "Impedance, Bandwidth and Q of Antennas," *IEEE Transactions on Antennas and Propagation*, vol. 53, pp. 1298-1324, April 2005.
- [26] James Adams Stratton, *Electromagnetic Theory*. New York and London, United States: McGraw Hill Book Company, 1941.
- [27] C. D. Cantrell, "Numerical Methods for the Accurate Calculation of Spherical Bessel Functions and the Location of Mie Resonances," University of Texas at Dallas, Center for Applied Optics, Dallas, 1988.
- [28] R.C. Hansen, "Fundamental Limitations in Antennas," *Proceedings of the IEEE*, vol. 62, no. 2, p. 170, Feb 1981.
- [29] A.R Lopez, "Fundamental Limitations of Small Antennas: Validations of Wheeler's Formulas," *IEEE Antennas and Propagation Magazine*, vol. 48, no. 4, pp. 28-36, August 2006.

[30] R.E. Collin and S. Rothschild, "Evaluation of Antenna Q," *IEEE Transactions on Antennas and Propagation*, pp. 23-27, January 1964.